DAMPING PROPERTIES OF SURFACE LAYERS PRODUCED BY FRICTION STIR PROCESSING

Submitted in partial fulfilment of the requirements for the award of the degree of

DOCTOR OF PHILOSOPHY

in

METALLURGICAL AND MATERIALS ENGINEERING

by

K. Venkateswara Reddy

(Roll. No. 714140)

Under the Supervision of

Dr. R. Arockia Kumar

Assistant Professor

DEPARTMENT OF METALLURGICAL AND MATERIALS ENGINEERING

NATIONAL INSTITUTE OF TECHNOLOGY

WARANGAL-506004, TELANGANA, INDIA.

July-2021

DEPARTMENT OF METALLURGICAL AND MATERIALS ENGINEERING

NATIONAL INSTITUTE OF TECHNOLOGY

WARANGAL-506004, INDIA.

CERTIFICATE

This is to certify that the work presented in the thesis entitled "**Damping properties of surface layers produced by friction stir processing**" which is being submitted by **Mr. K. Venkateswara Reddy** (Roll No. 714140), is a bonafide work submitted to National Institute of Technology, Warangal in partial fulfillment of the requirement for the award of the degree of Doctor of Philosophy in Metallurgical and Materials Engineering.

To the best of our knowledge, the work incorporated in the thesis has not been submitted to any other university or institute for the award of any degree or diploma.

Date: 30/7/2021

Dr. R. Arockia Kumar
Thesis Supervisor
Assistant Professor
Department of Metallurgical and Materials Engineering
National Institute of Technology, Warangal, India.

DEPARTMENT OF METALLURGICAL AND MATERIALS ENGINEERING

NATIONAL INSTITUTE OF TECHNOLOGY

WARANGAL-506004, INDIA.

DECLARATION

This is to certify that the work presented in the thesis entitled "**Damping properties of surface layers produced by friction stir processing**", is a bonafide work done by me under the supervision of Dr. R. Arockia Kumar and was not submitted elsewhere for the award of any degree.

I declare that this written submission represents my idea in my own words and where other's ideas or words have not been included. I have adequately cited and referenced the original sources. I also declare that I have adhered to all principles of academic honesty and integrity and have not misinterpreted or fabricated or falsified any idea/data/fact/source in my submission. I understand that any violation of the above will be a cause for disciplinary action by the Institute and can also evoke penal action from the sources which have thus not been properly cited or from whom proper permission has not taken when needed.

Date: 30/07/21

Place: NIT Warangal

Kvedy 30/07/21

(Mr. K. Venkateswara Reddy)

Research Scholar

Roll No. 714140

Thesis Approval for PhD

The thesis entitled "**Damping properties of surface layers produced by friction stir processing**" by **K. Venkateswara Reddy** is approved for the degree of **Doctor of Philosophy** in Metallurgical and Materials Engineering.

Examiners

Supervisor

Dr. R. AROCKIA KUMAR
Assistant Professor

Chairman

Date:

ACKNOWLEDGEMENT

It is my pleasant duty to acknowledge the people who have helped me during the tenure of the research work reported in the present thesis.

I express special gratitude to my supervisor and mentor **Dr. R. Arockia Kumar**, Assistant Professor, Department of Metallurgical and Materials Engineering, National Institute of Technology Warangal for his inspiring guidance, keen interest, motivation, involvement and constant supervision throughout the course of this work and preparation of thesis. Without his patient mentorship, constant inspiration, valuable discussions and suggestions, this thesis would not have been possible.

Besides my supervisor, I take this privilege to thank all my Doctoral Committee (DSC) members Dr. Asit Kumar Khanra, Associate Professor (Chairman and Head), Prof. G. V. S. Nageswara Rao, and Dr. D. Jaya Krishna, Associate Professor (Department of Mechanical Engineering) for their useful suggestions and periodical review of my progress during this course of PhD work. I also would like to thank all the faculty members of MMED for their support and help during the course of PhD.

I thankfully acknowledge the financial support received from Science and Engineering Research Board (SERB) of Department of Science and Technology (DST), Govt. of India.

I would like to express my sincere thanks to Dr. G. Malakondaiah (Former Director, DMRL and CCR&D, DRDO Hyderabad), Dr. G. Madhusudhan Reddy (Director, DMRL Hyderabad) Mr. Rama Rao Golla, (Scientist E, ASL, DRDO, Hyderabad) and NIT Jaipur for providing research facilities required during my Ph. D work.

I take this opportunity to acknowledge with sincere gratefulness to my friends and colleagues Mr. C. Ravikanth Reddy, Mr. Shiva Kumar, Dr. Bheekya Naik, Mr. T. Sravan Kumar, Dr. Shiva Bejjugama, Dr. G. Eshwar Gowd, Dr. Venkat Rao, Mr. Vidhish Naik, Dr. K.N.B. Kumar and all research scholars of NIT Warangal.

I also thank technical staff G. Savvaiah, Mechanic A grade (Retired), Mr.Md. Fayaz, Nandu and ramya (Technical Assistants) and other technical and office staff of Metallurgical and Materials Engineering Department, NIT Warangal for their help during this research work. Also I want to thank Mr. Vijay Kumar (DMRL, Hyderabad) and Mr. Khannan (ASL, DRDO, Hyderabad). Finally, I express my sincere thankfulness to my family for their love, patience and encouragement.

K. Venkateswara Reddy

ABSTRACT

A structure under motion (e.g. vehicles and aircraft) vibrates, resulting in unavoidable massive noise levels. The vibrations are minimised by using materials with high damping capacity. Despite of inadequate damping capacity, aluminium and its alloys are being used in the automotive/ aircraft industry owing to its lightweight. Introducing ceramic reinforcements into a metal matrix, known as metal matrix composites (MMC), is one method to improve the damping capacity. Microstructure refinement is another method for improving the damping capacity of aluminium. Friction stir processing (FSP), a modification of the friction stir welding process, can simultaneously incorporate reinforcements and refine microstructure. However, FSP has majorly been used to improve the hardness, tensile strength, wear-resistance and corrosion behaviour. The use of FSP to alter damping properties is rare in the literatures. Hence, the current study is planned to investigate the damping properties of metallic and composite layers prepared by friction stir processing.

First, the damping capacity of friction stir processed commercial-grade aluminium, copper and magnesium metals were studied. A fixed set of variables was used to process the plates. Samples cut from the stir-zone were characterised for their microstructure, hardness, dislocation density, and damping capacity. The frequency-dependent and temperature-dependent damping properties were studied using the dynamic mechanical analyser. The room temperature damping capacity of aluminium (+58%) and copper (+135%) increased after friction stir processing due to an increase in the grain boundary area. In contrast, magnesium's damping capacity decreased (—60%) due to increased dislocation density after processing.

In the second step, the role of friction stir process variables, i.e. tool rotational speed, tool traverse speed and number of passes, on the damping capacity of commercial-pure aluminium was investigated. The increase in rotational speed and the number of passes enhanced the damping at high temperatures. But an increase in traverse speed decreased the damping.

In the third step, surface composites prepared by FSP were studied for their temperature-dependent damping capacity. AA6061 was chosen as the matrix, and SiC, BN, and graphite particles were chosen as reinforcements to prepare composites. The role of process variables, the fraction of reinforcement and the particle size were investigated in these studies. A decrease in rotational speed significantly improved the damping (585%) in AA6061/BN composites. In the case of AA6061/graphite composites, an increase in graphite fraction increased the damping capacity at ambient and high temperatures. As particle size increased, the damping

increased in AA6061/SiC composite system. For a fixed set of process variables, among the three selected reinforcements, BN was observed to be an effective reinforcement for enhancing the damping capacity of AA6061.

Finally, surface composites with metallic reinforcements, i.e. Fe and Ni, were prepared and studied. Both the elements were observed to improve the high-temperature damping; however, Ni was better among them. The results undoubtedly established that friction stir processing is an effective method to improve the damping capacity of metallic materials.

Keywords: AA6061, surface composites, friction stir processing, damping capacity, dynamic mechanical analyser, impulse excitation technique, RFDA

TABLE OF CONTENTS

LIST OF FIGURES

LIST OF TABLES

Nomenclature

SYMBOLS

δ	Logarithmic decrement
E'	Storage modulus
E''	Loss modulus
η	Loss factor
ζ	Damping ratio
ψ	Specific damping capacity
Q^{-1}	Inverse quality factor
f_r	Resonance frequency
η_c	Damping capacity of composite
η_p	Damping capacity of the reinforcement
η_m	Damping capacity the matrix
Vf_P	Volume fractions of particle
L_N	Dislocation segment length
ρ	Dislocation density
B	Damping constant
b	Burgers vector
t	Dimension of reinforcement
V_f	Volume fraction of matrix
ΔT	Temperature
$\Delta\alpha$	Difference between the CTE of reinforcement and matrix.
v	Poison ratio
$A_{g,}$	Area of the groove
A_p	Projected area of pin
W_g	Groove width,
D_g	Groove depth

D_p	Pin diameter
L_p	Pin length
ϵ	Average lattice strain
D	Crystallite size
λ	Radiation wave length
θ	Half of the diffraction angle.
E	Elastic modulus
f_f	Resonance frequency (Hz)
m	Mass of the sample
T_1	Correction factor
f_{zp}	Plastic zone volume fraction
G_c	Shear modulus
σ	Stress
ε	Strain
S_V	Grain boundary area per unit volume
$\bar{N}_L$	No. of intercepts per unit length

ABBREVIATIONS

Severe plastic deformation	SPD
Equal channel angular extrusion	ECAE
Friction stir process	FSP
Friction stir welding	FSW
Silicon Carbide	SiC
Boron Nitride	BN
Graphite	Gr
Nickel	Ni
Iron	Fe
Metal matrix composite	MMC
Damping capacity	Tanδ
Impulse excitation technique	IET
Dynamic mechanical analysis	DMA
Resonance frequency damping analyser	RFDA
Aluminium matrix composites	AMCs
Metal matrix composites	MMCs
Rule of mixtures	ROM
Coefficient of thermal expansion	CTE
Equal channel angular pressing	ECAP
Carbon nanotubes	CNT
Rice husk ash	RHA
Carbon fibres	C_f
Dynamic recrystallization	DRX
Stir zone	SZ
Thermos-mechanically affected zone	TMAZ
Heat affected zone	HAZ

X-Ray diffraction	XRD
Scanning electron microscope	SEM
Electron back scattered diffraction	EBSD
Grain boundaries	GB
Vickers hardness	Hv
Traverse speed	TS
Rotational speed	rpm

Chapter 1

Introduction

1.1 Motivation

Progress in materials science requires the development of newer materials/processes to cater to the needs of strategic industries. In addition to the materials offering high structural efficiency, the aerospace industry requires the materials to serve as good dampeners [1]. The structures in a dynamic system are often subjected to the varying magnitude of vibrations that result in an unavoidable huge noise level and therefore causes discomfort to human passengers and may damage sensitive electronic components. It is imperative to protect the payload from vibrations during the lift-off of a launch vehicle, provide comfort to the passengers of an aircraft during its cruise, and isolate tremendous vibrations to the crew cabin helicopter as the engine and crew cabin are situated adjacent each other. Consequently, the materials used for structural applications (e.g. automotive and aerospace automobile industries) should have a high damping capacity to nullify the noise generated due to vibrations. Thus there is a considerable demand for the material possessing the combination of properties such as low density, high damping coefficient and high specific strength [2].

The aerospace sector extensively uses aluminium and its alloys due to its inherent advantages, and AA6061 is one such candidate material with good formability. It is actively selected for many aerospace structures. The automotive/ aerospace industries exploit aluminium and its alloys due to their high specific strength and inherent properties. However, they possess inadequate damping capacity to isolate vibrations and reduce noise. It would benefit these industries if aluminium and its alloys can be tuned to have a better damping coefficient. Several efforts have been made to improve the damping capacity of aluminium and its alloys and one such method is the introduction of ceramic reinforcements to aluminium and its alloys, which has resulted in the improvement of damping capacity and other mechanical properties [3].

Processing is another route to engineer the damping properties of aluminium alloys. Many researchers have done investigations on improving damping capacity of materials through severe plastic deformation (SPD) techniques like equal channel angular extrusion (ECAE) [4], extrusion [5] and roll bonding [6]. These processes found to refine the microstructure further changes the mechanical and damping properties of materials. Friction stir process (FSP) is also a severe plastic deformation process to refine grain structure. Studies showed that materials

with an ultrafine grain structure could be obtained by FSP [7]. Using the FSP technique, it is possible to produce high damping materials because FSP produces fine grain structures with man defects like dislocation and grain boundary area, which are responsible for improving the damping capacity [8]. Moreover, the manufacture of surface composites through friction stir processing has evolved itself as one of the newer synthesis methods over the conventional melt route or powder metallurgy route and has witnessed enormous growth due to its host of advantages [9].

Over the twenty years, friction stir welding/ friction stir processing has been established as a reliable method for processing light alloys, i.e. aluminium and magnesium. There were enough efforts to understand the effect of FSP on the mechanical and wear properties [10]. However, the detailed literature survey revealed, as described in Chapter 2, minimal efforts have been made to investigate the effect of FSP on the damping properties of metallic materials. Therefore, it is believed that analysing the influence of FSP on damping properties would help the engineering community. In the present study, an effort is made to investigate the damping properties of pure metals (pure Al, Cu and Mg) and surface composites, i.e. AA6061 + (SiC/ BN/ Graphite/ Ni/ Fe) prepared by friction stir processing.

1.2 Aim and objectives of the research work

The present research work aims to study the damping properties of surface layers produced through friction stir processing.

The objectives are

- To study the damping capacity of friction stir processed (FSP) pure metals
- To analyse the influence of FSP process parameters on the damping capacity of aluminium
- To study the damping capacity of AA6061 based surface composites with ceramic reinforcements
- To study the damping capacity of AA6061 based surface composites with metallic reinforcements

1.3 Organization of thesis

The thesis is organized into six chapters, and the following is the objectives of each chapter.

Chapter 1 aims to motivate the research work and list the aim and objectives of the research work.

Chapter 2 introduces the damping capacity of materials, mechanisms of damping capacity, and it measurement. The chapter reviews the published literature on the damping of fine-grained

structures achieved through various routes, including FSP. Then damping properties of composites fabricated using different routes are presented. Finally, the gaps identified are listed.

Chapter 3 presents the research work and details the materials, processes, and characterisation methods employed in the research work.

Chapter 4 presents the results then correlates the properties with the microstructure.

- The effect of grain refinement on the damping capacity of pure metals, i.e. magnesium, copper and aluminium, is presented and discussed in 4.1.
- The ability of friction stir process parameters, i.e. tool rotational speed, traverse speed and number of passes, on the damping property of aluminium is compiled in 4.2
- The effect of three different ceramic reinforcements (Gr, SiC and BN) on the damping property of AA6061 is presented and discussed in sections 4.3, 4.4 and 4.5.
- The effect of two different metallic reinforcements (Fe and Ni) on the damping property of AA6061 is discussed in section 4.6
- The final part of Chapter 4.7 highlights the significant contributions of this research work.

Chapter 5 lists the major conclusions of the work and the scope for future work. This chapter is followed by references and a list of publications.

Chapter 2

Literature review

2.1 Introduction

This chapter is organized as follows: (i) the chapter starts with defining damping capacity and its measurement method. Then mechanisms of damping are summarized. (ii) The next part provides an overview of the damping capacity of various metals, and composites fabricated using different processing routes, i.e. casting, powder metallurgy, severe plastic deformation processes. (iii) The third part discusses the friction stir process, its pros and cons, and key process variables' effect on microstructure development. (iv) Fourth part reviews the efforts on improving the damping capacity applying friction stir processing. In the end, the identified gaps in the literature are listed.

2.2 Measurement of damping capacity

The damping measure of a material is its ability to absorb energy when it is under cyclic loading. Cyclic loading cause's vibrations and noises, and high-damping materials are capable of suppressing the noise and vibrations. Thus, their development has become increasingly important for dynamic structures and other high precision devices. Several vital metals and alloys have low damping capacity, thus making them not usable for dynamic systems. However, it is possible to improve the damping capacity of such materials by reinforcing with particles that have high damping capacities to form metal matrix composite (MMC) [4]. Material damping is measured either by the decay of vibration amplitude in free vibration (***impulse excitation technique***) or by suppressing resonant amplitude and the phase lag of deformation behind the applied load in forced vibration (***dynamic mechanical analysis***).

The damping capacity of all specimens was measured in terms of tan δ, and it is defined as follows [11] [12].

$$\tan \delta = E'' / E' \qquad (1)$$

Where E′ is the storage modulus, corresponding to the material's stiffness, proportional to the energy stored during a cycling loading. Loss modulus (E″) relates to the viscous component, proportional to the dissipated energy.

The common measures of damping are Loss factor (η), damping ratio (ζ), Specific damping capacity (ψ), Logarithmic decrement (δ) and inverse quality factor (Q^{-1}).

For small damping capacity values (< 0.1.), all of the mentioned qualities are interchangeable and are related by the following equation [13].

$$\tan \delta = \delta = \eta = \zeta = \frac{\psi}{2\pi} = \frac{\Delta}{\pi} = Q^{-1} \qquad (2)$$

Logarithmic decrement (δ), is derived from the amplitude decay of a specimen under free vibration is defined as [4]

$$\text{Logarithmic decrement } (\delta) = \frac{1}{n} \ln \frac{Ai}{Ai+n} \qquad (3)$$

Where Ai and $Ai + n$ are the amplitudes of the ith cycle and (i+n)th cycle, at times t1 and t2 respectively, separated by n periods of oscillation.

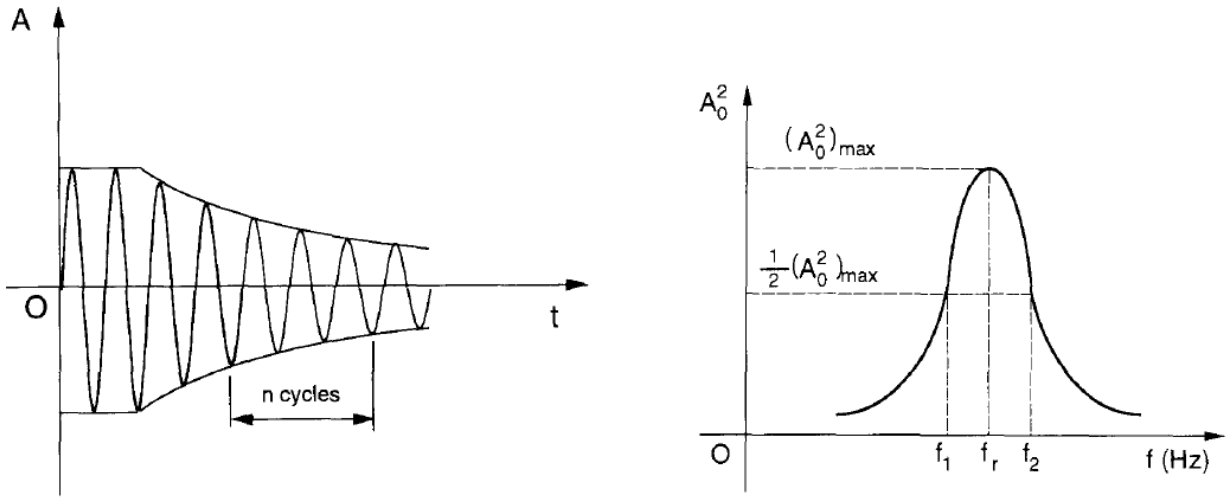

Fig. 2.1.1 Schematic diagram showing (a) amplitude decay under free vibration (b) Amplitude square vs frequency [3].

The inverse quality factor (Q^{-1}) is calculated for a specimen under forced vibration by [4]

$$Q^{-1} = \frac{f2-f1}{fr} \qquad (4)$$

Where f_r is the resonance frequency and f_1 and f_2 are the half-power bandwidth of the frequencies.

The damping capacity was measured by two techniques

1. Dynamic mechanical analyzer (DMA)
   Damping measurements were performed using a dynamic mechanical analyzer in three-point bending mode. Two types of tests are performed
   (a) Frequency-dependent damping capacity at constant strain amplitude and temperature
   (b) Temperature-dependent damping capacity at constant frequency and strain amplitude.
2. Impulse excitation technique (IET)
   The damping capacity of materials was measured at the resonance frequency of materials using a resonance frequency damping analyzer (RFDA)

2.3 Damping mechanisms

A variety of mechanisms are responsible for improving the damping behaviour of materials. During processing formation of defects like dislocations, point defects, interfaces between reinforcements and matrix and grain boundaries are dominant factors in defining the damping capacity of materials. Zhang et al. [14] reported the primary damping mechanisms for AMCs. The dislocation damping plays a significant role at room temperature during interface sliding and grain boundary damping at high temperatures. The following are some of the factors which are active in improving the damping of materials [3].

2.3.1 Intrinsic damping

The resultant damping capacity of the composites is directly related to the damping capacity of the individual components. The improvement in damping of composites is mainly based on the selection of reinforcement. One simple and important mechanism in improving the damping rule of mixtures (ROM) [15].

$$\eta_c = \eta_p V_{fp} + \eta_m (1 - V_{fp}) \qquad (5)$$

Where η_c is the damping capacity of composite, η_p and η_m are the damping capacity of the reinforcement, and the matrix, V_{fp}, $(1-V_{fp})$ are volume fractions of particle and matrix.

2.3.2 Dislocation damping

During the MMCs cooling process, dislocations are generated due to the large mismatch (six times higher) between the matrix's coefficient of thermal expansion (CTE) and the reinforcement. According to Deng and co-workers [16], this difference in CTE values and consequent dislocation generation explains the higher damping capacity of composites compared to the unreinforced matrix.

The mechanism behind the dislocations influence on the damping behaviour is well described by the Granato-Lucke theory [17], where dislocations are segments of length L_N (shown in Fig. 2.1.2). At room temperature and under cyclic loading, dislocations can drag the weak pinning points (such as vacancies) moving, dissipating energy and contributing to damping. With increasing temperature, dislocations movement becomes faster, although their concentration and consequently contribution to damping are expected to fall [13].

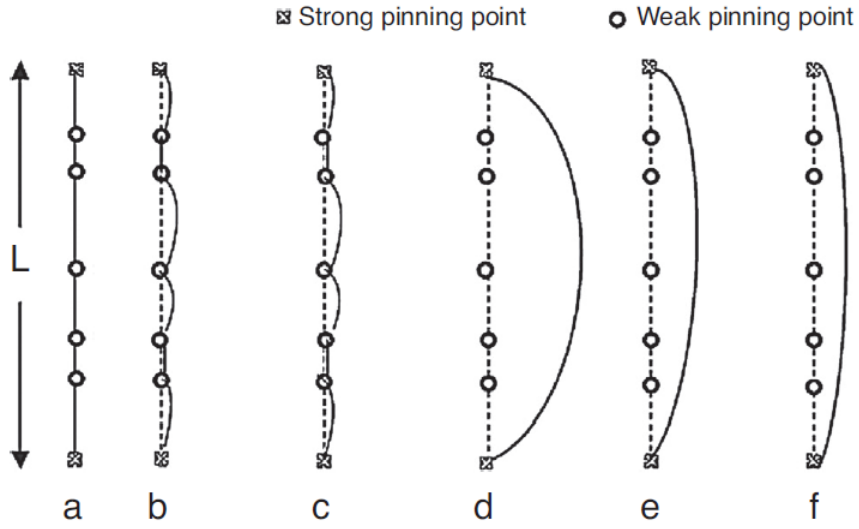

Fig. 2.1.2 Schematic representation of Granato and Lucke vibration string model [18]

The density of dislocations generated due to mismatch between the matrix and the reinforcement particle can be calculated using the following equation [18]

$$\rho = B\Delta\alpha\Delta T V_f/(bt(1-V_f)) \quad (6)$$

Where B is damping constant, b the Burgers vector, t is the smallest dimension of reinforcement, V_f is the volume fraction of matrix, ΔT is the temperature, and $\Delta\alpha$ is the difference between the CTE of reinforcement and matrix.

2.3.3 Grain boundary damping

The grain boundary sliding is another possible mechanism contributing to damping capacity at high temperatures. Polycrystalline metal shows viscous properties at grain boundaries. The mechanical energy produced at the grain boundary due to cyclic loading is converted into thermal energy due to internal friction (damping) [16].

2.3.4 Particulate matrix interface

The interface is a two-dimensional defect where the crystal structure of the metal matrix is distorted [10]. Several works suggested that the interface plays a role in increasing the damping of Al composites [10]. When the temperature exceeds 100 °C, the Al matrix softens, and a movement occurs at the interface [11]. The frictional energy loss from the interfacial movement between the reinforcement and the Al matrix is responsible for generating the damping. The contribution of the interface/matrix to the damping can be measured by the following equation[16][18].

$$Q^{-1} = 4.5(1-\nu)/\pi^2(2-\nu)*V_f \qquad (7)$$

Where Q^{-1}: Quality inverse factor (damping capacity), v: poison ratio, V_f: volume fraction of particles. This correlation suggests that the interface damping is directly proportional to the volume fraction of reinforcement.

2.4 Damping properties of materials

The introduction of crystal defects during deformation processing is responsible for enhancing damping properties. The movement of crystal defects (such as dislocations and grain boundaries) under external vibrations helps to dissipate energy, thereby contributing to damping [19]. Hence, it becomes necessary to understand the influence of deformation processing on the damping properties of materials. Shyi-Kaan Wu [20] studied the influence of cold rolling on the damping capacity of pure Al and Al-12%Si. This study used 99.99% virgin Al, and Al-12% Si alloy was fabricated through the direct chill casting method. The cast Al-12% Si alloy was homogenised and extruded at 350°C. Zhang [4] studied the damping behaviour of grain refined pure aluminium through Equal channel angular pressing (ECAP). The damping capacity of Aluminium increases with temperature and decreases with increasing frequency. Also, they reported that increased frequency decreased dislocations' movement, thereby reducing the damping capacity. Fan et al. [21] studied the mechanical and internal friction (damping capacity) of pure Mg through (ECAP). They found increased internal friction values in the strain-independent part due to abundant mobile dislocations induced by the ECAP

processing. Jingfeng Wang et al. [22] investigated the dislocation configurations on the damping capacity of Pure Mg by arc bending deformation. The entangled dislocation configuration caused by introducing excessive dislocations in Mg is difficult to move under alternating stress, suggesting that this dislocation configuration cannot effectively activate the dislocation damping capacity.

2.5 Damping capacity of metal matrix composites (MMCs)

The damping capacity of materials can be improved by combining them with reinforcing particles with high damping capacities to form metal matrix composites (MMC). Composite materials with high damping reinforcement in a matrix find significant applications in lightweight structures such as aerospace, military, and automotive to suppress vibrations [13].

J.N. Wei et al. [23] studied the damping behaviour of pure Al/Gr composites prepared by pressure infiltration. And also, R.J. Perez [15] studied the damping behaviour of Al6061/Graphite composites using spray atomisation and co-deposition. The damping capacity increases with graphite content. They concluded that, at low temperature, dislocation damping, intrinsic damping of Graphite and interface between Al and Graphite are effective mechanisms by which damping is improved. At high temperatures, grain boundary sliding and interface sliding are substantial.

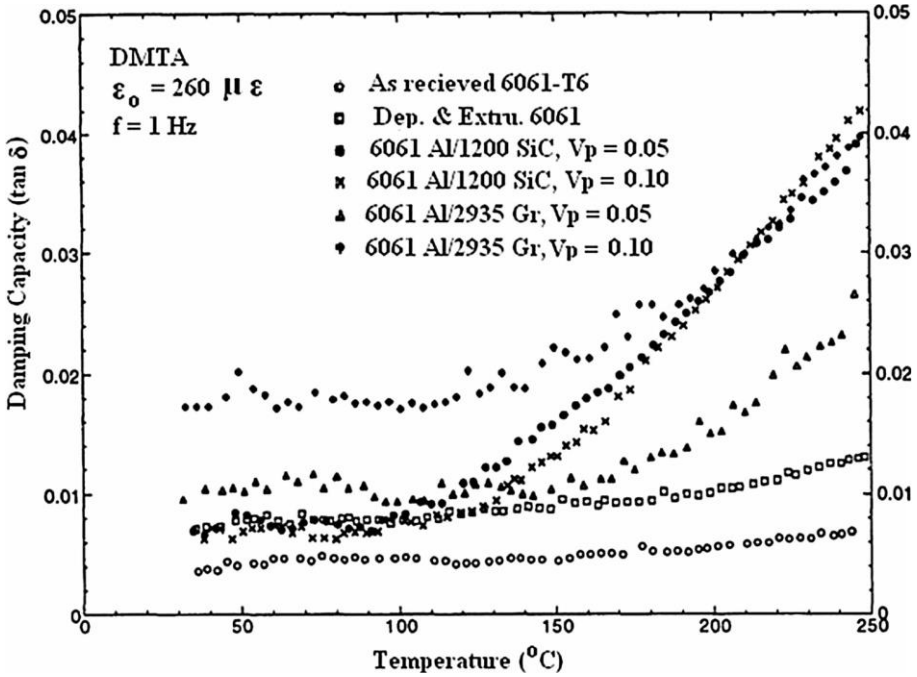

Fig. 2.1.3 Comparison of 1 Hz damping capacity for spray deposited MMCs and unreinforced alloy [24].

Rohatgi et al. [24] prepared Gr and SiC reinforced Al alloy composites and studied the damping capacity. The damping capacity increases with increasing Gr. content in Al/Gr composites. Whereas in the case of Al/SiC, no significant improvement was observed.

Bouri et al. [25] produced Al8090 alloy composites with 8, 12 and 18 % SiC particles through stir casting. The damping capacity of the alloy and composites were analysed over a temperature range of 27 to 300°C with different frequencies. The results confirmed that the damping capacity decreases with increasing frequency. The composites displayed better damping properties than the Al alloy. J. Zhang et al. [26] fabricated Al6061/SiC, Graphite (Gr.) composites were processed through spray atomisation and deposition technique. The Al6061/SiC and Al6061/Gr composites exhibited better damping capacity than the base alloy. Based on the results, it was concluded that at lower temperatures, the major damping mechanisms are intrinsic damping of reinforcement particles, dislocation damping and grain boundary and interface damping at high temperatures (Fig. 2.1.3).

Jinhai Gu et al. [27] produced Al6061/SiC/Gr hybrid composites through spray atomisation and deposition and analysed damping and mechanisms. O. Carvalho et al. [28] fabricated AlSi–CNT, AlSi–SiC and AlSi–(CNT–SiC) hybrid composites by hot pressing. The results demonstrated that the hybrid composites showed better damping capacity than the single reinforced composites.

S. Madeira et al. [29] studied the effect of particle size on damping capacity and dynamic young's modulus of AlSi/SiC composites produced by hot pressing. Studies showed that all AlSi- SiC_p composites displayed superior damping capacity than unreinforced AlSi alloy. The improvement in damping capacity is due to plastic zone radius and dislocation density at low temperature and interface; grain boundary sliding is significant at high temperature.

Siva Prasad [18] fabricated hybrid composites Al/SiC/Rice husk ash (RHA) with various weight per cent using stir casting process. It was observed that damping capacity increases with the percentage of reinforcement. The increase in damping capacity is related to the rise in dislocations generated due to the large coefficient of thermal difference between matrix and reinforcement. Jinhai Gu et al. [30] studied the damping properties of aluminium MMCs reinforced with coated continuous carbon fibres (C_f). The composites were fabricated by pressurised liquid metal infiltration technique, the temperature of fibre preform and that of melt were set as 600 and 750 °C, respectively. The same process also prepared the Cf/Al composite without coating. Finally, the damping capacity of hybrid composites was higher than the single reinforced composite.

2.6 Friction stir processing (FSP)

Friction stir welding (FSW), which was developed at The Welding Institute in the United Kingdom, is considered the most significant development in metal joining in the past few decades. FSP was developed based on the principle of FSW [31]. Friction stir processing (FSP) has been established as a reliable method of engineering the microstructure of light alloys, and it is one of the unique and emerging severe plastic deformation (SPD) techniques for substantial grain refinement and is capable of producing surface composites, particularly in aluminium and magnesium alloys [32]–[34]. FSP utilises a non-consumable spinning tool that is plunged into the base alloy and moved at a specific speed (i.e. traverse speed), which results in the stirring action of base metals, causing a recrystallised zone at the nugget based on the process parameters. This method has also been shown to incorporate ceramic particles, thereby producing metal matrix composites. Such composites exhibit better wear and mechanical properties [35]–[38].

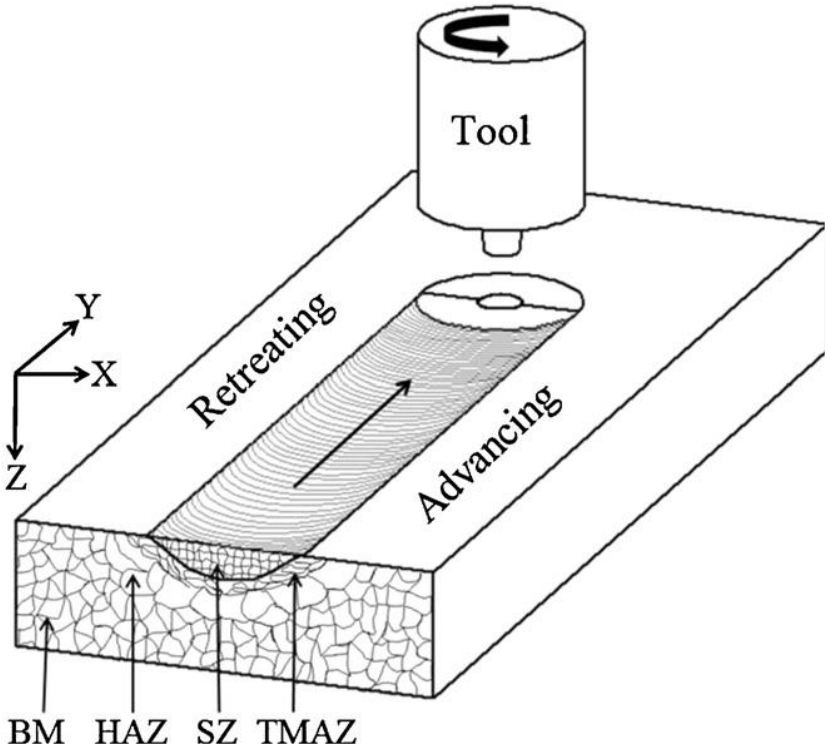

Fig. 2.1.4 Schematic representation of friction stir processing [39].

A schematic of the process is shown in Fig. 2.1.4. The rotating/stirring tool serves two main functions: (i) heating and (ii) deformation of work-piece material. The stirring action of the tool creates a frictional heat between the tool shoulder, tool pin, and work pieces. Due to this, the materials are plasticised during FSP. This plasticised material flows around the rotation tool pin, and the material moves the front and back of the rotating tool pin. During the tool rotation,

the materials undergo intense, severe plastic deformation and thermal exposure, finally, which causes significant refinement for the microstructure of the processed region. The repetitive dynamic recrystallisation (DRX) causes the generation of refined and equiaxed grains in the stir zone (the processed region). After the processing, the processed region consists of the four distinct regions, which are named as stir zone (SZ), thermos-mechanically affected zone (TMAZ), heat affected zone (HAZ), and base metal zone [10], [40]. The various regions of the processed zone are shown in Fig. 2.1.5. These distinct regions are formed during the FSP due to the rotations of the non-consumable rotating tool that causes material flow behaviour. The heat-assisted plastic deformation causes grain refinement at the processed zone. The proper selections of the FSP variables give a defect-free FSPed zone. Several researchers have attempted to improve the mechanical properties of materials [41], [42] through FSP.

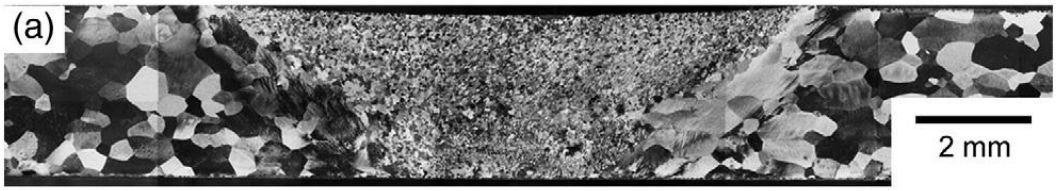

Fig. 2.1.5 Cross-sectional macrostructure of friction stir processed pure aluminium [43]

2.6.1 Applications of Friction Stir Processing

It is always essential for finding a suitable material for the required properties for various industries and engineering applications. It is always challenging to choose a material with the required design and desired property of material for particular areas. However, there are many limitations in terms of time, environment, energy, and production cost to satisfy these desired properties with conventional processing techniques. It is always difficult to have high strength accompanied by high ductility. Materials having homogenous and fine grain structures are helpful to achieve it.

FSP is being developed for this purpose, and its potential applications are:

1. Producing fine-grain microstructure (superplasticity, formability, and microstructural homogenisation)
2. Refining microstructure of cast light alloys (eliminate casting defects, enhancing mechanical and tribological properties)
3. Preparing metal matrix micro-and nano-level surface composites.

Fig. 2.1.6 Lists the attributes of FSP and its link to achieve the desired property in a material.

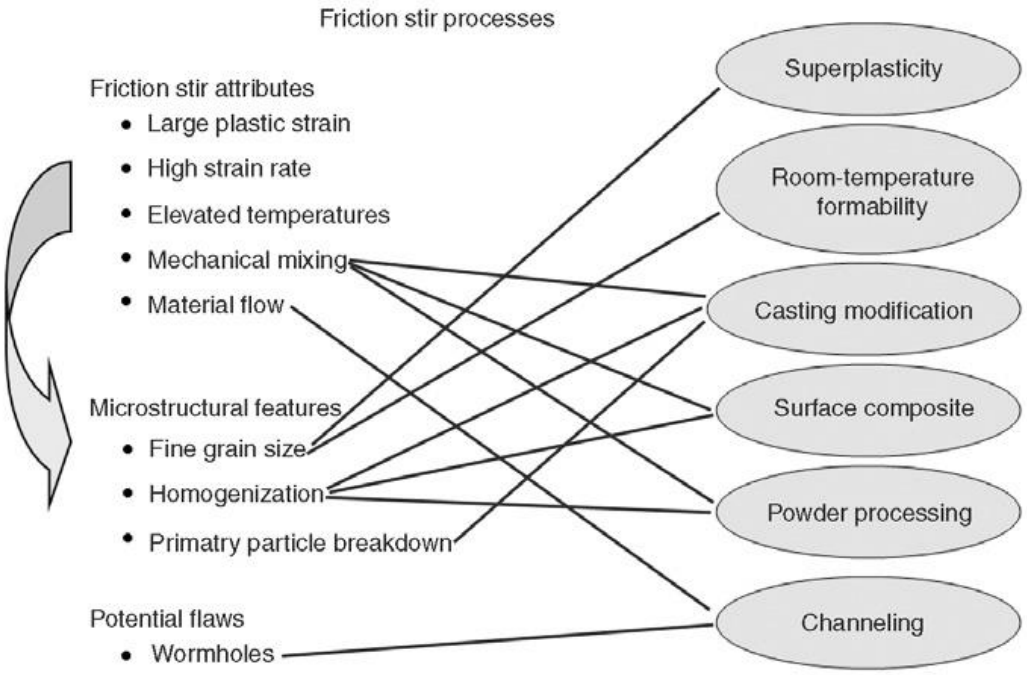

Fig. 2.1.6 Schematic lists attributes of friction stir processing and links to the friction stir processes [44].

2.6.2 Effect of Friction Stir Processing parameters

In fact, at low temperature, processing surface composite, which is below the melting point of materials, can prevent the interfacial reaction between metal matrix and reinforcement particles and the development of any unrequired phases [45]. The perfect solidified microstructure with good interfacial bonding between particles and matrix material in the surface layer can also be achieved by monitoring FSP parameters effectively than by other conventional techniques. As discussed earlier, the continuous dynamic recrystallisation causes the refined grains and equiaxed grains to be generated in the processed zone during FSP. However, the process parameters play a significant role in the final fine grain microstructure. The added reinforcement particles always help improve the properties and grain refinement and recrystallisations in friction stir processed MMCs. The influence of FSP parameters on various properties and for developing the surface composite [46] are shown in Fig. 2.1.7. The main process parameters and their effects in preparing surface level MMCs by the FSP route are given in Table 2.1.1.

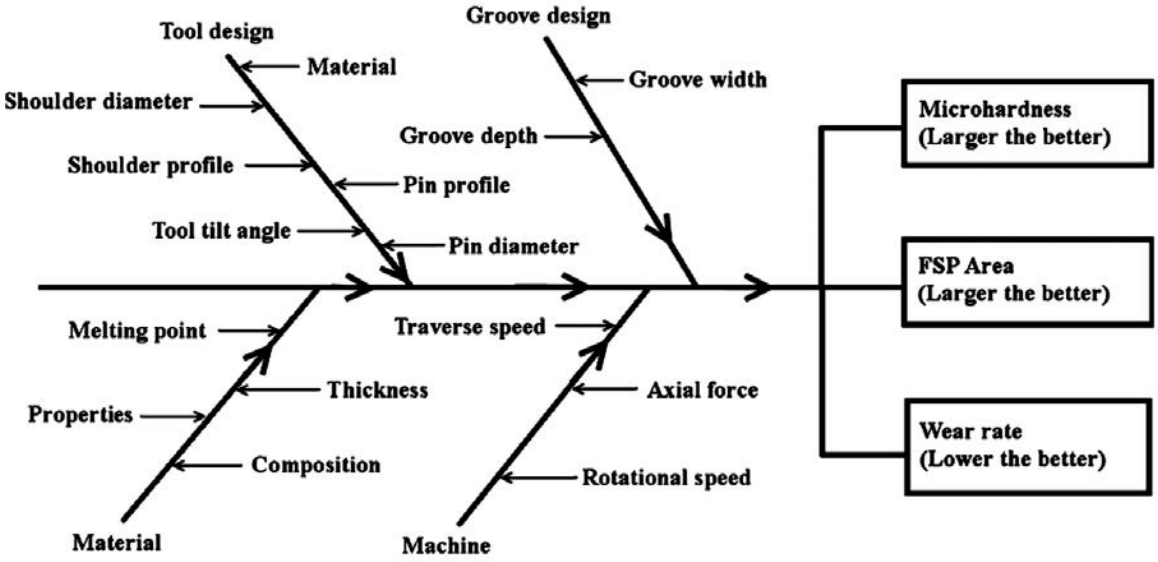

Figure 2.1.7 FSP parameters influencing the properties of the surface composite [45]

Table 2.1.1 Effects of FSP parameters on preparing the surface or surface composites

S. No	FSP parameters	Effects in preparing surface composites
1	Tool rotational speed	Frictional heat, heat input, stirring, oxide layer breaking and mixing of material
2	Traverse (processing) speed	Heat input, Appearance
3	Tool tilt angle	Forging, Compaction, Appearance, Thinning, Stirring
4	Downward force	Frictional heat, maintaining contact conditions
5	Tool plunge depth	To achieve compaction of reinforcements
6	Multi-pass	To achieve uniform microstructure, to achieve uniform distribution of reinforcements

2.6.3 Friction stir processing of pure metals

FSP produces fine grain structure with many defects like dislocations and grain boundary area, which are responsible for improving the properties of the materials. The influence of FSP on the microstructure and hardness of pure aluminium (pure aluminium) was studied by Wen-ying Gan et. al.[47]. The grain size is reduced in the stir zone compared to the base metal. There is a reduction in the hardness of the FSPed sample than the base metal. After FSP, it is shown that the dislocation density of base metal is significantly reduced and results in a drop in hardness. Taiki Morishige et al. [43] investigated the grain size of aluminium with different purity levels using FSP. Ultra-high purity of aluminium (99.999%) showed large recrystallised grains compared to the grain size of low purity aluminium (99% and 99.99%). This work shows that FSP allows deformation to get a microstructure with specific minimum grain sizes despite the

high-temperature deformation process. Surekha and Els-Botes [48] studied the effect of traverse speed on mechanical and electrical properties. With increasing the traverse speed, grain size decreased, and the mechanical properties improved compared with the base metal. There is no significant variation in the electrical conductivity of the FSPed sample compared to the base metal. Salar Salahi and Vahid Rezazadeh [49] studied the ductility of the FSP'ed Cu by using a tensile test at 20 °C temperature. The traverse speed varied from 40 to 100 mm/min, and rotational speeds ranged from 300 to 600 rpm. After FSP, the ultrafine grain microstructure was achieved. Further, at 300 rpm, the defects were observed in the nugget zone, and by increasing the traverse speed at a constant 600 rpm, the microstructure is refined and improved the ductility. Fracture behaviour depends on the grain size and porosity formed while processing Cu. The controlled heat input can be produced through a rotational tool; the produced heat input reduces the porosity formations and modifies the grain size.

Barmouz et al. [50] studied pure Cu through FSP, processed using various process parameters, and increased the number of passes. The enhanced ultimate strength and elongation (300% and 47%) properties were observed with selected processes parameters. There was a considerable decrement in the grain size (ultrafine grains up to 700-800 nm) processed with a higher number of passes.

Initially, FSP is applied to modify the material's surface properties by changing grain recrystallisation. In the 20th century, reinforced metal matrix composites (MMCs) were fabricated by FSP. Many researchers improved the hardness and wear properties of soft matrix materials by incorporating hard reinforcement particles into the matrix [10], [40]. By adding an appropriate amount of reinforcements, the specific strength of pure metals or alloys can be improved.

2.6.4 Friction stir processing of composites

Initially, on the required metallic plate, a groove with required width and depth dimensions or a hole with required dimensions of depth and diameter is machined. Further, the selected metallic/ceramic reinforcement particles are contriving in the groove or hole with the required volume. The volume of the particles depends on the chosen groove dimensions. After filling the holes or grooves with particles, they are processed with the pin-less tool to avoid the spilling/escaping of the particles. This process is known as compaction. Subsequently, the material is processed with a rotating tool with the required pin dimensions and adequate axial force. Then the material plastically deforms with applied axial force and rotational motion of the tool and forms the MMC's. The significant approaches in surface composite fabrication via

FSP is presented schematically in Fig. 2.1.8 [33]

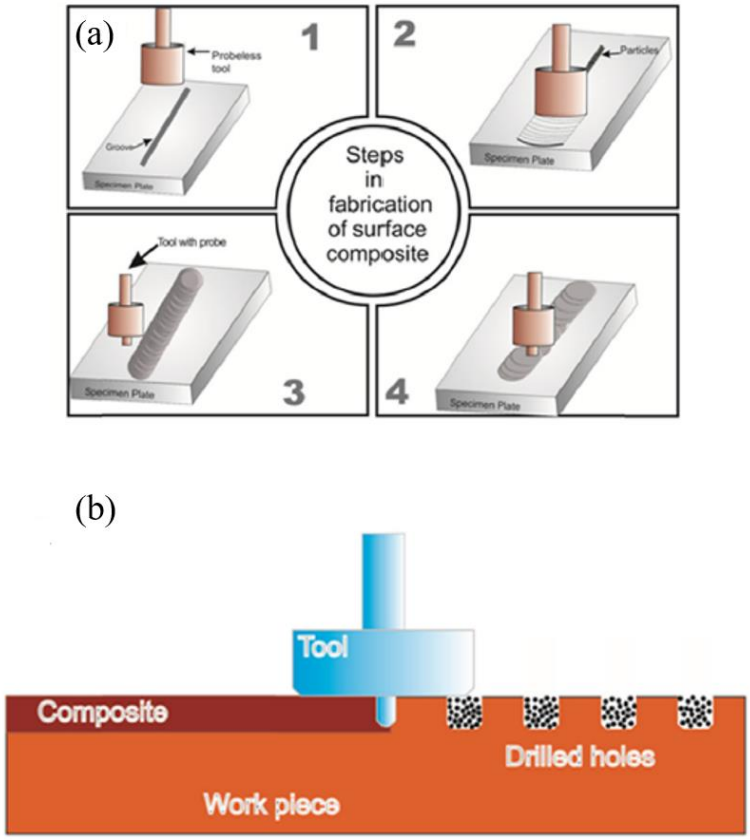

Fig. 2.1.8 Common methods for placing reinforced particles in the fabrication of surface composites (a) by a groove (b) by drilled holes.

Aluminium, copper and magnesium are examples of matrix materials and SiC; Gr, SiO_2, Al_2O_3 TiC are a few examples of reinforcement particles. The potential applications of metal matrix composites (MMCs) can be found in automobile, aerospace, marine and power generation industries [51]. Silicon carbide (SiC) ranks high among the most popular aluminium MMC reinforcements. There is a significant difference in the coefficient of thermal expansion between Al and SiC leading to solidification issues during conventional manufacturing methods. FSP being a solid-state technique, resolves these issues. Several authors reported Al/SiC surface composites fabricated using FSP. Mishra et al. [52] produced the Al5083/SiC surface composites using FSP. An increase in 51% hardness with better wear resistance is achieved for surface composites than the base metal. Wang et al. [53] also investigated the surface composites of 5A061/SiC and improved the hardness of 10% reported. In another study, 139% in microhardness enhancement was obtained in Al1050/SiC composites. Ke. et al. [54] synthesised in situ Al/Ni intermetallic composites via FSP at 1500 rpm and 23.5 mm/min. and 3° tilt angle. Three pass FSP was conducted to increase the reaction between Al and Ni. FSP successfully produced al/Ni intermetallic composites with subsequent heat treatment at 550 °C

for 6 Hrs. After FSP, Al intermetallic composites' microhardness and tensile strength increased due to the grain refinement and precipitation hardening of Al_3Ni intermetallic. Essam R.I. Mahmoud et al. [55] studied the effect of Al_2O_3 and SiC reinforcement particles into the Al alloy by FSP. By varying the combination (20/80, 50/50 & 80/20) of Al_2O_3 and SiC volume percentages into the aluminium alloy, good wear resistance and hardness properties were achieved. But superior wear resistance properties were achieved at 20% Al_2O_3 +80% SiC combination than the other combination of SiC and Al_2O_3. Thangarasu et al. [56] fabricated the AA6082/TiC surface composites with varying volume content of TiC particles. They studied that the area of the FSP zone decreases, and the mechanical properties improve with an increase in volume content. The maximum hardness and ultimate tensile strength obtained were 149Hv and 382 MPa, respectively, for 24 % TiC composite. Wanchuck Woo et al. [57] studied the influence of the FSP tool pin and shoulder on the microstructure and hardness of Al6061T6 Aluminium alloy. The FSP was conducted at 1250 rpm and 4.7mm/s with H-13 tool of 19.05 mm shoulder diameter and 6.35mm pin diameter with 6.23mm pin height. The microstructural softening that occurs due to the dissolution of precipitates is displayed by the significant hardness decreases in the stir zone.

Naresh Parumandla and Kumar adepu [58] fabricated Al/Al_2O_3 and Al/SiC surface nanocomposites. Al6061T6 was selected as the base metal. The FSP was conducted at 1150rpm and 50 mm/min. by varying the volume per cent of (2, 4 and 6) nanoparticles and studying the nanocomposites' microstructural, mechanical and wear properties. Barmouz et al. [59] investigated the effect of traverse speed on the grain size of Cu/SiC composites by FSP. Increasing the traverse speed in constant rpm causes reducing grain size and agglomeration of SiC particles to increase. The reason is related to the effect of the heat input on grain growth. Increasing the traverse speed leads to a decrease in the duration of the time in which the material is affected by the process heat. Therefore, the grain size decreases in the stir zone. Asadi et al. [60] produced SiC/AZ91 composite by FSP and observed that an increase in rotational speed leads to an increase in grain size while the increase in traverse speeds leads to a decrease in grain size. This was explained by noting that increasing traverse speed reduces the time of exposure to the process heat.

Sarmadi et al. [61] studied Cu/graphite composite and reported the effect of tool pin profile and increasing graphite content on microstructure and wear behaviour. The triangular pin profile tool provided better and homogeneous distributions of the Gr particles in the processed zone. The hardness decreased with increasing Gr particle content, which is soft. The wear loss was reduced with increased Gr particles content compared to the pure Cu. Sathiskumar et al. [46]

processed the Cu/B_4C composite and investigated the influence of the FSP parameters such as the rotational speed of the tool, traverse speed, and groove dimensions on grain size and hardness of the Cu/B_4C composite. Increased tool rotational speed and lower tool traverse speed produced the homogeneous distribution of the added B_4C particles in the processed region. The increased composite area formed due to higher heat development during the process. The higher heat development is due to the intense stirring action of the tool and leads to more material transportations. Finally, the improved hardness in composite was observed compared with the pure Cu. Sathiskumar et al. [62] investigated the FSP of Cu/B_4C composites and studied the influence of the volume fractions of B_4C particle on the microstructure and wear properties using the process parameters of tool traverse speed of 40 mm/min and tool rotational speed of 1000 rpm and axial force of 10 KN applied. Increased B_4Cp, improved the microhardness and wear resistance of the produced composite.

V Kishan et al. [63] produced nano Titanium Boride (TiB_2) reinforced Al6061T6 composites with different volume per cent by FSP. The effect of the volume per cent of TiB_2 particles on tribological properties was studied. Microstructure revealed that all composites showed the distribution of reinforcement in the stir zone. The microhardness increases with increasing the volume per cent of TiB_2 particles. It is noticed that the composite produced with 4% TiB2 composite showed better wear resistance than the 2 and 8%.

2.6.5 Damping capacity of FSPed materials

Very few researchers studied the damping capacity of friction stir processed materials. H.J. Jiang et al. [64] employed friction stir processing (FSP) on an Al-Mg-Si alloy (AA 6082-T4) at a low tool rotational speed of 200 rpm and better mechanical and damping properties were noticed after FSP. The high mechanical and damping capacity of the FSPed sample is due to recrystallised grains and the dissolution of metastable phases. Y. Chen et al. [65] studied the influence of FSP on the mechanical and damping capacity of Al7075 by adding Scandium (Sc). The study revealed that a low tool rotation rate of 300 rpm effectively inhibited the grain coarsening and grain size reduced to 1.7 μm during FSP. The FSPed 7055-0.25Sc alloys exhibited higher strength and ductility than the FSP Al7055 alloys under the same processing conditions. The temperature-dependent damping capacity of the Al7055 alloys was improved after FSP and Sc addition. Also, processing at low rotational speed improved the damping of Al7055- 0.25Sc alloy; this was due to its fine microstructure. Subhash Singh and Kaushik Pal [14] produced aluminium matrix composites incorporated with SiC, MgO grafted SiC and $MgAl_2O_4$ grafted SiC particles stir casting. Additionally, the composites were processed using

FSP to analyse the effect of grain refinement on mechanical and damping properties. Grain refinement of these composites played a significant role in improving the damping characteristics of FSPed samples. After FSP, the tensile strength of Al/SiC/ $MgAl_2O_4$ is increased by a factor of 3.9 and 3.3, respectively, compared to pure Al. Subhash Singh et al. [51] also fabricated Al composites by incorporating pristine SiC and decorated SiC and SiC/$ZnAl_2O_4$/Al composite via FSP technique. The better damping behaviour of composites was attributed to dislocation motion at particle/matrix interfaces. Very few researchers have investigated the effect of reinforcement on microstructural, and damping capacity of friction stir processed Al materials.

2.6.6 Gaps identified

The following gaps are identified through the detailed literature survey

- The friction stir processed materials rarely characterised for the functional properties
- Limited efforts on characterising the damping properties of friction stir processed metals/ alloys, and those works only on aluminium alloys
- Only a few expensive reinforcements, such as NiTi was explored to improve the damping properties.
- Systematic studies exploring the feasibility of FSP to alter damping properties is required.
- The usage of economic reinforcements to improve the damping (such as Fe, Ni, cast iron) can be explored.

Based on the above literature, it is clear that the authors have not studied the microstructural and damping capacity of the metals and Al surface composites produced by FSP. Thus the present thesis is concerned with the microstructure and damping capacity of pure metallic materials (Aluminum, Copper and Magnesium) and A6061T6 alloy surface composites produced through FSP.

Chapter 3

Experimental methods

This chapter describes the methods employed to fabricate the samples using friction stir processing further extraction samples for various characterisations, i.e. microstructural observations using optical and electron microscopes, hardness measurements and evaluation of damping capacity.

3.1 Work plan

Fig. 3.1.1 illustrates the overall work plan in the form flowchart. The chart provides information about raw materials used in the study, friction stir processing conditions, and the characterisation methods employed in the study.

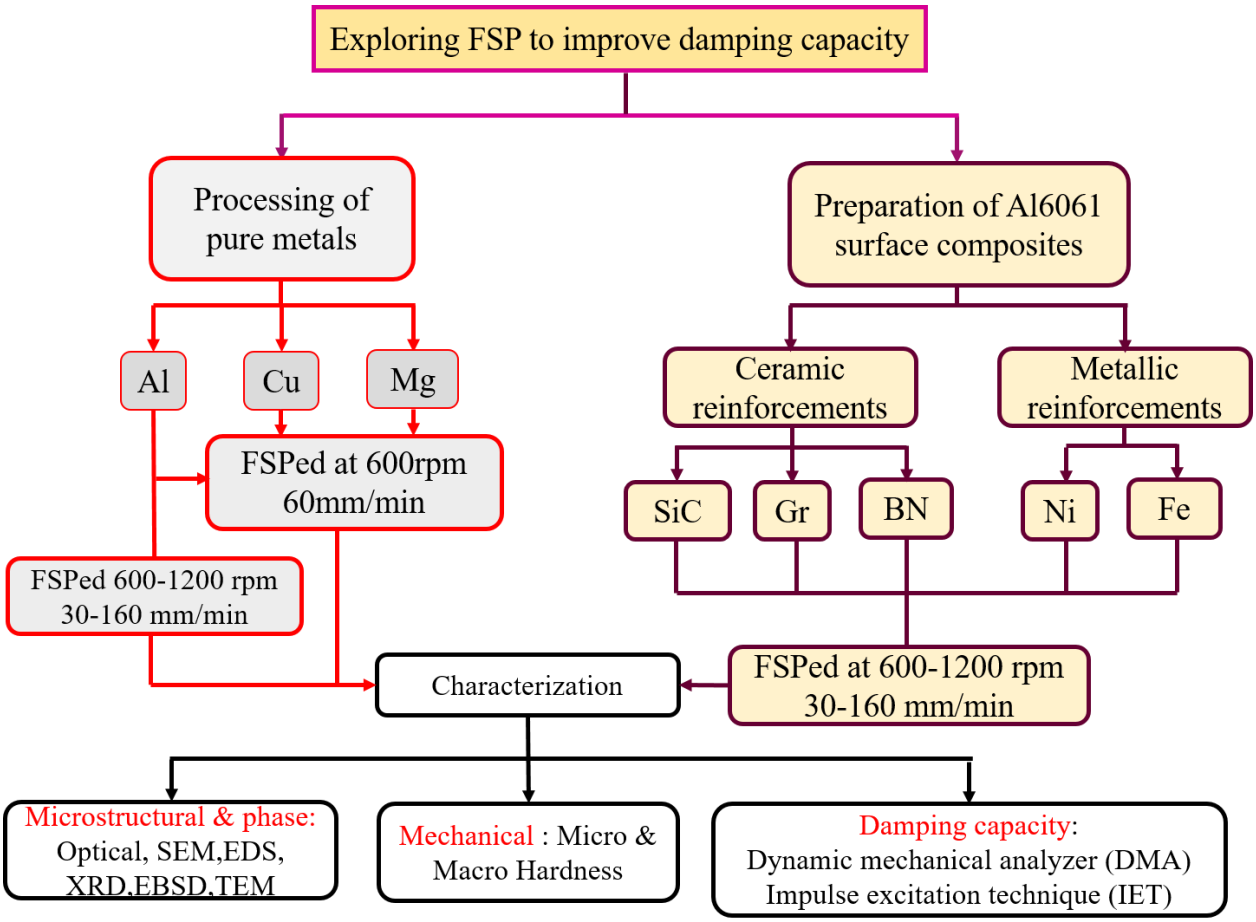

Fig. 3.1.1 Flow chart illustrating the overall work plan of the research work

3.2 Selection of base materials and tool material

The commercial pure aluminium, magnesium, copper and AA6061 alloys are the primary raw materials used in the study. To prepare surface composites, metallic (Fe and Ni) and ceramic particles (SiC, BN and graphite) were used as reinforcements. The raw materials' purity form and the supplier information are provided in Table 3.1.1. The damping capacity of reinforcements was adopted from the literature [66]. The chemical composition of AA6061 as provided by the supplier is given in Table 3.1.2.

Table 3.1.1 Basic information of raw materials used in the study

S. No.	Material	Purity (%)	Form (thickness)	Damping capacity (10^{-3})	Supplied by
1	Commercial pure aluminium	99	Plate (5 mm)	--	M/s. Andhra Steels, Hyderabad
2	Commercial pure copper	99.9	Plate (5 mm)	--	
3	Commercial pure magnesium	99	Cast ingot	--	Sri Venkateswara Tools, Hyderabad
4	AA6061-T6	--	Plate (6 mm)	--	M/s. Chowdhary Metals, Hyderabad
5	SiC	99	Powder	1.1 – 2.5	Alfa Aesar
6	Graphite	99	Powder	8 – 10.5	Alfa Aesar
7	BN	99	Powder	28 - 40	DRDO-DMRL
8	Nickel	99	Powder	31.8	DRDO-DMRL
9	Iron	99	Powder	23.9	DRDO-DMRL

Table. 3.1.2 Chemical composition of the AA6061 as provided by the supplier

Element	C	Mn	P	S	Si	Cr	V	Mo
Amount (wt. %)	0.42	0.28	0.015	0.003	1.00	5.20	1.05	1.45

Table 3.1.3 Chemical composition of AISI H13 tool steel as provided by the supplier

Element	Si	Fe	Cu	Mg	Zn	Ti	Cr	Mn	Al
% wt.	0.723	0.231	0.213	0.983	0.126	0.021	0.163	0.033	Remaining

The FSP tool, made up of hardened H13 steel, has a hardness of 55HRC, was used to process the workpiece material. Composition of tool provided in Table 3.1.3. A tool with a shoulder diameter of 15mm and a conical pin of 4mm in length was used for processing. The FSP was carried out on a machine designed and developed by the Indian Institute of Science, Bangalore and manufactured by M/s. ETA Technologies, Bangalore. The machine has a unique capability of choosing the plunge depth, rotational speed and traverse speed during processing.

The reasons for choosing a specific raw material are given below.

- Commercial pure metals, i.e. Al, Cu and Mg, have been selected as our purpose was to understand the response of these materials to friction stir processing from a damping perspective.
- AA6061 was chosen as a matrix for preparing the composite layers as this alloy was used in aircraft industries.
- The listed reinforcements (Table 3.1.1) were chosen either for their excellent inherent damping capacity (e.g. BN, graphite) or their extensive usage as a reinforcement (e.g. SiC) in several studies.

3.3 Preparation of surface layers by FSP

Fabrication of surface composites by single groove technique is a very flexible and easy process. Fig. 3.1.2 (a) shows the plate before FSP. In the case of preparing surface composites, a groove was machined on the plate (Fig. 3.1.2b); the groove dimension was decided based on the amount of reinforcement has to be incorporated. Then groove was filled with reinforcements (Fig. 3.1.2c). Subsequently, friction stir processed (Fig. 3.1.2d).

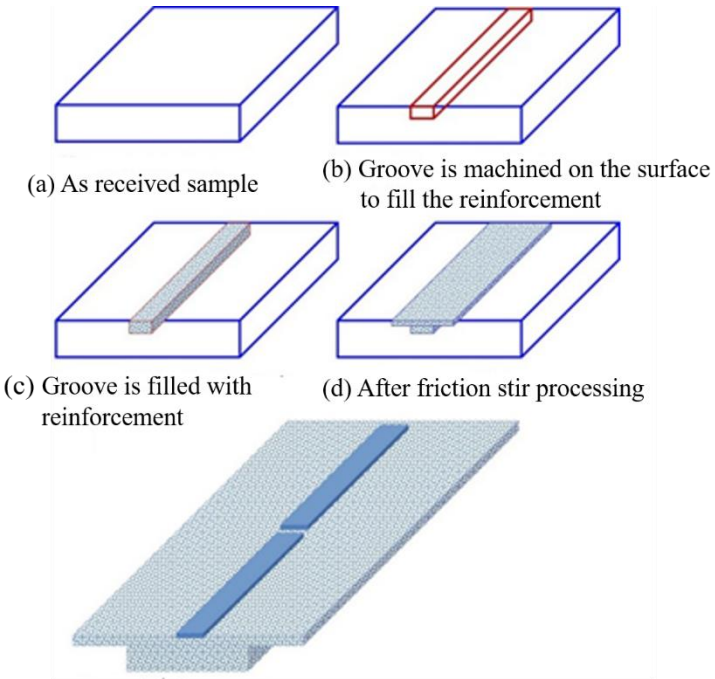

Fig. 3.1.2 Diagram shows the step-by-step preparation of surface composites. Note that samples for damping properties were prepared completely from the processed regime.

Fig. 3.1.2 (e) shows how samples are extracted from the processed regime for damping measurements. The formula used to calculate groove dimension was [67]

$$V_{fr} = \frac{A_g}{A_p} \times 100 \qquad (8)$$

$$A_g = W_g D_g$$

$$A_p = D_p L_p$$

Where, $V_{fr,}$: volume fraction of the reinforcement, $A_{g,}$: area of the groove, A_p:projected area of a pin, $W_{g,}$: groove width, $D_{g,}$: groove depth $D_{p,}$: pin diameter *and* L_p: pin length.

3.4 Characterization

3.4.1 Microstructural studies

3.4.1.1 Sample preparation

Specimens were obtained from the centre of the processed regime and perpendicular to the friction stir processed direction. To study microstructural characterisation, samples were ground with emery papers with different grades as shown in Table 3.1.4; later, samples were polished using a disc polishing machine. Alumina powder was used to obtain surfaces with a mirror finish during fine polishing. After polishing, samples were cleaned using water and dried for 5 minutes. Poulton's reagent containing 6 ml HNO_3, 12 ml HCl, 1 ml HF and 1ml water was used to etch specimens.

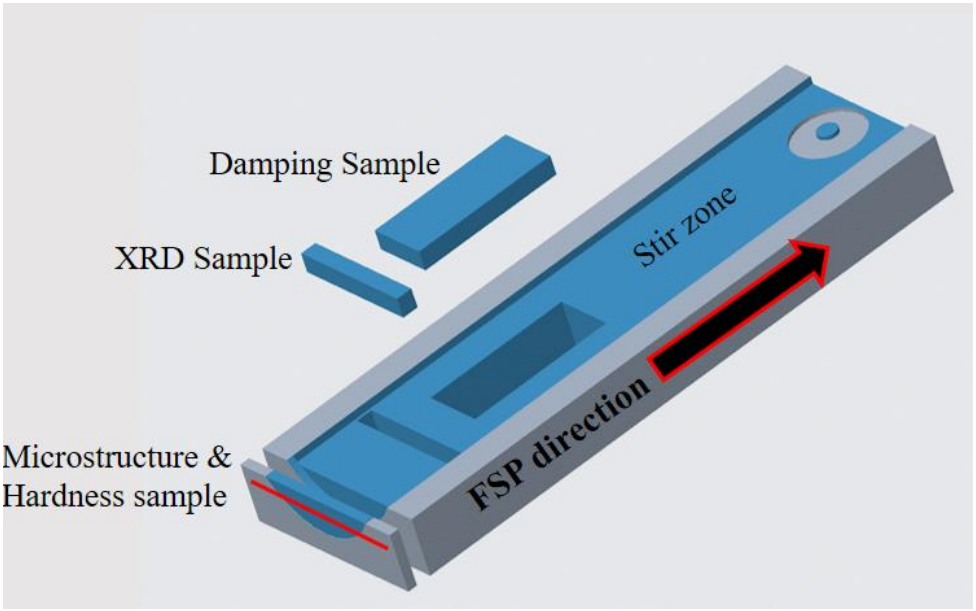

Fig. 3.1.3 Illustration shows method adopted to extract samples for characterisation.

Table 3.1.4 Polishing procedure for microscopy

S. No.	Abrasive (Grit SiC paper)	Time (sec)
1	200	120
2	400	120
3	600	120
4	800	120
5	1000	120
6	1500	180
7	2000	180

Microstructural characterisation was conducted on base metal and in the stir zone of FSPed samples to observe the microstructural features (presence secondary phases, grain size, and distribution of reinforcement particles). The way samples were extracted from the stir zone for various characterisations (metallographic, XRD, hardness and damping capacity) is displayed in Fig. 3.1.3. The polished samples were examined using the optical microscopy technique to find the interface between the base metal and stir zone (SZ). JEOL JSM-T330A scanning electron microscope (SEM) equipped with energy dispersive spectroscopy (Oxford EDS detector) was used for the microstructure/ composition analysis of the monolithic and composite samples. SEM was used to investigate: (i) the distribution of particulates, (ii) the interfacial bonding, and (iii) the grain size. Electron backscattered diffraction (EBSD) was used to determine the microstructure, particularly in FSPed aluminium.

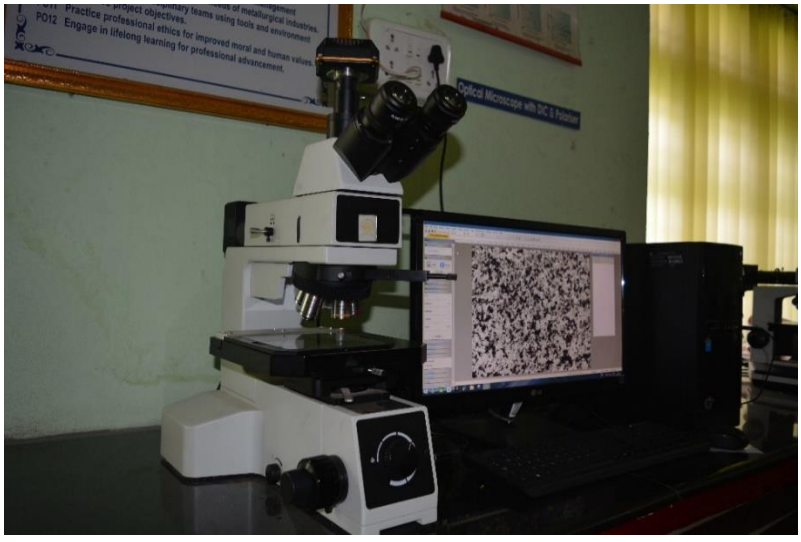

Fig. 3.1.4 Quasmo QX4RT model optical microscope used to investigate the microstructure

3.4.1.2 X-ray diffraction studies

X-ray diffraction is used to find the phases present in the materials and to determine dislocation density. Enough care has been taken while extracting the samples from the friction stir processed regime so that the extracted sample contains only the processed regime and not the base material.

The dislocation density of base metal and the composites was estimated using the following expression [68], [69].

$$\rho = 2\sqrt{3}\,\epsilon/Db \qquad (9)$$

Where, ρ: dislocation density, ϵ: average lattice strain, b: Burgers vector (0.286 nm [68]) and

D: Crystallite size. The crystallite size of Al samples was obtained by using the Williamson-Hall equation (Eq. 2).

$$B\,\mathrm{Cos}\,\theta = \lambda K/D + 4\epsilon\,\mathrm{Sin}\,\theta \qquad (10)$$

Where B: diffraction peak width, λ: radiation wavelength (0.154056 nm), K = 0.89 and θ: half of the diffraction angle.

Fig. 3.1.5 TESCAN VEGA 3LMU **s**canning electron microscope used to observe the microstructure

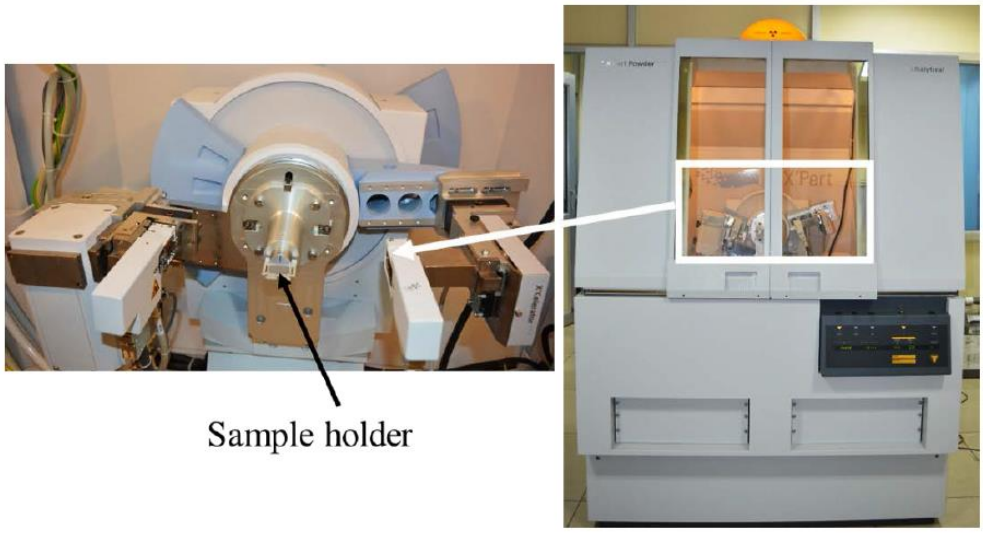

Fig. 3.1.6 PANalytical X'Pert Powder XRD used in the study

3.5 Hardness measurements

The samples were prepared by grinding and polishing the surface of the processed region. The Vicker's microhardness measurements were made at the mid-plane of the processed cross-section at each 0.5 mm using a Shimadzu HMV G21 Vicker's hardness testing machine with 100 kgf load and 15 s dwell time. The photograph of the microhardness tester is shown in Fig. 3.1.7.

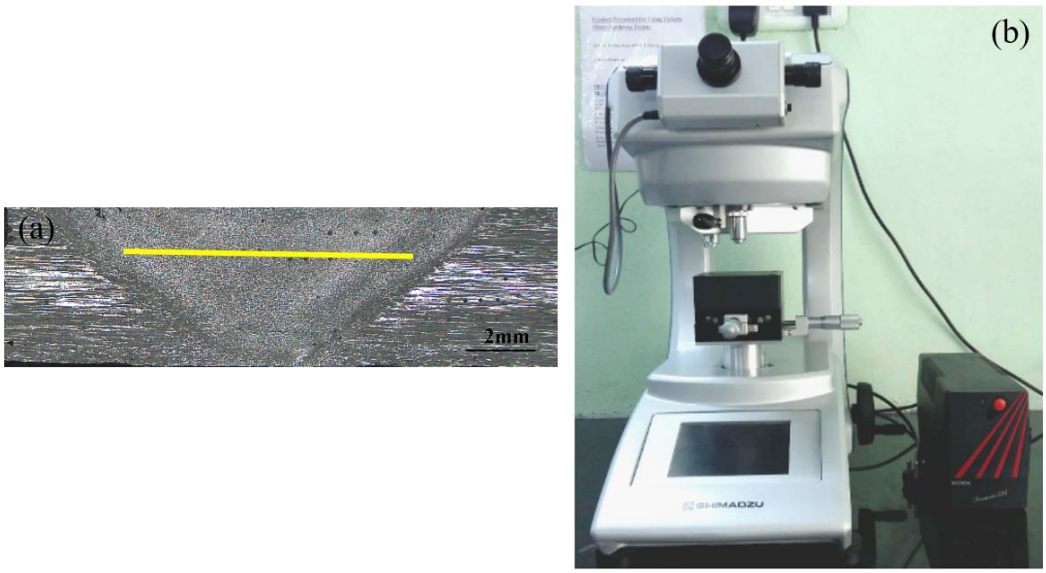

Fig. 3.1.7 a) Schematic diagram shows the measurement of hardness across the processed zone or stir zone and (b) Shimadzu HMV G21 Vicker's microhardness tester

3.6 Dynamic mechanical analyzer (DMA)

The dynamic mechanical analyser (DMA) works by deforming a known-geometry sample using a sinusoidal deformation. A controlled stress or a controlled strain can be applied to the sample. The sample will then deform a particular amount in response to a known stress. The sinusoidal wave is generated by a force motor and sent to the sample through a drive shaft. Modulus and damping capacity are measured using DMA (tan delta). The storage modulus has an in-phase component and the loss modulus has an out-of-phase component. The elastic behaviour of a sample is measured by the storage modulus, which is either E' or G'. The tan delta is the ratio of the loss to the storage modulus, and it's also known as damping. It is a measurement of a material's energy dissipation.

The damping measurements were carried out using Dynamic Mechanical Analyser (TA instruments RSA-G2) at frequency 1 Hz and temperature ranging from 25°C to 300℃ using three-point bending mode; heating rate used: 5 °C/min. Samples of dimension 50 × 7 × 1.6 mm^3 were used for damping measurements. Room temperature frequency-dependent measurements were obtained in the range of 1 to 20 Hz. The applied strain amplitude was (ε) 260 × 10^{-6} (kept constant).

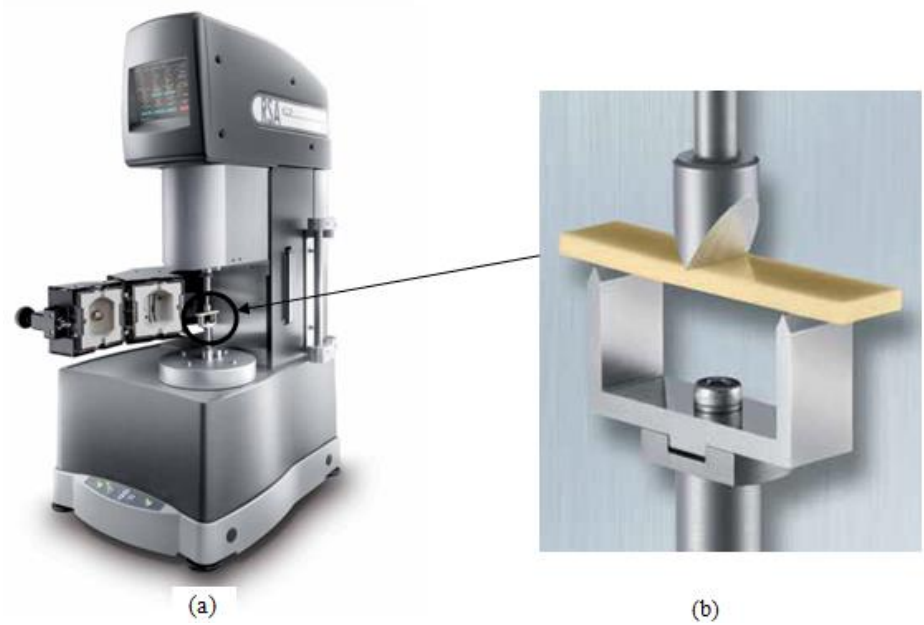

Fig. 3.1.8 Experimental set-up for measuring damping (a) dynamic mechanical analyzer (b) illustrates 3-point bending mode configuration.

3.7 Impulse excitation technique (IET)

Impulse excitation technique (IET) is a non-destructive technique for determining damping capacity and elastic constants. The basic approach is to tap the sample with a projectile and then

record the resulting vibration signal using equipment like a microphone. After that, a rapid fourier transformation is used to translate the acquired vibration signal from the time domain to the frequency domain. Dedicated software will calculate the elastic characteristics and damping capacity by determining the resonance frequency with high accuracy.

The impulse of a light mechanical impact excites the suspended sample into the resonance frequency. A microphone collects the sample's vibration as a function of time. This signal (amplitude of vibration vs time) is processed by a software-based analysis program to calculate the resonance frequency, elastic modulus, and damping.

The elastic modulus can be calculated as following formula [70] for rectangular samples.

$$E = 0.9465 \frac{m f_f^2}{b} \left(\frac{L^3}{t^3}\right) T_1 \qquad (11)$$

Where E is the elastic modulus (Pa), f_f is the resonance frequency (Hz), m is the mass of the sample (g), T_1 is the correction factor and L, b, and t are the length, width and thickness of the sample (mm).

The damping factor or internal friction (Q^{-1}) can be calculated from

$$Q^{-1} = \frac{K}{\pi f_f} \qquad (12)$$

Where K is the exponential decay parameter.

Fig. 3.1.9 RFDA basic impulse excitation technique set up as supplied by M/s. IMCE, Belgium.

Chapter 4

Results and discussions

4.1 Damping capacity of pure metallic materials

4.1.1 Objective

The objective is to study the microstructure, mechanical and damping properties of friction stir processed commercial-grade aluminium, copper and magnesium.

4.1.2 Experimental methods

Aluminium and copper have been obtained in plates from the supplier. These plates were received in rolled condition. Whereas plates were cut from cast ingot of magnesium for friction stir processing. The following are dimensions of plates on which friction stir processing was performed as per the conditions listed in Table 4.1.1.

Pure Aluminium (Al) plate dimensions (rolled condition): 200×100×5 mm^3

Pure Copper (Cu) plate dimensions (rolled condition): 200×100×5 mm^3

Pure Magnesium (Mg) plate dimensions (cut from the cast ingot): 200×100×12 mm^3

Table 4.1.1 Friction stir processing conditions employed for processing pure metals

Rotational speed (rpm)	Traverse speed (mm/min.)	Axial load (KN)	Tilt angle (^{o})
600	60	10	2.5^o

4.1.3 Microstructural characterisation

Fig 4.1.1 shows the optical micrographs of the base metals and the FSPed metals. The stir zone can be clearly distinguished from the base metals in each sample. The FSP zone of this sample consists of equiaxed grains; the grain size was smaller in the FSP zone than in the base metal. The microstructure in the stir zone (SZ) was discernibly different from that of the base material. The grains in the SZ were particularly small compared to the grains of the pure metals. The average grain size of FSP-ed pure metals is shown in table 4.1.2. The final grain size after FSP depends on the processing parameters and the tool geometry rather than the initial grain size. FSP is a thermo-mechanical process during which the material deforms at elevated temperature with the strain rate in the range of 10-100 s^{-1} [43]. Therefore, the occurrence of dynamic recrystallisation is expected during the process. The microstructure obtained through transmission electron microscopy (TEM) for the Mg samples subjected to FSP revealed the formation of dislocation tangles as shown in Fig. 4.1.1g and Fig. 4.1.1h.

Table 4.1.2 Grain size of pure metals

S.No	Material	Grain Size (μm)		Dislocation density (ρ) $\times 10^{12}/m^2$	
		Before FSP	After FSP	Before FSP	After FSP
1	Pure Aluminium (Al)	50.1 ± 15	6.5 ± 1.2	4.24	2.57
2	Pure Copper (Cu)	20.4 ± 2.3	4.1 ± 0.6	1.49	0.84
3	Pure Magnesium (Mg)	780 ± 30	25.6 ± 0.9	1.67	2.99

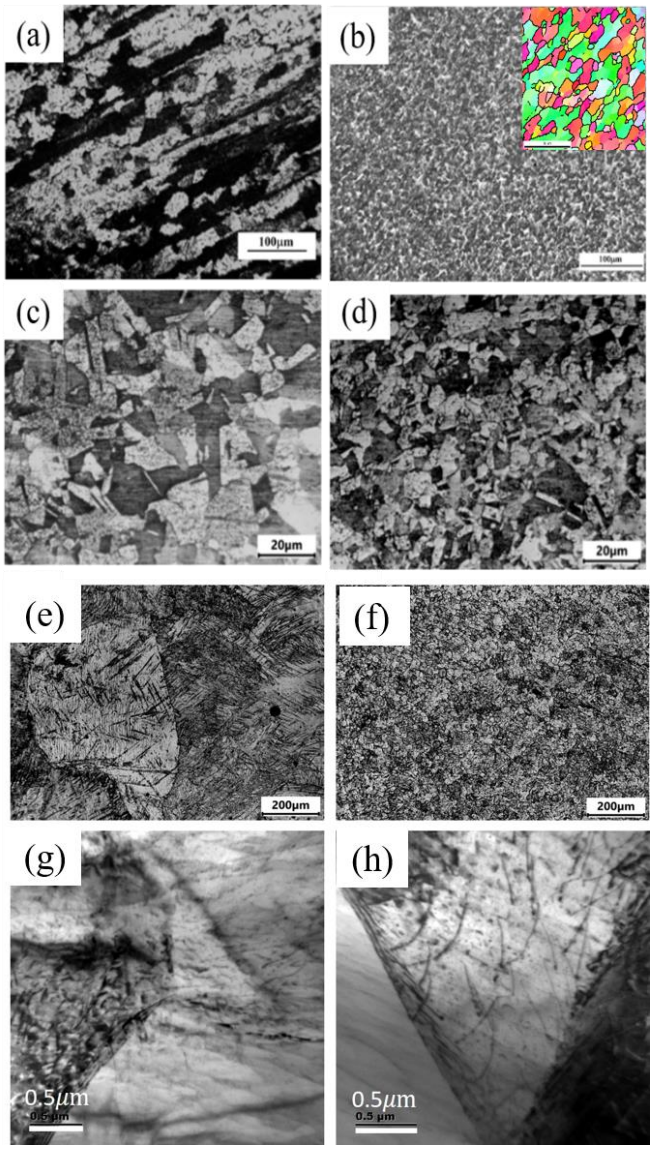

Fig. 4.1.1 Optical micrographs of pure Al, Cu, Mg (a), (c), (e) and (b),(d),(f) are stir zone of pure metals, respectively. (g) and (h) is the TEM images of pure Mg and FSPed Mg. The inset figure in (b) is an EBSD image of stir-zone to show clear grain boundaries.

4.1.4 X-Ray diffraction analysis

Fig. 4.1.2 shows the XRD results of the as-received and FSPed samples (obtained from the cross-section of the processed regime, Fig. 3.1.3). The peaks were shifted to higher 2θ values. This can be attributed to the associated process features, i.e., ~~texturing and~~ straining. Furthermore, the FSPed samples peaks are broadened. Peak broadening indicates the introduction of higher dislocation density [71] and smaller grain size of the processed regime or at the stir zone, and the same was calculated (Table 4.1.2)

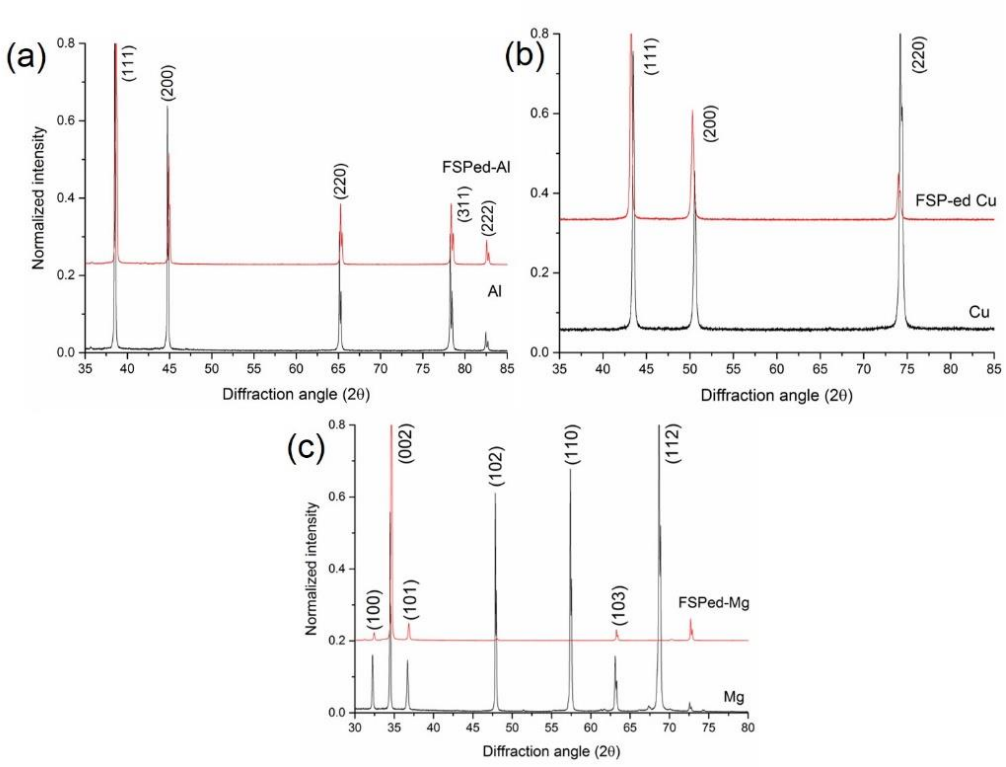

Fig. 4.1.2 XRD peaks of pure metals before and after FSP.

4.1.5 Hardness

Hardness was measured across the cross-section of the sample at a load of 200 g and 15 s. dwell time. The hardness of the FSPed Al in the stir zone is reduced by 27% than the Pure Al (Fig.4.1.3 (a)). The FSP/W produces two competitive factors that affect the hardness of the stir zone. The first factor, the FSP/W, resulted in remarkable annealing softening, thereby reducing the hardness of the stir zone; the second factor, the significant grain refinement resulting from the FSP/W, increased the hardness of the nugget zone. A softening effect was dominant in the stir zone, reduction in hardness was observed at the stir zone of aluminium. Similar results were reported for aluminium by Wen-ying GAN et al. [47].

In the case of pure Cu, the hardness in the stir zone was increased by 14%. Because the fine grain strengthening exceeded the softening effect at the lower rotation speed of 600 rpm [72].

The average hardness of cast Mg was 31.8Hv. At the same time, the hardness of the stir zone was about 36.7Hv. There was an approximately 15.4% increase in hardness after friction stirring. This increase in hardness can be attributed to microstructure refinement and dislocations (Table 4.1.2).

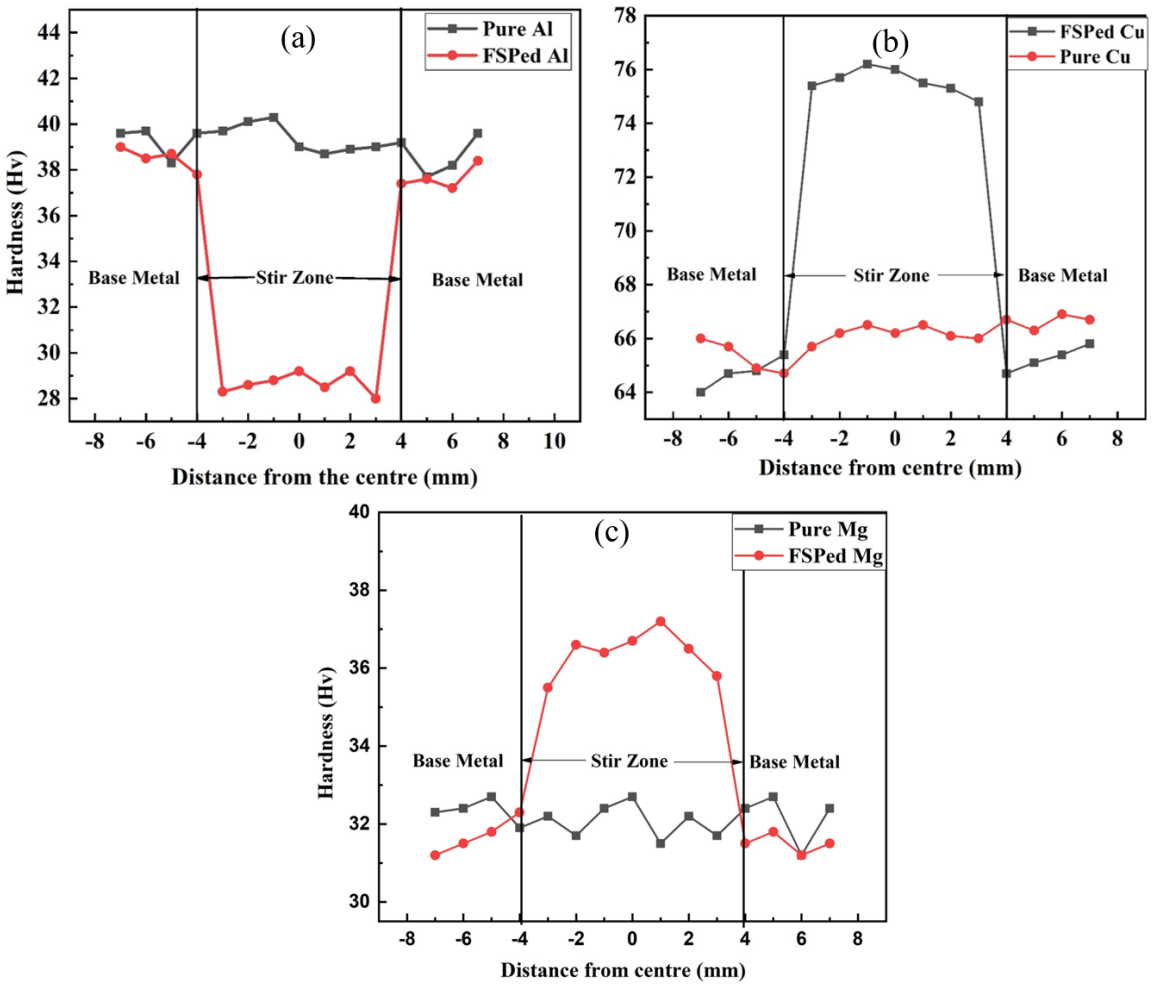

Fig. 4.1.3 Hardness of the pure metals before and after FSP (Note: Y-axis scale is not same for the plots)

4.1.6 Damping capacity measurements by DMA

Fig. 4.1.4 shows the variation of damping capacities with temperature for the base and FSPed samples. The damping of base samples continuously increased with the temperature. The same trend was seen after FSP. The damping capacity for the as-received samples gradually increased with the temperature till 130 °C, and then steeply increased beyond 130 °C; a similar trend was observed for FSPed Al and Cu, respectively. The damping at higher temperatures was remarkably higher for FSPed Al and Cu, respectively. However, at temperatures below 80°C, the damping of FSPed Mg was lower than that of cast-Mg. At temperatures above 80°C, FSPed Mg exhibited better damping than the cast-Mg. The damping capacities of all samples were improved with increasing temperature due to the viscous flow at grain boundaries (GB)s converting mechanical energy into thermal energy due to internal friction at GBs [64]. At lower temperatures, the damping capacity of FSPed samples showed less than the pure metals. This may be due to decrease in dislocations during re-crystallization (Table 4.1.2). The damping capacity of the FSPed samples, at high temperatures e.g. 200°C, is three times higher than the base metals. An equiaxed, fine grain structure characterised the microstructure of the FSPed samples.

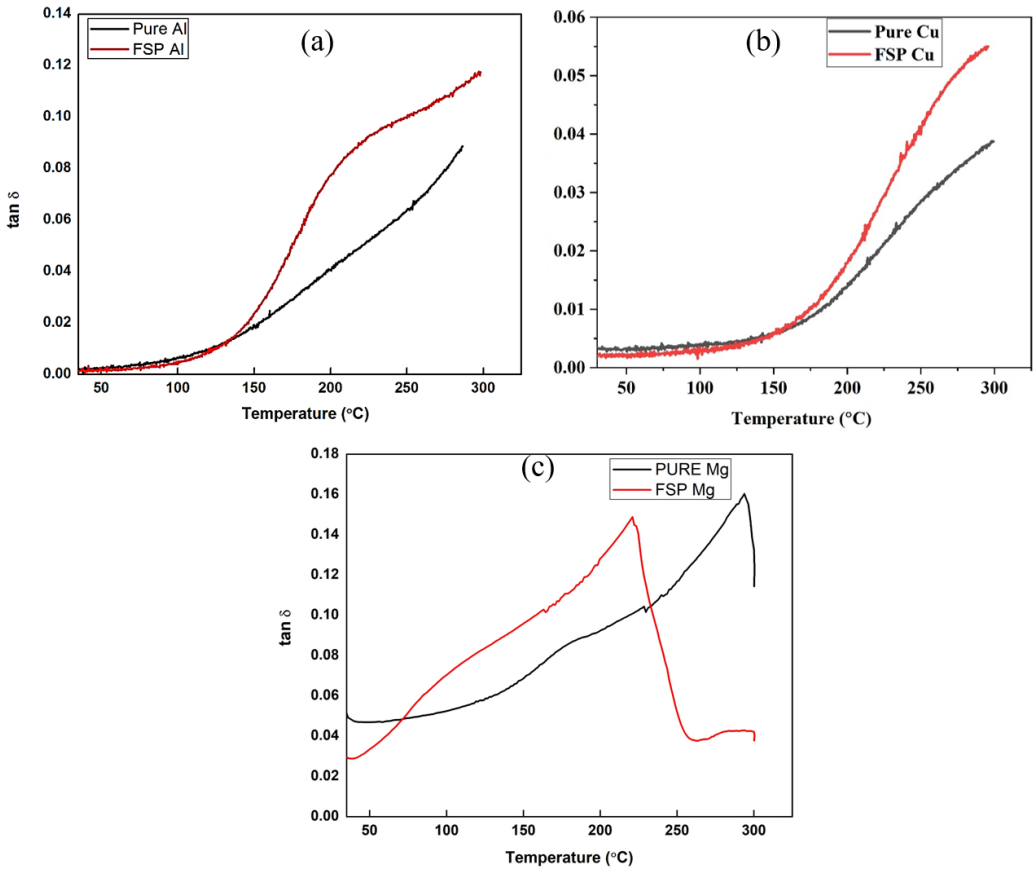

Fig. 4.1.4 Temperature-dependent damping capacities of base samples and FSPed samples.

This special microstructure always contributes to excellent GB sliding capacity above 200 °C [63]. Thus, the FSPed samples exhibited much higher temperature damping capability than the base samples.

4.1.7 Damping capacity and elastic modulus using impulse excitation technique

Fig. 4.1.5 shows the decay of sound vibration as a function of time. The time required to decay the sound vibration represents the damping ability of the material. If the vibration amplitude decays quickly, it has better damping properties. It is evident from Fig. 4.1.5 that the time for decaying the vibration reduced in the case of friction stir processed aluminium and copper. At the same time, it takes more time to decay the vibration in the case of processed magnesium. It was implied from Fig. 4.1.6 that the damping factor increased for aluminium and copper after processing. Indeed, for copper, the damping factor doubled after FSP, whereas the improvement in the damping factor for aluminium was marginal. However, the damping factor for magnesium considerably decreased after FSP. The elastic modulus of copper and aluminium, in general, decreased after processing. However, magnesium is unchanged. The observed changes in damping factor and elastic modulus might have been due to the microstructural changes during FSP.

It was observed that dislocation density decreased after processing in copper and aluminium, whereas in magnesium, it increased after processing (Table 4.1.2). The aluminium and copper plates used in this study was received in rolled condition. Then it is expected to have high dislocation density in the as-rolled condition. But after FSP, the dislocation density was low because the microstructures were fully recovered and recrystallised by thermo-mechanical cycles endured by the metal during FSP [63]. Whereas magnesium was received in the as-cast condition. ~~As-cast ingots are expected to have only an equilibrium number of dislocations~~ The number of dislocations increases after processing in the case of magnesium.

The defects, i.e. dislocations, grain boundaries, present in the material helps to improve the inherent damping factor [8]. The vibrational energy dissipates at defects. The decrease in grain size (Table 4.1.2) implies an increase in grain boundary area [73]. This was believed to be responsible for improving damping properties in aluminium and copper.

The significant change in the damping capacities of as-cast Mg and friction stirred Mg can be explained considering the roles of dislocations and grain boundaries, as there was about 79% increase in dislocation density and significant grain refinement after FSP.

The significant increase in dislocation density led to the formation of tangled dislocations, as substantiated by X-ray and TEM analysis (4.1.1 g & 4.1.1 h). The increased dislocation density resulted in the higher resistance for their movement, and thereby a decrease in damping at low

temperatures was witnessed. A decrease in damping was reported for ECAE processed pure magnesium supports the present observation [21].

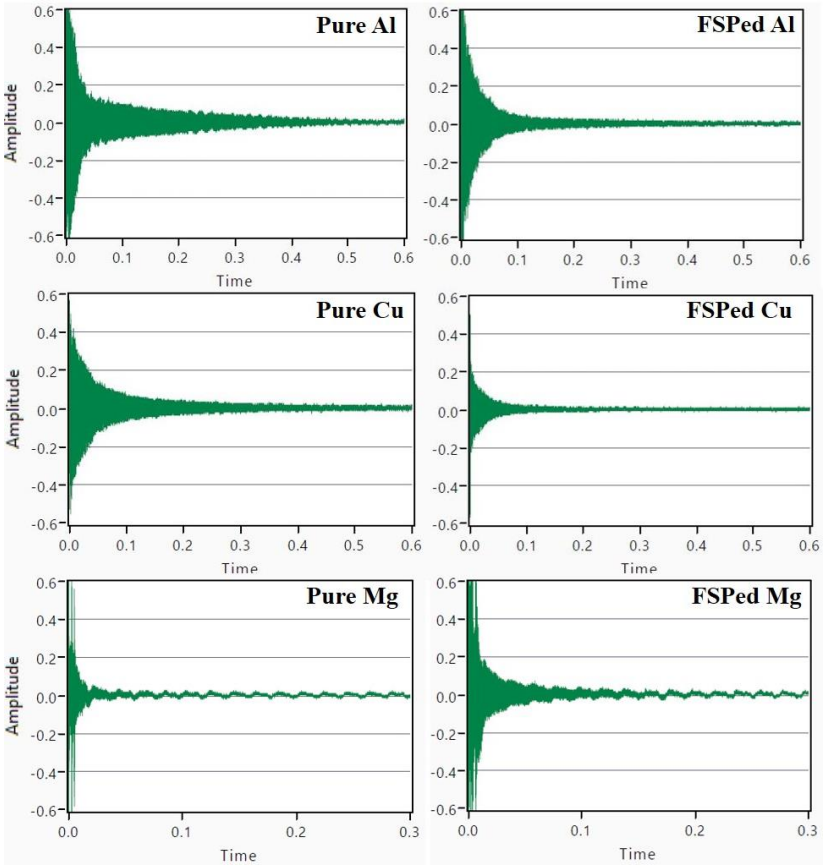

Fig. 4.1.5 Decay of sound vibration as a function of time (sec) for materials before and after FSP.

The creation of defects, particularly an increase in grain boundary area, led to a decrease in density. Otherwise, free volume increases as grain boundary fraction increases. As a result elastic modulus also decreases. It is evident from Fig. 4.1.1 that the microstructure of aluminium and copper is significantly refined after FSP, i.e. increase in the grain boundary area. Pal-Val et al. [74] also observed that materials exhibit reduced elastic modulus after being subjected to severe plastic deformation, supporting the present findings.

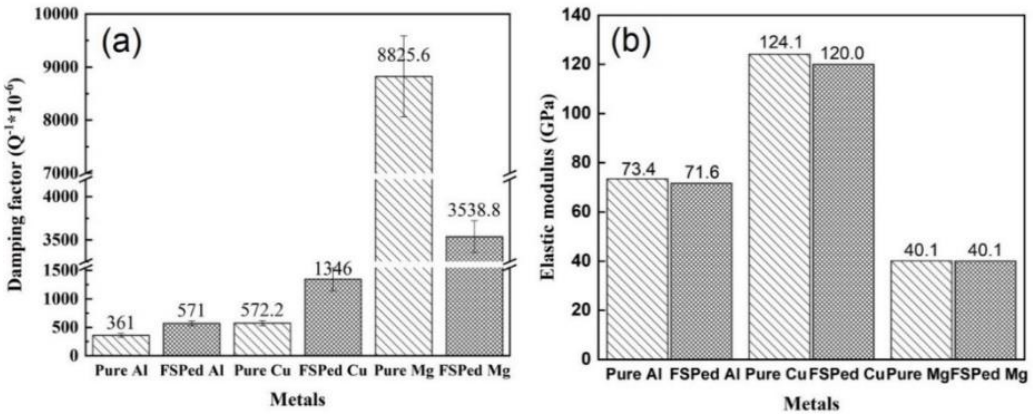

Fig. 4.1.6 (a) Damping factors and (b) elastic modulus of pure metals before and after FSP.

4.1.8 Summary

1. The grain size was refined to 6.5, 4.1 and 26 μm for pure Al, Cu and Mg, respectively, through friction stir processing.
2. The hardness of FSPed Al decreased by 27% due to softening in the stir zone,
3. The hardness increased by 14% and 15% in Cu and Mg, respectively, due to structure refinement dominating the softening.
4. The damping capacity of FSPed metals decreased at lower temperatures due to a reduction in dislocation density.
5. At high temperatures (>130°C), the damping capacity of FSP-ed Al, Cu and for Mg (>80°C) was better than the base metal; this was due to increased grain boundary area.
6. The damping factor measured by IET of aluminium (+58%) and copper (+135%) was increased, and magnesium decreased (−60%) after friction stir processing due to an increase in the grain boundary area.
7. The elastic modulus of aluminium and copper was marginally decreased and unchanged for magnesium after processing.

4.2. Effect of process parameters on damping capacity of pure Al

4.2.1 Objective

To study the role of friction stir process variables on the damping capacity of commercial-grade aluminium.

4.2.2 Experimental methods

Commercial pure aluminium plates (200×100×5 mm^3) were used for the study. Table 4.2.1 provides the details of experiments carried out in this work.

Table. 4.2.1 FSP process parameters

Variable	Fixed parameters
Tool rotational speeds (RS): 600, 900 and 1200 rpm	TS: 40 mm/min; Pass: 1
Tool traverse speed:40, 80 and 120 mm/min	RS: 900rpm; Pass: 1
Number of passes: 1,2 and 3	RS:900rpm; TS:80mm/min

4.2.3 Microstructure

4.2.3.1 Effect of rotational speed

The as-received aluminium was observed to have elongated grains of an average size of 45 μm (Fig. 4.2.1a). As a result of FSP, severe microstructure refinement was observed at the stir-zones (Fig. 4.2.1b-j); the grains were equiaxed. The average grain size of the specimen processed with 600 rpm was 8.52 μm. The grain size was observed to increase with the rotational speed (Table 4.2.2). Due to the rotation of the tool against the aluminium work piece, the samples experienced concurrent application of mechanical load and heat that enabled the onset of dynamic recrystallisation resulting in structure refinement [47]. The increase in the rotational speed increased the number of interactions between the tool and the work piece, thus increasing the frictional heat imparted in the processing region [68]. The following equation has been proposed in the literature [75] for the relation between heat-input and rotational tool speed (ω, rpm) and traverse speed (ν, mm/min).

$$\text{Heat input} = \frac{\omega^2}{\nu \times 10^4} \qquad (13)$$

Where ω= tool rotational speed

ν = tool traverse speed

For a constant traverse speed, an increase of rotational speed increased the heat-input as per the above relation. Consequently, high heat input promotes grain growth, which could be the reason for the increase of grain size with the rotational speed.

4.2.3.2 Effect of traverse speed

Fig. 4.2.1 (e-g) shows the microstructures of the stir zone (SZ) of the specimens produced at traverse speeds of 40, 80, 120 mm/min and the rotational speed of 900 rpm. The average grain size sample specimen processed at 900 rpm and 40 mm/min. was 8.64 μm. The grain size was observed to decrease with the traverse speed (Table 4.2.2). The increase in the traverse speed decreases the time of interaction between the tool and the work piece, thus decreasing the frictional heat imparted in the processing region. For a constant rotational speed, an increase of traverse speed decreases the heat-input as per the above relation. Consequently, low heat input promotes grain refinement, which could reduce grain size with the traverse speed [58].

4.2.3. Effect of number of passes

Fig. 4.2.1 (h-j) shows the microstructure of pure Al processed with no of passes (1, 2, 3 pass) at 900rpm and 80mm/min. The average grain size after a single pass was 6.55 μm. The grain size was observed to decrease with the no. of passes (Table 4.2.2). Increasing the number of passes imparts more amount of strain into the region being processed. This strain assists nucleation of grains at several locations thereby promotes grain refinement.

Table. 4.2.2 Average grain size of stir zone (as measured from Fig. 4.2.1)

S. No.	Rotational speed (rpm)	Traverse speed (mm/min.)	No. of passes	Grain size (μm)	Dislocation density (ρ) $\times 10^{11}/m^2$	Heat input index
Base metal	--	--	--	45±2.1	4.03	--
1	600	40	--	8.52±1.7	3.63	9
2	900	40	--	8.64±1.3	3.01	20
3	1200	40	--	21.30±1.9	2.57	36
4	900	80	1	6.55±0.9	4.25	10.1
5	900	120		5.12±0.7	1.44	6.7
6	900	80	2	5.08±0.6	1.45	--
7	900	80	3	3.95±0.9	2.08	--

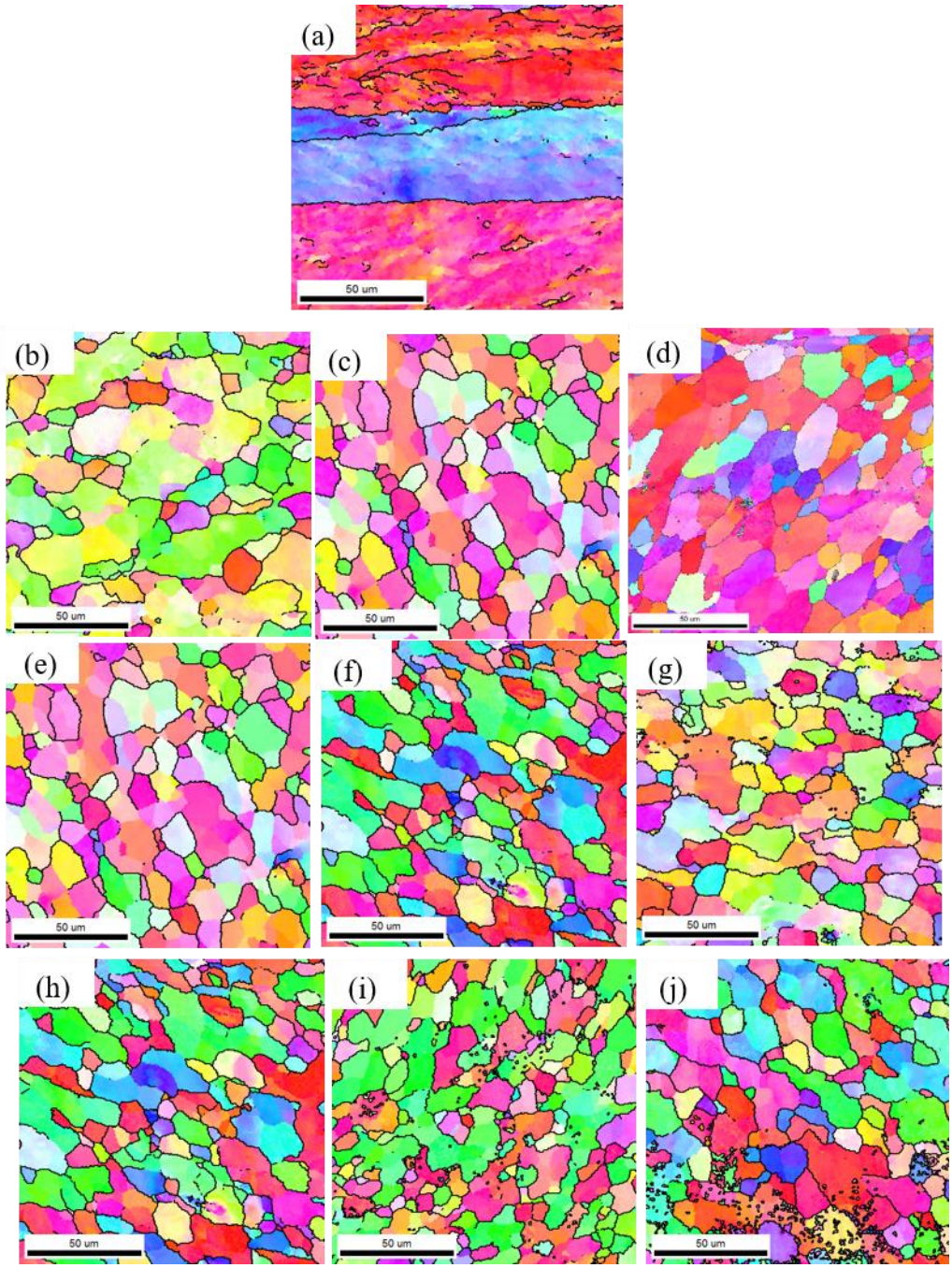

Fig. 4.2.1 EBSD images (a) pure Al (b-d) effect of rotational speed at 600, 900, 1200 & 40 traverse speed (e-g) effect of traverse speed at 40, 80, 120 & 900 rpm and (h-j) effect of no. of passes at 900 rpm and 80 mm/min.

4.2.3 XRD Analysis

Figure 4.2.2 shows the XRD results of the as-received and FSPed samples on the cross-sections. All the FSPed Al samples peaks were shifted to higher 2θ values than the base metal. These can be attributed to the associated process features (i.e. strain). Furthermore, the FSPed Al peaks are broadened. Peak broadening indicates the introduction of higher dislocation density [71]

and smaller crystalline size. The dislocation density in the stir zones was calculated following the procedure provided in Section 3, further listed in Table 4.2.2

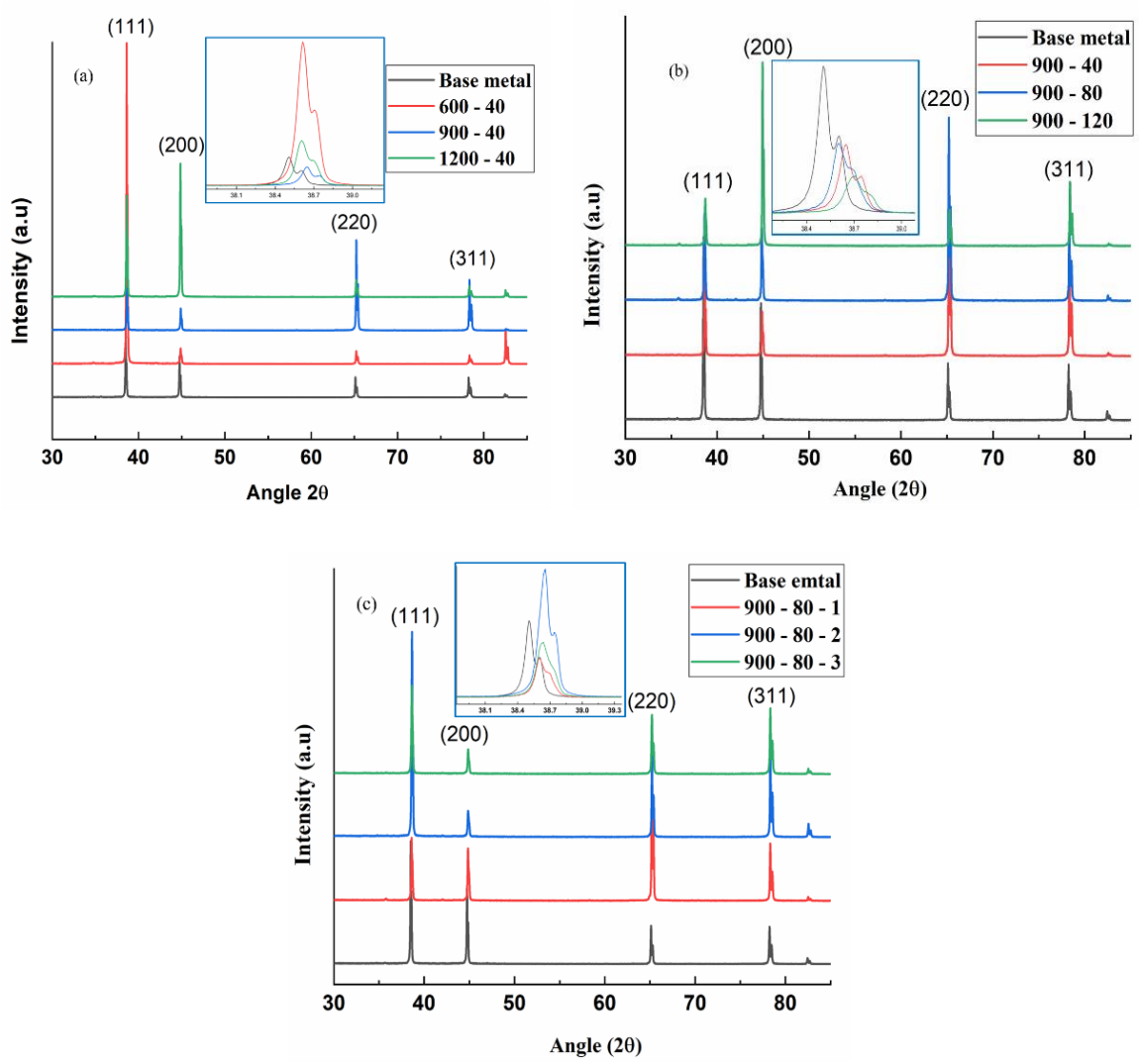

Fig. 4.2.2 Shows XRD peaks of pure Al and FSPed Al processed at (a) 900 rpm and 40, 80, 120 mm/min. (b) 40 mm/min. and 600, 900, 1200 rpm and (c) 900 rpm and 80 mm/min.1,2, 3 passes.

It can be readily noted the Table 4.2.2 that dislocation density decreased as rotational speed increased from 600 to 1200 rpm. As described above, increasing the rotational speed increases the heat input to the processed region. The heat enables the annihilation of dislocations, which could be why dislocation density decreases as rotational speed increases.

On the other hand, increasing traverse speed decreases the heat input to the processed region (Table. 4.2.2). Hence, one may expect dislocation density to increase with the traverse speed. However, the observed trend was different from the expectation. Similarly, the increase in the

number of passes would result in more dislocations. Once again, the observed trend was opposite to this expectation. The reasons for the observed contrary in the trends are unknown and need to be explored.

4.4.5 Hardness

4.4.5.1 Effect of rotational speed

The hardness measurements (Fig. 4.2.3) complemented the above observations noted in grain size variation and the dislocation density. The microstructure with a high dislocation density was supposed to exhibit better hardness (38 ± 3.6 Hv). The same was observed (Table. 4.2.2), i.e. the as-received sample showed the highest hardness among all the samples. The hardness continuously decreased with the rotational speed, which could be due to the reduction of dislocation density [47]. Apart from dislocation density, the continuous increase in the grain size due to high heat input (Table.4.2.2) also could be a reason for the observed reduction in hardness (Fig. 4.2.3 a). When rotational speed increased, the residing time of the frictional heat also increased. As per the equation, the high heat input can be expected for a rotational speed of 1200 rpm. Then grain size increased with increasing rotational speed. Hence, the hardness of FSPed Al decreased with increasing rotational speed.

4.4.5.2 Effect of traverse speed

Fig. 4.2.3 (b) shows stir zone micro hardness values of pure Al after processing w.r.t. traverse speeds. After FSP, the hardness values were decreased, and with an increase in traverse speed increase in hardness was observed. The stir zones had hardness values in the range 26.5-32 ± 2.9 HV depending on the processing conditions (Fig. 4.2.3 b). The decrease in hardness after FSP is due to the reduction in the dislocation density. The heat input decreases with increasing traverse speed (Table. 4.2.1). The heat input decides the grain size in the stir zone. The grain size variation in the stir zone is shown in the Table. 4.2.1. When traverse speed increased, the residing time of the frictional heat decreased. The high heat input can be expected for a traverse speed of 40mm/min as per equation (13). The grain size decreases with increasing traverse speed. Hence the hardness of FSPed Al increased with increasing traverse speed.

4.4.5.3 Effect of number of passes

The effect of no. of passes on the micro hardness of pure Al is shown in Fig. 4.2.3 c. After FSP, the hardness of pure Al decreased. An increase in the number of passes increased the hardness. The observed variation in the grain size supports this data. As the number of passes increased, the grain size was reduced. The fine grains strengthen following the well-known Hall-Petch relation [51]. Hence, fine-grained samples, i.e. 3-pass samples, exhibited better hardness.

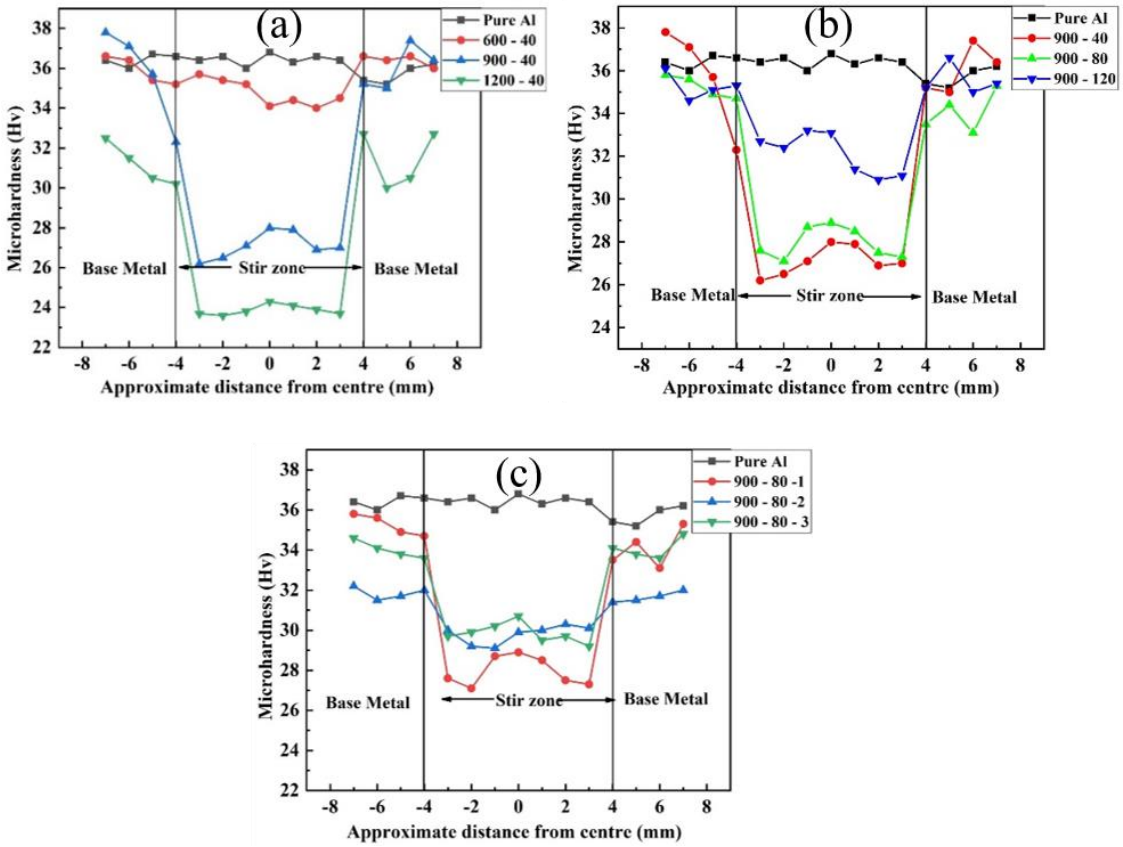

Fig. 4.2.3 Microhardness measurements of pure Al and FSPed Al (a) effect of rotational speed (b) effect of traverse speed and (c) effect of no. of passes.

4.2.6 Damping capacity

4.2.6.1 Effect of rotational speed

Fig. 4.2.4 (a) shows the effect of rotational speed on frequency-dependent damping capacity of friction stir processed Al. The damping capacity marginally decreased with increasing frequency. Interestingly, the damping got reduced after subjecting the samples to FSP, whereas a declining trend in the damping capacity was also observed with an increase in rotational speed. Classical Granto- Lücke damping theory states that dislocations are significant damping contributors at low frequencies and ambient temperatures, i.e. dislocations move under the application of dynamic loads and dissipate energy, thereby improving the damping capacity [15] [76]. By applying this model to the current observation, it can be deduced that the high number of dislocations present in the as-received Al could be the reason for its high damping capacity. At the same time, reduction of dislocations led to reduction of damping after FSP. The increase of frequency decreases dislocations' movement, thereby reducing the damping

capacity [8]. The observed decrement in damping capacity with the frequency could be ascribed to this.

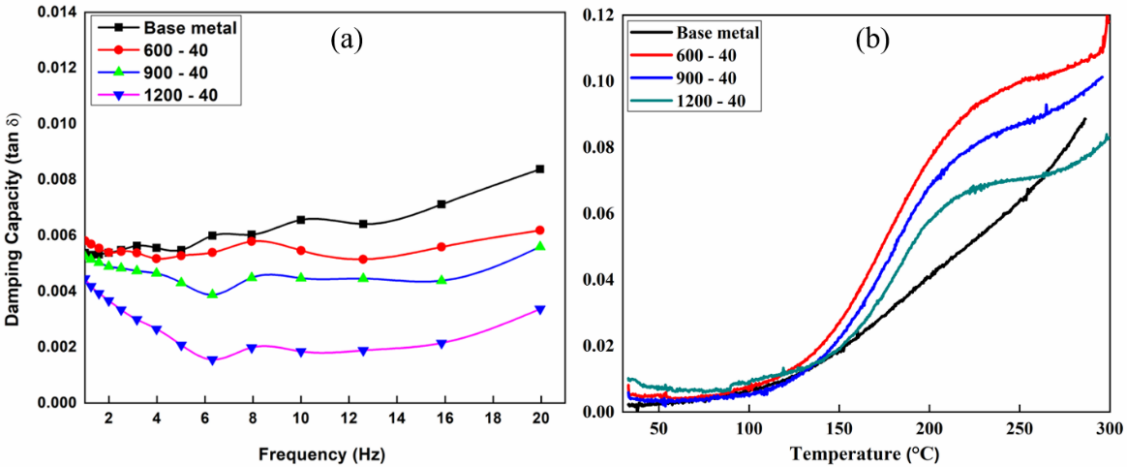

Fig. 4.2.4 Effect of rotational speed on (a) frequency-dependent and (b) temperature-dependent damping capacity of pure Al (base metal) and FSPed Al.

The influence of rotational speed on the temperature-dependent damping capacity of FSPed Al is shown in Fig. 4.2.4 (b). The damping capacity gradually increased with the temperature to 100 °C then steeply increased. The damping at high temperatures is remarkably higher for FSPed specimens. However, the increase in rotational speed decreased the damping. There was about a 121% increase in damping than the as-received Al (or base metal) for the sample processed at 600 rpm. The FSPed Al at 600 rpm sample exhibited more refined grains than two other FSPed samples because of the low heat input (Table. 4.2.2). Finer the grain size higher the grain boundary area, consequently FSPed Al at 600 rpm showed better damping than 900 rpm and 1200 rpm.

4.2.6.2 Effect of traverse speed

Fig. 4.2.5 shows the damping capacity of specimens before and after FSP. Fig. 4.2.5 (a) shows the effect of traverse speed on the frequency-dependent damping capacity of pure Al. The damping capacity was reduced after FSP. Increasing the traverse speed increased the damping ability. As described earlier, dislocations play an important role in room temperature damping. However, the observed dislocation density and damping variation could not be matched. The increase of frequency decreases dislocations' movement, thereby reducing the damping capacity [4]. The observed decrement in damping capacity with the frequency could be ascribed to this.

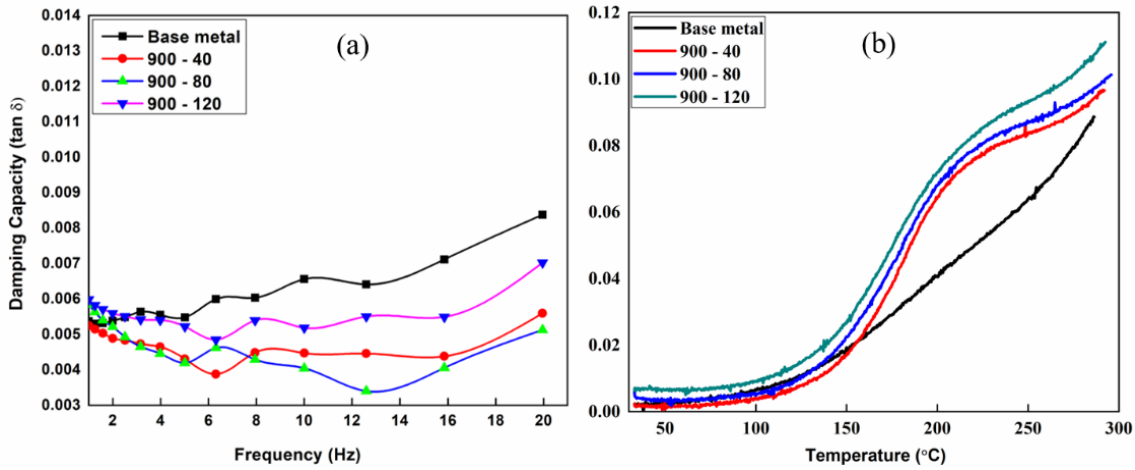

Fig. 4.2.5 Effect of traverse speed on (a) frequency-dependent and (b) temperature-dependent damping capacity of pure Al (base metal) and FSPed Al.

Fig. 4.2.5 (b) shows the effect of traverse speed on the temperature damping capacity of pure Al. The damping capacity increases with increasing traverse speed, and the highest damping capacity is observed for FSPed Al processed at 900 rpm and 120 mm/min. There was about a 107% increase in damping compared to the as-received Al. The fine grain structure of the sample processed with 120 mm/min can be ascribed to its better damping capacity than the other samples. This is because of an increase in the grain boundary area as grains are refined. Grain boundaries significantly contribute to damping at high temperatures as they can easily move against externally applied load. The movement enables energy dissipation.

4.2.6.3 Effect of no of passes

Fig. 4.2.6 (a) shows the frequency-dependent damping capacity of specimens before and after FSP. The damping capacity marginally increased with increasing frequency. The damping got reduced after subjecting the samples 1 and 2 passes of FSP. Whereas the damping capacity, surprisingly, increased for three pass FSP. Once again, the observed damping trend with the number of passes could not be explained with the help of dislocation density data.

Fig. 4.2.6 (b) shows the effect of no. of passes on the damping capacity of pure Al and FSPed Al at 900 rpm and 80mm/min. The damping capacity increases with increasing no. of passes, and the highest damping capacity is observed for FSPed Al processed for three passes. There was about a 92% increase in damping compared to the as-received Al. With the increase in no. of passes, grain size decreases (Table. 4.2.2) due to severe deformation and material flow, which will refine grain structure. Damping peaks are observed for FSPed samples at 210°C. The damping peaks are associated with viscous sliding along the GBs. The refined equiaxed

grains in the FSP samples provide these alloys' excellent GB sliding capacities at high temperatures. Thus, the peaks caused by GB relaxation were observed in the temperature-dependent damping curves of the FSP samples [8].

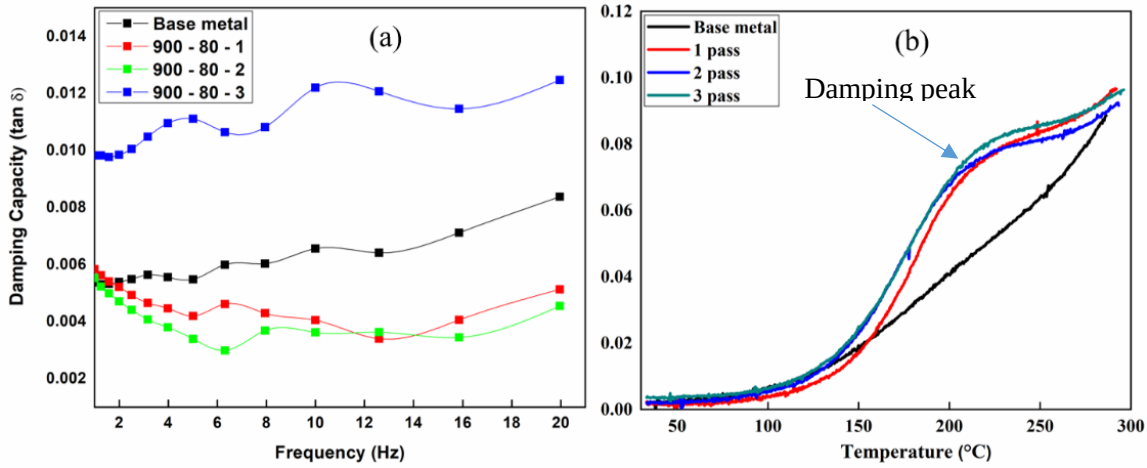

Fig. 4.2.6 Effect of no of passes on (a) frequency-dependent and (b) temperature-dependent damping capacity of pure Al (base metal) and FSPed Al.

4.2.7 Summary

The fine-grained microstructure developed after friction stir processing of pure Al. The grain size increases with increasing rotational speed and decreases with increasing traverse speed and no. of passes.

1. The hardness of the FSPed Al is decreased due to the softening effect in the stir zone.
2. The frequency dependant damping capacity of FSPed Al decreased after FSP.
3. At higher temperatures, the damping capacity of FSPed Al is better than pure Al. The increase of tool rotational speed decreased the damping capacity of pure aluminium. Whereas the increase of tool traverse speed and the number of passes increased the damping.
4. Highest damping is obtained at 600 rpm & 40 mm/min (121% than pure Al) at 200 °C.

4.3 Damping capacity of Al6061/Graphite surface composites

Previous chapters discussed the effect of friction stir processing on the damping capacity of pure metals and the effect of process parameters on the damping capacity of pure Al. In the following chapters, the results of three different surface composites are presented. The details of the other composites are as follows:

1. Al6061/Gr surface composites produced with 0, 5, 10, 15 volume fraction at 1120 rotational speed and 40mm/min traverse speed using friction stir processing.
2. Effect of particle size on damping capacity of Al6061/SiC surface composites produced by FSP.
3. Effect of different process parameters on the damping capacity of Al6061/BN surface composites.

4.3.1 Objective

The objective is to analyse the effect of volume fraction on the damping capacity of Al6061/Gr surface composites produced through FSP.

4.3.2 Experimental methods

AA6061 alloy received in T6 condition machined into the size of 200×100×6 mm^3 used for friction stir processing. The graphite reinforcement was incorporated into the alloy employing tool rotational speed of 1120 rpm and traverse speed of 30 mm/min. The volume fraction graphite was varied as 5, 10, 15 and 20%. The method of specimen preparation for various characterisations is presented in Chapter 3.

4.3.3 Microstructural characterisation

Fig. 4.3.1 shows the optical images of base metal (Al6061) and FSPed Al. The base metal was observed to have coarse grains (Fig.4.3.1a). The microstructural investigation revealed that the cross-section of the FSPed plate has three distinct regions, namely (i) stir-zone, (ii) thermo-mechanically affected zone (TMAZ) and (iii) parent or base-metal (Fig.4.3.1b). The boundary between the base metal and stir zone becomes clear in Fig. 4.3.1b. It can be readily inferred that the microstructure was severely refined by friction stirring, i.e. grain structure in stir-zone is not distinguishable as in the base-metal. The grain structure at the stir-zone is visible at high magnifications (Fig.4.3.2 a-f), and their size was determined through the linear intercept method. The grain size drastically reduced to 4.32 μm just after FSP from its initial value of 45 μm. The grain size of composites is also significantly smaller than the base-metal (4.32 μm, 5.24 μm 5.34 μm and 5.96 μm for composites containing 5, 10, 15 and 20 vol.% graphite). It may be noted that grain size slightly increased with the graphite fraction. The severe stirring

generates intense heat that softens the metal, thereby eases plastic deformation. At the same time, the generated heat is enough for recovery and recrystallisation. The rise in temperature during friction stirring of aluminium alloys is as high as 450 °C [64]. Thus, the heat-assisted plastic deformation and recrystallisation facilitated microstructure refinement in the stir-zone, which was evident from the microstructures.

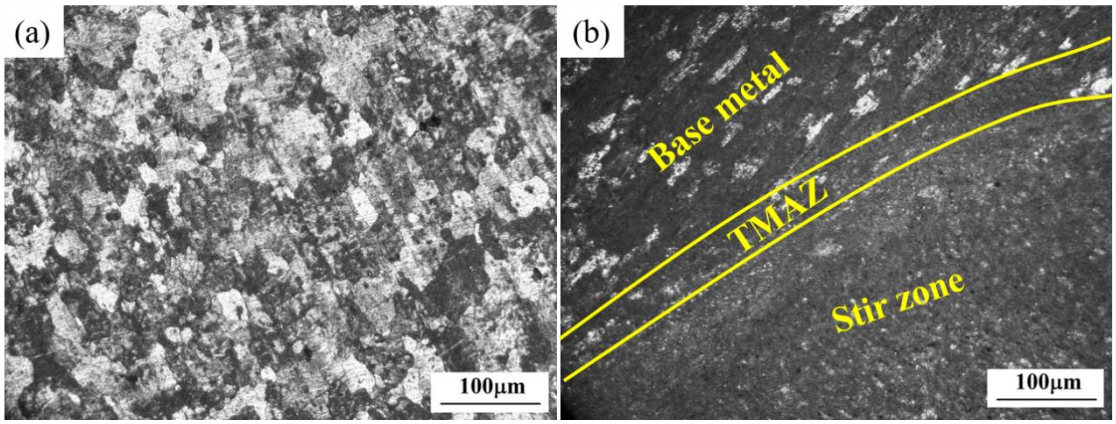

4.3.1 Optical images of (a) base metal (b) transition zone between the base metal and FSPed sample.

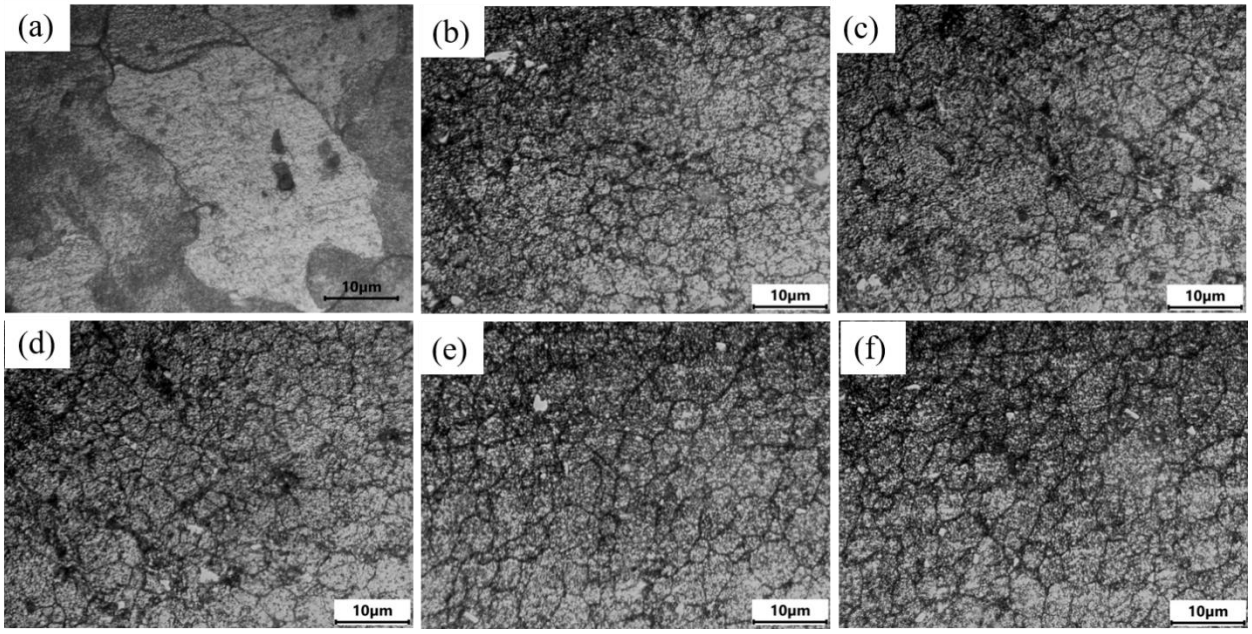

Fig. 4.3.2 Optical images of the (a) base metal, FSPed Al/Gr composites in stir zone processed at 1120 rpm and 30 mm/min (b) 0 vol. % (c) 5 vol. % (d) 10 vol. % (e) 15 vol. % (f) 20 vol. %.

Fig. 4.3.3 (c-f) shows the distribution of Gr particles in the stir zone. The distribution of Gr particles was reasonably uniform for 5 – 15 vol. % of Gr containing composites, whereas agglomeration of particles was observed in 20 vol. % composite. Further, the presence of graphite was ensured by analysing the elements through energy dispersive spectroscopy (EDS) (Fig. 4.3.4). The stir-zone area was divided into four quadrants then an areal EDS analysis was performed to ensure the homogeneous distribution of graphite in the stir-zone. The spectrum contained three peaks assigned to Al, Mg, Si, which are basic elements of AA6061. It also confirms that carbon has been identified.

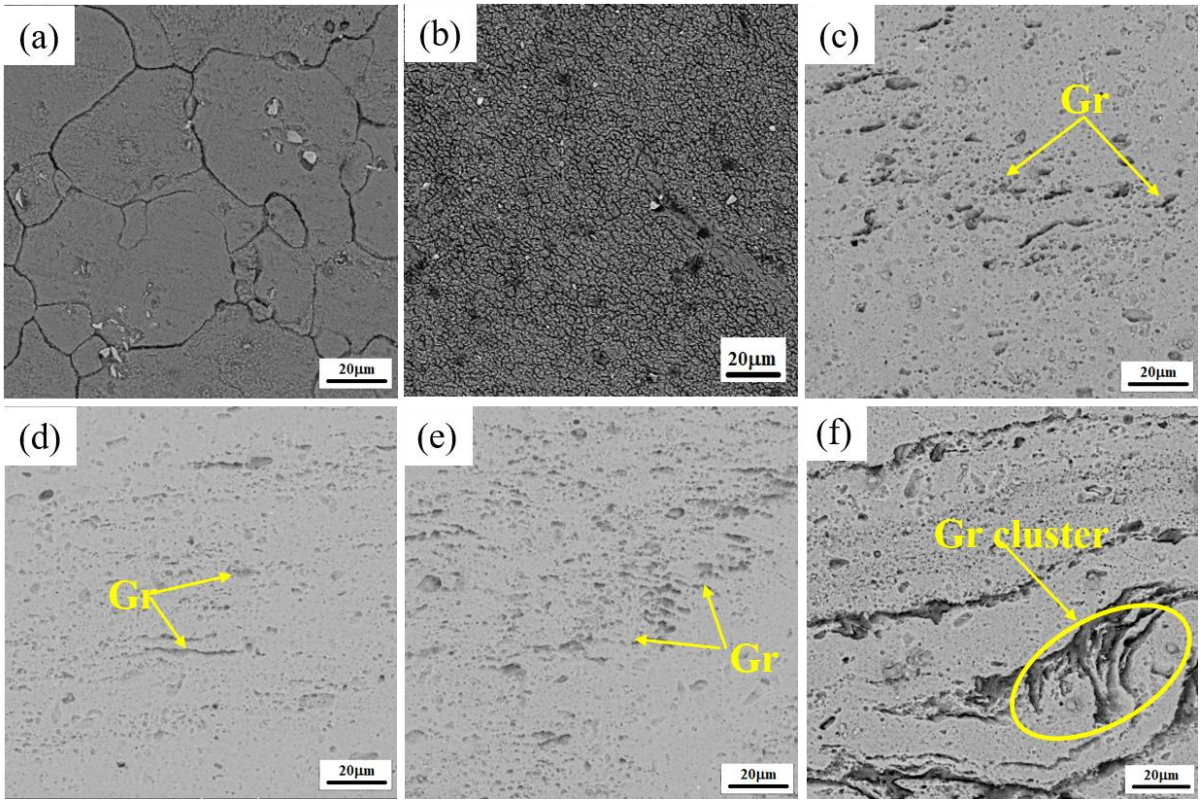

Fig. 4.3.3 SEM images of the (a) base metal, FSPed Al6061/Gr composites in stir zone processed at 1120 rpm and 30 mm/min (b) 0 vol. % (c) 5 vol. % (d) 10 vol. % (e) 15 vol. % (f) 20 vol. %.

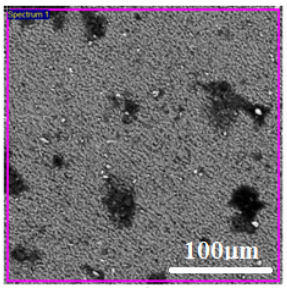

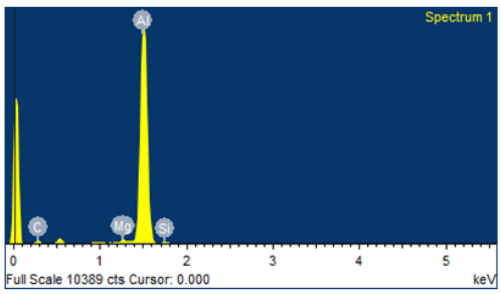

Element	Weight%	Atomic%
CK	30.78	49.97
Mg K	0.63	0.50
Al K	67.49	48.77
Si K	1.10	0.76
Totals	100.00	100.00

Fig. 4.3.4 EDX Spectrum of Al/15 vol. % Gr composite.

4.3.4 XRD Analysis

Fig. 4.3.5 shows the XRD results of the base metal and FSPed samples on the cross-sections. The peaks corresponding to the FCC phase was identified in patterns. Peaks were observed to shift to higher 2θ values. This could be due to the straining of the lattice. Furthermore, the Al6061/Gr surface composites peaks are broadened. Peak broadening indicates the introduction of higher dislocation density [71] and smaller crystalline sizes of these particles. The intensity of the FSPed composites is higher than the as-received sample. This implies that the (111) plane tends to lie on the transverse plane of the FSPed samples (or perpendicular to the pin travel direction).

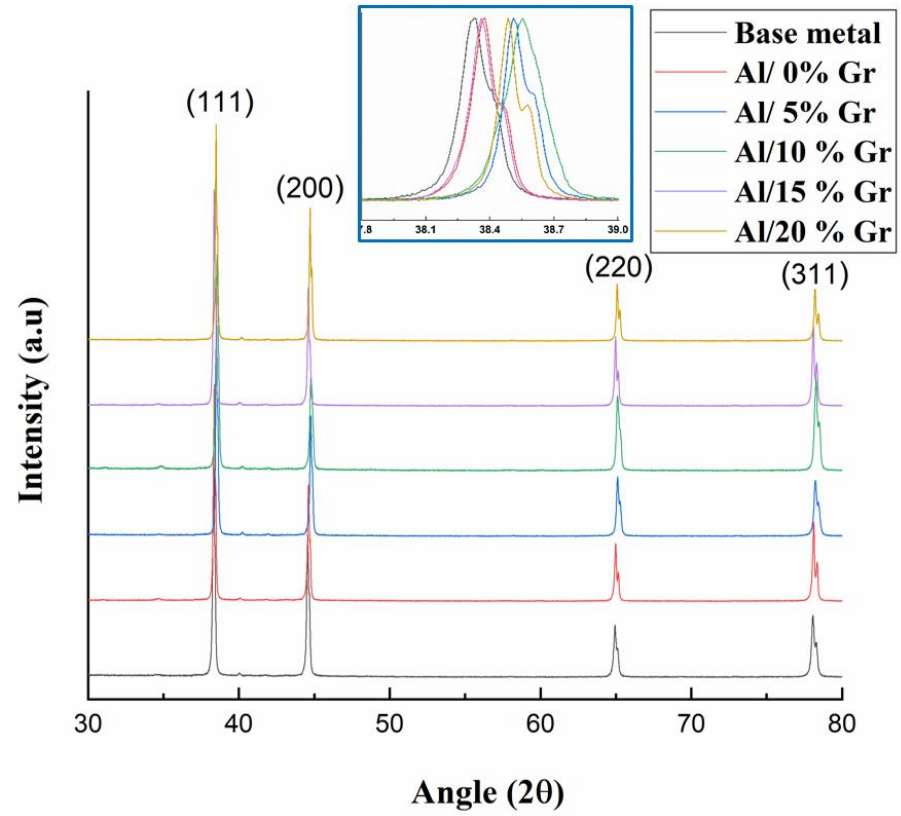

Fig. 4.3.5 X-ray diffraction patterns base metal (Al6061) and Al6061/Gr surface composites. The inset figure shows the shift of (111) peak after FSP.

4.3.5 Microhardness

Microhardness of all surface composites with various amounts of reinforcement and as received alloy shown in Fig. 4.3.6. It was revealed that the hardness of the matrix decreased due to the heat generated during processing. Mainly, the hardness values depend on the heat generation in the stir zone and the distribution of particles. Hardness was measured using Vicker's hardness test at load 500 g and time 15 sec. The hardness of the as-received sample was 88 ± 4.3 Hv and 71.6 at 0 vol. %. There is a decrease in hardness after FSP. The hardness

reduction in the stir zone could be associated with the dissolution or coarsening of precipitates. This was due to high heat that causes matrix softening, decreasing the microhardness. The softening of the SZ owing to coarsening and dissolution of precipitates in the aluminium matrix was reported while processing peak aged aluminium alloys [63]. As increasing the Graphite vol. % there is a further decrease in hardness values. It is found that there is not much difference in hardness between 15 vol. % and 20 vol. %. This drop-in hardness is due to the softness of graphite particles [2][37]. The soft dispersions do not contribute to the hardness of the composites as they cannot act as barriers to the movement of dislocations within the matrix [9]. The graphite particles are softer than the matrix metal, which causes a reduction in hardness by about 26 %.

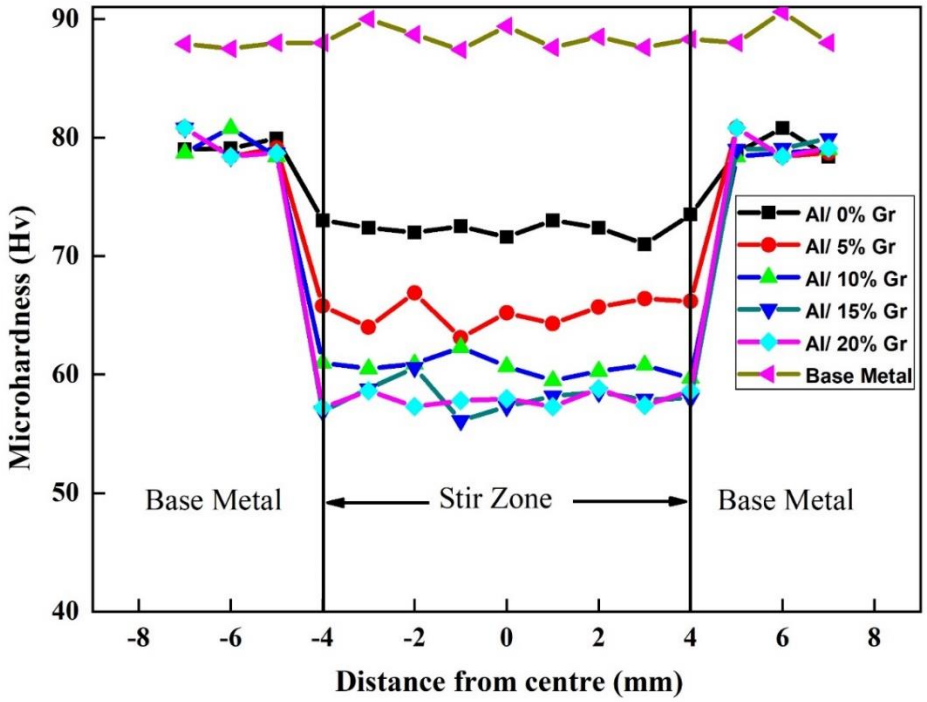

Fig. 4.3.6 Microhardness survey of base metal and Al6061/Gr surface composites.

4.3.6 Damping capacity

The damping capacity of all the surface composites with various amounts of graphite and as received alloy with frequency is shown in Fig. 4.3.7. It was noticed that the damping capacity of the as-received alloy was 1.13×10^{-3} at 1 Hz, which indicated low damping for Al6061-T6 alloy. From the plot, it was observed that increasing the amount of graphite, up to 15%, increased the damping capacity. However, composite with 20 vol.% of graphite measured to have lower damping than 15 vol.% graphite. The poor distribution and agglomeration of graphite could be a reason for the poor damping of 20 vol.% sample. It was also observed that no significant improvement in damping capacity in the as-FSPed sample and the surface composite with 5 vol. % of graphite. However, composite with 15 vol.% of reinforcement

exhibited better damping capacity than all samples. It showed a higher damping capacity (tan δ = 9.1× 10^{-3}) at 6.3 Hz. Fig. 4.3.8 (a) shows the percentage increase in damping capacity of all surface composites. It is observed that maximum damping is observed at 15 vol. % of graphite which is four times the as-received alloy at 1Hz.

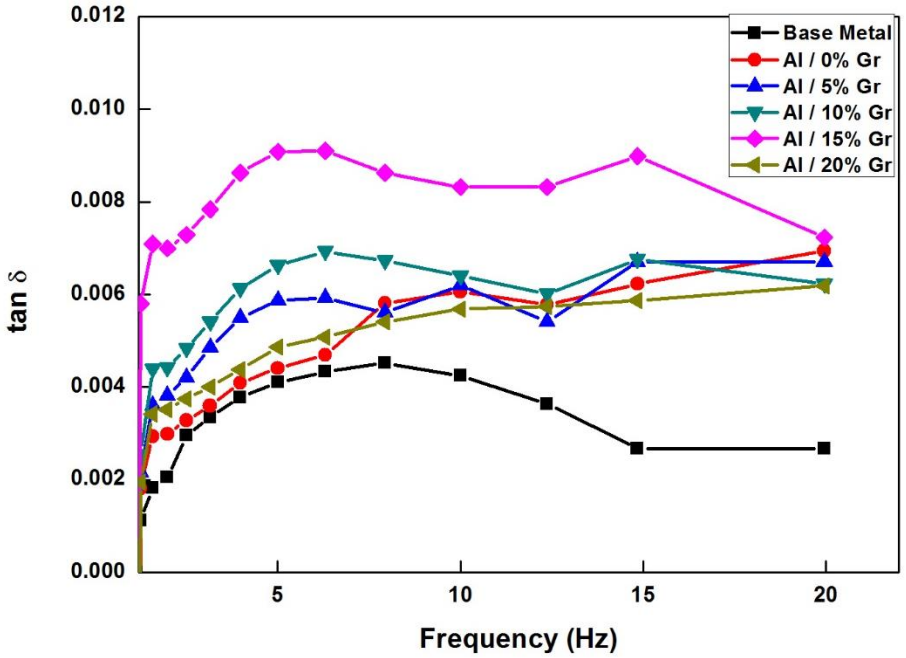

Fig. 4.3.7 Damping capacity for base metal and Al6061/Gr composites as a function of frequency.

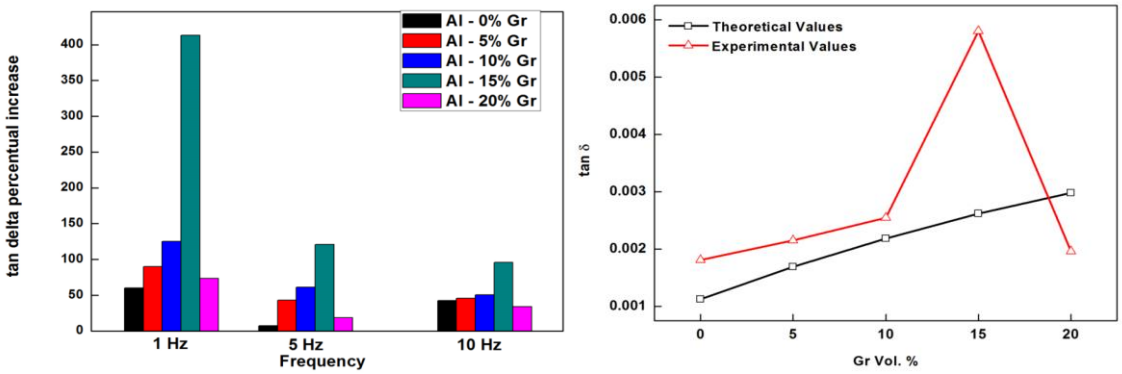

Fig. 4.3.8 (a) Percentual increasing damping of Al6061/Gr composites (b) theoretical and experimental damping of the composites.

Fig. 4.3.9 Shows the damping capacity of the surface composites and as received alloy from 50 to 250 ^{o}C at 1 Hz. From the figure, it was observed that there is an increase in damping with an increase in temperature. Similar results were reported by the R.L Perez and co-workers [15]. It was observed that there is no significant increase in damping up to 120^{o}C after that increase in

damping can be observed. The difference between the damping capacities of the composites is small at lower temperatures (50-120 ºC) than the higher temperature (200-250 ºC). The highest damping capacity (tan δ = 25 × 10^{-3}) was observed with 15 vol. % of graphite at 250 ˚C which is 3.25 times the as-received alloy. The remarkable improvement in damping can be observed at low frequency, high vol. % of graphite and at high temperature.

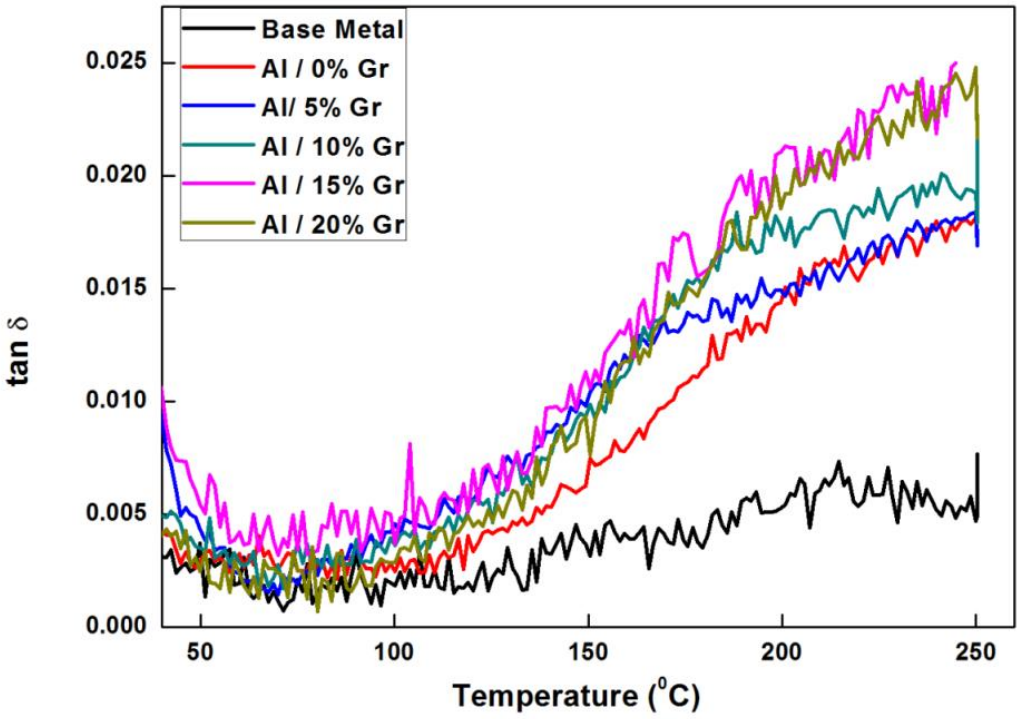

Fig. 4.3.9 Damping capacity for base Metal and Al6061/Gr composites as a function of temperature at 1Hz.

A variety of mechanisms are responsible for improving the damping behaviour of Al composites. Lattice defects such as dislocations, point defects, interfaces between reinforcements and matrix and grain boundaries are primarily responsible for defining the damping characteristics. Primarily, Zhang et al. [77] were explained the potential governing mechanism of damping for MMCs. The difference in the coefficient of thermal mismatch (CTE) between dispersoids and matrix at low temperature is the principal cause of dislocation damping, whereas interface sliding and grain boundary play a critical role in damping at high temperatures.

The following are some of the factors which are active in improving the damping of Al6061 /Gr surface composites.

The observed enhancement in damping discussed in the light of the following mechanisms [2,4, 12]

1. inherent damping or intrinsic damping
2. interface damping, i.e. AA6061 matrix- graphite interface
3. grain boundary damping
4. dislocation damping

According to Wolfenden and Wolla [3], the following relation can be used to predict the damping capacity of composites

$$\eta_C = \eta_p V_p + \eta_m V_m + \eta_i V_i \qquad (14)$$

Where η_c is the damping capacity of composite, η_p, η_m and η_i are damping capacity of the particle, matrix, and the interface V_p, V_m *and* V_i are volume fraction of particle reinforcement, matrix and the interface, respectively.

The inherent damping is determined by the composition and phases present in the material. The overall composition remains the same before and after processing; however, there is a phase change after processing, i.e. dissolution of precipitate phase in turn change in the matrix composition. Ignoring this effect as expected to be minimal also requires detailed investigation. The decrease in grain size or the grain boundary area can be attributed to the enhanced damping just after friction stirring (Fig . 4.3.7 & 4.3.9).

In the case of composites, the incorporation of graphite has significantly increased the damping and the grain boundary area. Graphite has a simple hexagonal structure in which the basal planes are weakly bonded along [0001] direction. The ease of movement of basal planes under vibrations provide better damping; thus, the inherent damping of composites is enhanced. Therefore, the incorporation of graphite has increased the inherent damping capacity of composites and increased grain boundary area. Moreover, the fraction of interface, i.e. matrix-graphite interface, also increases with the fraction of reinforcement. The interfaces are two-dimensional defects, move under dynamic loads, and enhance damping.

The contribution of interfaces to damping (Q^{-1}- quality inverse factor or damping capacity) can also be understood through Schoeck theory [74]

$$Q^{-1} = 4.5(1-\nu)/\pi^2(2-\nu) \times V_f \qquad (15)$$

Where v: Poisson's ratio, V_f: volume fraction of particles. This relation shows that the interface damping is directly proportional to the graphite volume fraction.

The contribution of grain boundaries to damping, particularly at high temperatures, has widely been reported and discussed in the literature [2], [3], [78]. The boundaries exhibit viscous properties at high temperatures. The energy due to dynamic or cyclic loading is dissipated at grain boundaries by moving them. The observed trends i.e. enhanced damping capacity and damping slope change with respect to temperature, attributed to microstructure refinement after

FSP. The base alloy had large grains, i.e. less grain boundary area, thus did not exhibit a significant change in slope. The slope change is visible just after FSP and in the surface composites due to the increase in the grain boundary area [64], [73].

Theories on damping suggest that dislocations significantly contribute to damping because their mobility under dynamic loads helps dissipate the energy. Moreover, its contribution is significant close to room temperatures. In the current study, the contribution of dislocations to damping can be ignored or assumed to be minimal due to the following reason; the microstructure refinement is through dynamic recrystallisation during friction stir processing. Such a microstructure is expected to have an equilibrium number of dislocations; thus, its contribution is expected to be the same across all specimens also to be minimal.

4.3.7 Summary

AA6061- (5 to 20 vol. %) graphite surface composites have been prepared by friction stir processing (FSP). Further, its vibration-damping properties were studied through the dynamic mechanical analyser. The following conclusions can be drawn from the current study

1. The chosen friction stir process parameters (1120 rpm and 30 mm/min) produced a defect-free processed regime.
2. The hardness of stir-zone reduced after FSP owing to the dissolution/ coarsening of precipitates. The incorporation of graphite has further reduced the hardness of surface composites.
3. The frequency-dependent damping was observed to increase after FSP with an addition of graphite. There was about a 400% increase in damping, at a frequency of 1Hz, for a specimen containing 15 vol. % graphite.
4. The damping capacity of 15vo l. % graphite composite is 3.5 times of the base alloy at 250 °C
5. The substantial enhancement in frequency and temperature-dependent damping is attributed to microstructural refinement (average grain size: 45 μm to 4.25 μm) as a result of friction stirring also due to the incorporation of graphite particles.
6. The poor damping of 20 vol. % graphite containing composite was due to agglomeration of particles.

4.4 Damping capacity of Al6061/SiC surface composites

4.4.1 Objective

The study the effect of particle size on the damping capacity of AA6061/SiC surface composites produced through FSP.

4.4.2 Experimental methods

AA6061 alloy received in T6 condition machined into the size of 200×100×6 mm^3 used for friction stir processing. The three different sizes of silicon carbide (SiC) reinforcement was incorporated into the alloy employing two-pass FSP at a rotational tool speed of 600 rpm and traverse speed of 60 mm/min. The volume fraction of SiC was kept constant (15%). The method of specimen preparation for various characterisations is presented in Chapter 3.

4.4.3 Microstructural characterisation

The microstructure of the base metal (Al6061) before and after subjecting it to FSP is shown in Fig. 4.4.1. The average grain size of the base metal as measured by linear intercept method, after FSP was found to be 5.6 μm as against the 45 μm of the base metal (Fig.4.4.1a & 1b, Table. 4.4.1). The shearing action during FSP results in the dynamic recrystallisation of the base metal, thereby refining the microstructure. The simultaneous application of heat caused due to friction and the mechanical forces aids the base metal to deform plastically. The stirring action of the tool displaces the base metal along with the advancing and retreating side of the tool, resulting in a severely deformed zone in the adjacent regions. The sub-grain boundaries that form due to dislocation cell walls transform to low angle boundaries and evolve to high angle grain boundaries by progressive accumulation of dislocations. The role of dynamic recrystallisation on microstructural refinement during FSP has been widely reported [9], [31], [33], [34].

The scanning electron micrographs of surface composites for various SiC particle sizes of 109 μm, 29.4 μm and 9 μm fabricated through FSP are shown in Fig. 4.4.1(c – e). The uniform distribution of SiC particles all over the alloy matrix for all the particle sizes reveals the homogeneity of the prepared composites. The average grain size of surface composites was found to be 5.5 μm, 6.05 μm, and 6.25 μm for SiC_p particles of 109 μm, 29.4 μm and 9 μm, respectively (Table. 4.4.1). This can be attributed to the phenomenon of heterogeneous nucleation of recrystallised grains along the particle boundaries. However, there was no significant variation in the grain size for different SiC_p particle sizes.

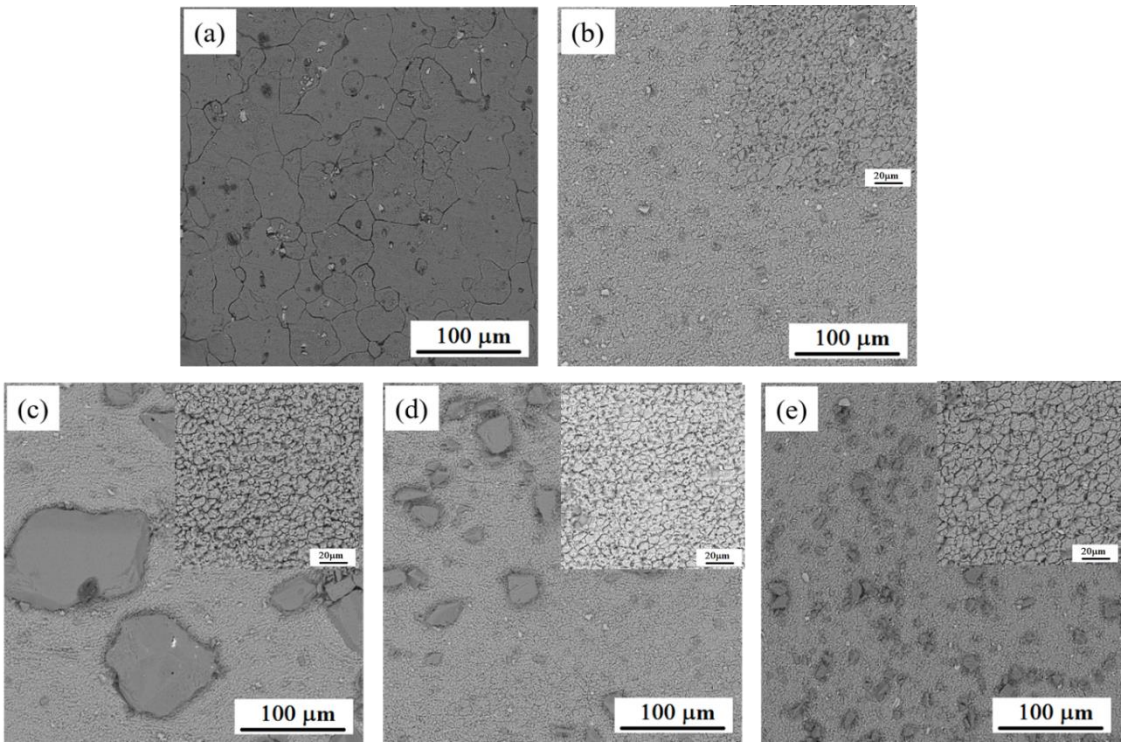

Fig. 4.4.1. Scanning electron microstructures of the base metal (a) before FSP, (b) after FSP and microstructures Al6061 surface composites reinforced with SiC particles of size (c) 109 µm (d) 29.4 µm and (e) 9 µm. Subset figures show the microstructure at high magnification in which grains are revealed.

4.4.4 XRD analysis

Fig. 4.4.2 shows the XRD pattern of the base metal and surface composites. The peaks in the diffraction pattern corresponding to the base metal and SiC reinforcements as indexed in the Figure. Peak shifting and peak broadening were observed for all the samples subjected to FSP, and this is attributed to the presence of lattice strain in the sample. Peak broadening also serves as an indication of the existence of higher dislocation density in the sample, and the same was calculated using the equation (Eq. 1) [68], [79].

$$\rho = 2\sqrt{3}\ \epsilon/Db \qquad (16)$$

Where ρ: dislocation density, ϵ: average lattice strain, b: Burgers vector (0.286 nm [68]) and D: Crystallite size.

The crystallite size of Al samples was obtained by using the Williamson-Hall equation (Eq. 2).

$$B\ \mathrm{Cos}\ \theta = \lambda K/D + 4\epsilon\ \mathrm{Sin}\ \theta \qquad (17)$$

Where B: diffraction peak width, λ: radiation wavelength (0.154056 nm), K = 0.89 and θ: half of the diffraction angle.

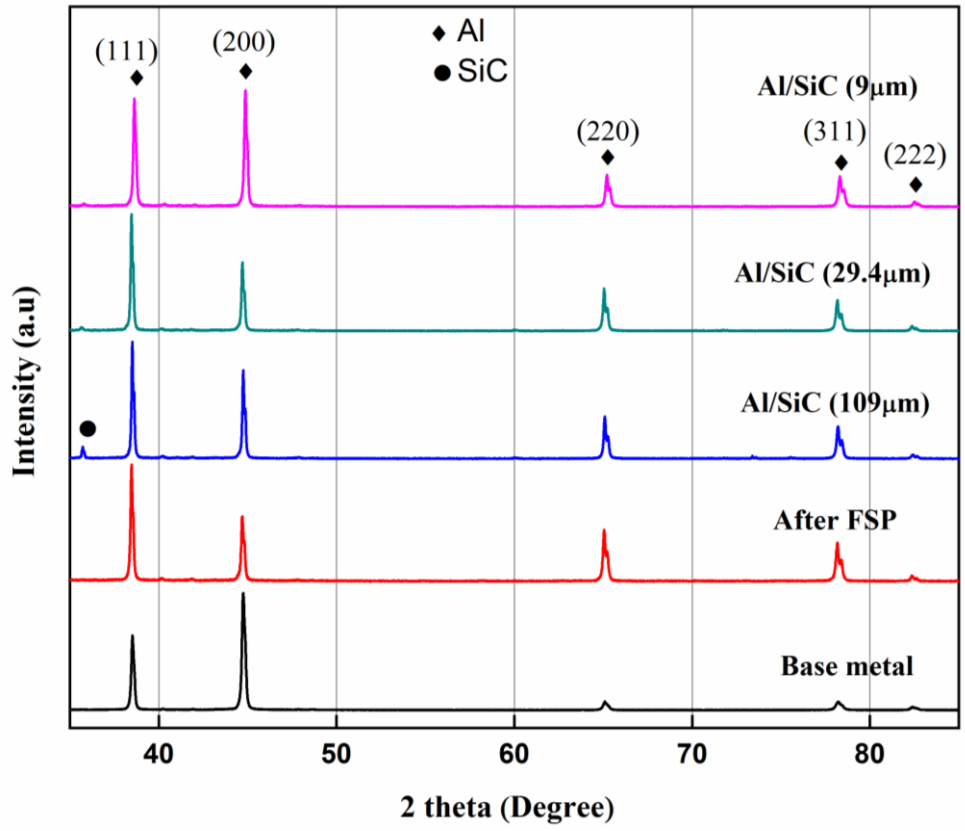

Fig. 4.4.2. X-ray diffraction patterns of specimens before and after friction stir processing.

Table 4.4.1. Estimated values of grain size, plastic zone size, grain boundary area, dislocation density and damping values predicted by rule of mixtures (ROM) for various specimen condition

S. No	Material	Average grain size(μm)	Grain boundary area (mm^2/mm^3)	Dislocation density ($10^{14}/m^2$)	Plastic zone radius (μm)	Experimental tan δ	tan δ estimated using ROM
1	Base metal	45 ± 3.1	50.9	17.2	--	--	--
2	FSPed Al	5.6 ± 1.7	293.0	10.2	--	--	--
3	AA6061/SiC (109μm)	5.51 ± 1.6	344.0	12.9	268.1	0.00324	0.00201
4	AA6061/SiC (29.4μm)	6.05 ± 1.2	321.6	13.6	72.3	0.00214	0.00201
5	AA6061/SiC (9μm)	6.25 ± 1.1	276.6	19	22.1	0.00116	0.00201

Table. 4.4.1 Summarises the calculated dislocation density values in the base metal and Al6061/SiC composites synthesised through FSP. It is clear from the table that the dislocation density decreased after subjecting the base alloy to FSP. The base metal had a dislocation density of 17.2 × $10^{14}/m^{2,}$ whereas the friction stir processed sample contained a dislocation density of 10.2 × $10^{14}/m^2$. The occurrence of dynamic recrystallisation resulted in the decreased dislocation density for the samples subjected to friction stir processing. However, with the introduction of SiC_p in the matrix, the dislocation density increased to 12.9× $10^{14}/m^2$ for a particle size of 109 μm. The metal matrix, in general, has a higher coefficient of thermal expansion (α) as compared to the reinforcing phase and the mismatch in the values between the base alloy matrix and SiC_p results in the generation of dislocation in the vicinity of the particles when cooled from the processing temperature and can be at the order of 10^{13} - $10^{14}/m^2$ [80]. The presence of SiC_p resists the deformation and thereby facilitates the formation of dislocations in its vicinity during FSP. This could also be a possible reason for an increase in dislocation density upon introducing the particles. The surface composites processed through FSP showed a trend of increased dislocation density with a decrease in the particle size from 109 μm to 9 μm. The introduction of lesser particle size in the alloy matrix increases the surface area associated with it and hence the higher dislocation density.

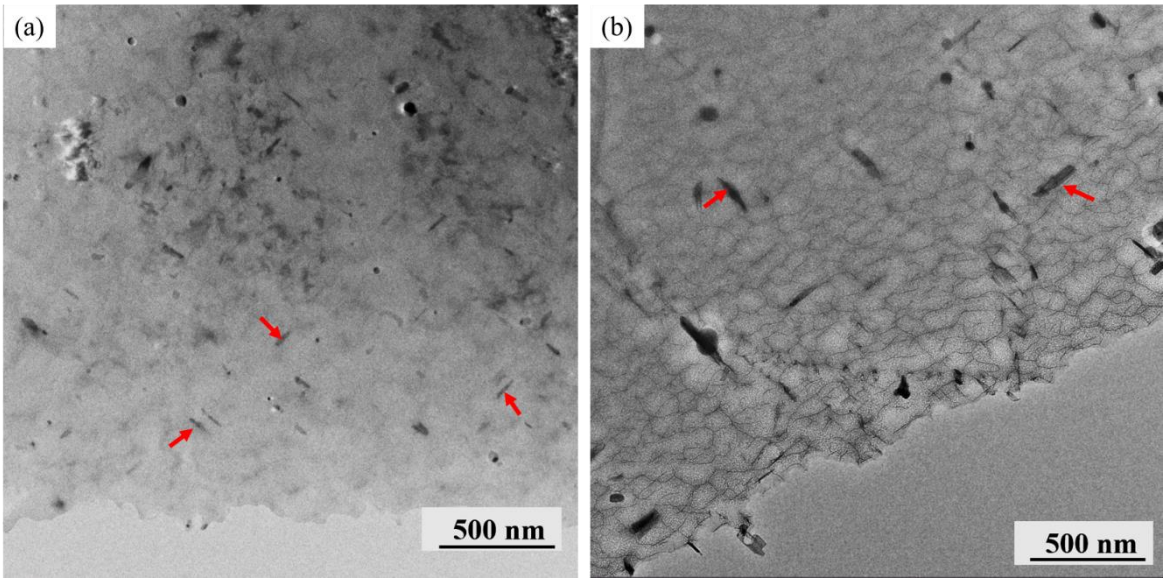

Fig. 4.4.3 TEM images of (a) base metal show fine needle precipitates (Mg_2Si) (b) FSPed sample shows coarsen needle precipitates.

4.4.5 Hardness

The hardness of base metal was measured to be 64 ± 5.3 HRB, which agrees with the earlier studies [81]. The base metal samples subjected to FSP showed a decrease in the hardness value (41.6 ± 3.9 HRB). The heat generated as a result of intense stirring can raise the local temperature to 400-600°C [54], [82], and this may lead to the dissolution/coarsening of Mg_2Si precipitates [64], [83], [84]. Though the dissolution temperature of Mg_2Si precipitates is about 300 °C [85], the coarsening or dissolution kinetics depends on the prevailing time-temperature conditions. Fig. 4.4.3 shows the images obtained through the TEM for the base alloy and the alloy subjected to FSP. The base metal in the T6 condition is exposed to the over-ageing phenomenon by which Mg_2Si precipitates in the base metal gets coarsened out due to the frictional heating during FSP (Fig. 4.4.3b). The coarsening of the precipitates results in decreasing the hardness values [57], [86]. On the other hand, the dynamic recrystallisation during FSP relieves the internal stresses, if any, during fabrication and thus leads to reduced hardness of the sample subjected to FSP. However, the hardness of samples with SiC_p of 9 μm as reinforcement subjected to FSP was found to be 57.26 HRB, and hardness values showed an increasing trend with decreasing particle size, as shown in Fig. 4.4.4.

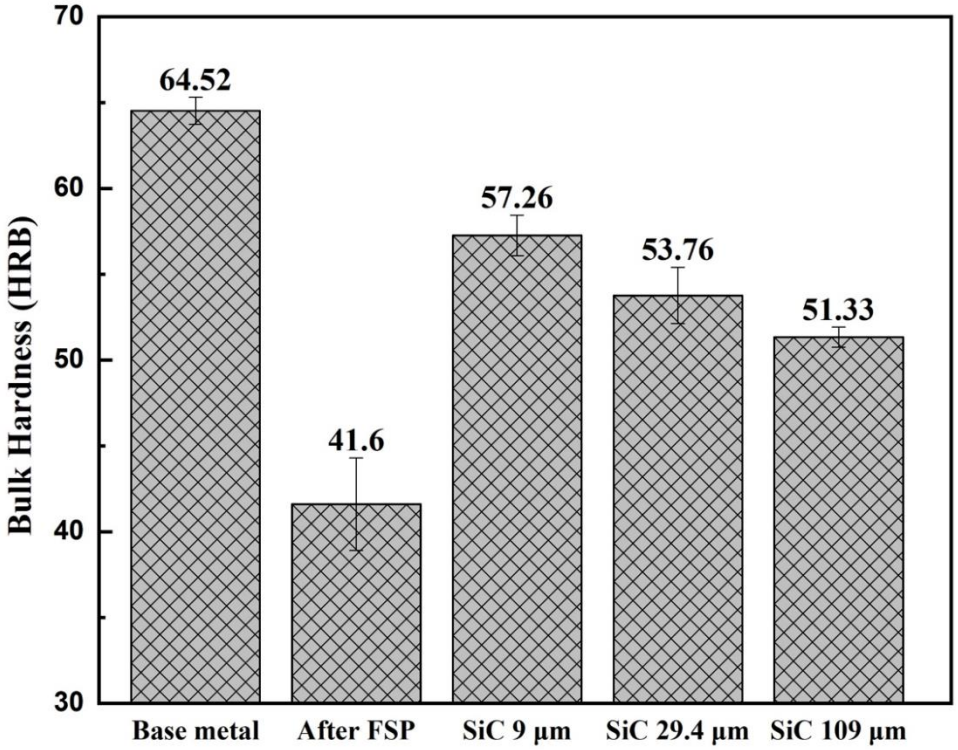

Fig. 4.4.4 Hardness measurements of base alloy and FSPed samples.

The presence of fine SiC_p in the base metal resists localised deformation, and thus it was observed to have higher hardness than the base alloy without any reinforcements. The higher value of hardness for the smaller particle size is due to the homogeneous distribution in the base alloy. The hardness data is also complemented by the data obtained through the X-ray analysis. The specimen with a higher dislocation density is expected to have better hardness, which has been observed (Table. 4.4.1 and Fig. 4.4.4). It is worth mentioning here that the hardness value obtained at heat-affected zones of processed specimens is about 35 ± 4.1 HRB. This drastic decrease in hardness after subjecting the samples to 2-passes was due to the dissolution of precipitates. Observation of this kind has been reported elsewhere [57], [81], [86].

4.4.6 Damping capacity

Fig. 4.4.5 shows the damping properties of specimens from 25 °C to 300 °C at a constant frequency (1Hz) and a constant strain amplitude of 12μm. It is evident from the data that the damping values close to room temperature are better for friction stir processed alloy and also for the composites. It is further noticed that the damping increased with an increase in the particle size. The damping capacity ($\tan \delta \times 10^{-3}$) of base-alloy, as FSPed, Al6061/SiC (9 μm), Al6061/SiC (29.4 μm) and Al6061/SiC (109 μm) at low temperature (50 °C) is 2.30, 0.26, 0.72, 2.40 and 2.76 respectively. The FSPed sample showed low damping capacity than the base-alloy. The low damping is attributed to the decrease in dislocation density after FSP (Table 4.4.1). The damping capacity of FSPed alloy and composites were significantly more significant than the base metal, particularly beyond 125 °C. Once again, the high-temperature damping increased with the particle size. It can be readily noticed from Fig. 4.4.5 that the damping steadily increased with temperature until a certain temperature, and beyond that temperature, it sharply increased. The temperature of the sharp change in damping slope is noted for all the specimens. The abrupt change in the damping-slope was observed at lower temperatures (approx. 125 °C) for the FSPed specimen and the composite specimens compared to the base metal (approx. 250 °C).

The increase in damping as with the particle size required an explanation. The damping properties of composites depend on (i) inherent damping capacity of the matrix and the reinforcement, (ii) contributions from defects [14] and (iii) the plastic zone in the vicinity of the particles. The inherent damping capacity of composites was estimated as 0.0021 applying the rule of mixtures (ROM) [78], and the estimated damping capacity remains the same for all the three composites as the volume fraction of reinforcement was kept constant (Table. 4.4.1).

The defects include grain boundaries, matrix-particle interface boundaries, porosity, and dislocations. The contribution of porosity can be ignored as it is evident from the micrographs (Fig. 4.4.1) that the stir zones are free from these kinds of defects. It is learned that the key factors influencing the damping of metal matrix composites are grain boundaries, dislocation density and plastic zone size [13]. Among these factors, dislocation density and plastic zone size determine the low-temperature damping behaviour [87], whereas grain boundaries play a crucial role in high-temperature damping [29].

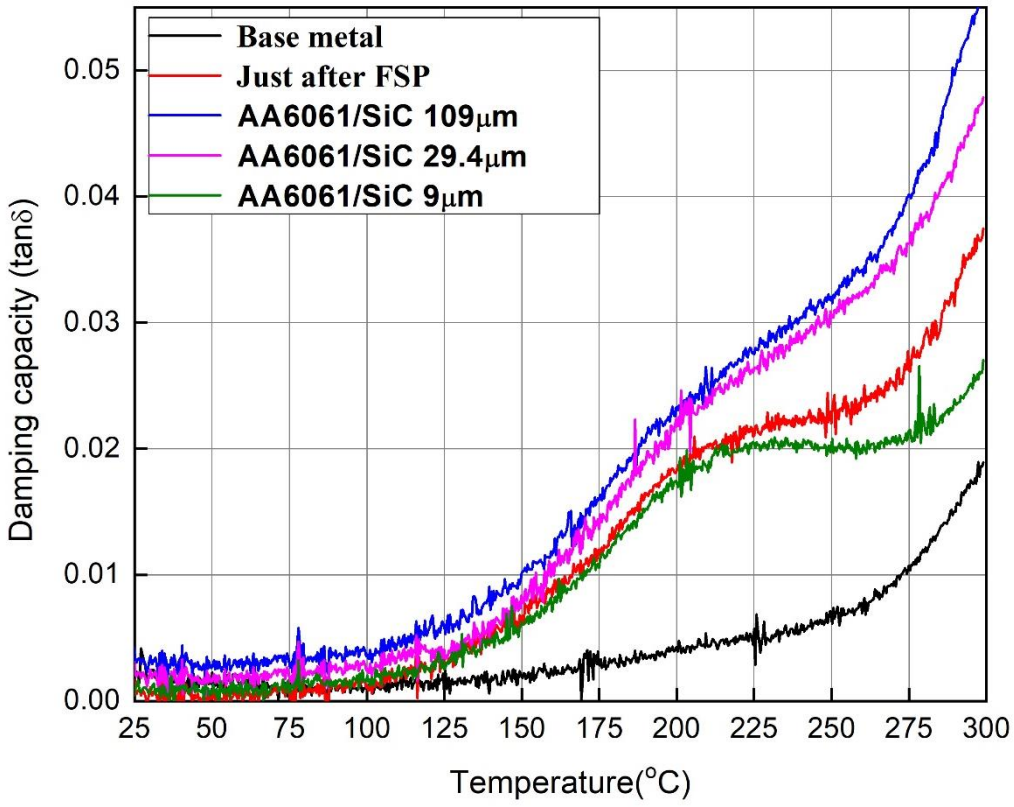

Fig. 4.4.5**.** The dynamic mechanical analyser measured the damping capacity of base metal and surface composites.

The Granato-Lucke theory [17] explains the mechanism of dislocation damping unambiguously at low temperatures. Dislocations drag the weak pinning points (such as vacancies), which are movable even at room temperatures under cyclic loading conditions, and this contributes to dissipation of energy, thereby improving damping.

The damping capacity of the friction stir processed sample was calculated using the following equation that relates the dislocation density with the damping.

$$Q^{-1} = \frac{a_0 B \rho L^4 \omega^2}{\pi^2 C b^2} \qquad (18)$$

Where Q^{-1}: damping capacity, a_0: numerical factor, B: damping constant, frequency, L: effective dislocation length, C: dislocation line tension and ρ: dislocation density.

The plastic zone radius along the particle boundaries was calculated using equation (4) that expresses the relation between the plastic zone radius and the damping [88].

$$tan\delta = \frac{f_{zp} G_c \oint \sigma . d\epsilon}{\pi \sigma_0^2} \quad (19)$$

Where f_{zp}: plastic zone volume fraction, G_c: shear modulus, σ and ε are the stress and strain, respectively.

The plastic zone radius, i.e. size of plastic strain build up around the SiC particles, was estimated using the following equation (5) [89].

$$f_{zp} = r_s \left(\frac{\Delta \alpha E \Delta T}{(1-\upsilon)\sigma y}\right)^{1/3} \quad (20)$$

Where $\Delta\alpha$: the difference between the coefficient of thermal expansion of SiC (4×10^{-6}/°C) and Al (24×10^{-6}/°C [90]), ΔT: the temperature difference between stir zone and room temperature, E: Al matrix elastic modulus (68.9 GPa), υ: Poisson's coefficient (0.3), σ_y: matrix yield stress (270 MPa) and r_s: is the reinforcement particle radius. The plastic zone radius increased with the particle size from 22.1 μm to 268.1 μm. The larger particles will have a higher volume to surface area ratio, and thus the contraction upon cooling from higher temperatures would be higher compared to smaller particles. The larger contraction associated with larger particle size results in a larger plastic zone in its vicinity [91][92]. As per the relations mentioned above, both dislocation density and plastic zone size are directly related to the damping. The measured values are indicated in Table. 4.4.1, and it can be observed that the (i) dislocation density decreased as particle size increased and (ii) plastic zone size increased with an increase in the SiC particle size. The observed trend in damping, i.e. increase in damping with the particle size, proves that plastic zone size is a significant contributor for improving the damping capacity than the dislocation density. It is evident from Fig. 4.4.5 that there is a substantial enhancement in damping just after friction stir processing for the composite specimens at elevated temperatures. At higher temperatures, the movement of dislocations becomes faster despite its concentration, and consequently, its contribution to damping vibrations decreases [13]. Indeed, grain boundary sliding is the primary damping mechanism at elevated temperatures. The enhancement of damping capacity beyond 125 °C is due to the fine grain structure in friction stirred specimens (Table. 4.4.1). Damping mechanisms associated with grain boundary was studied by Lavernia and Zhang [78]. At higher temperatures, grain boundaries display viscous

properties, i.e. they tend to slide over another. The viscous flow at grain boundaries translates mechanical energy generated by cyclic load into thermal energy, increasing the damping at grain boundaries [64]. It can be inferred from the grain size data that the grain boundary area increased with the particle size. Moreover, the grain boundary area significantly increased after friction stir processing (Table 4.4.1). The grain boundary area in the base metal and the composites was estimated using the following equation (6) [93].

$$S_V = 2\bar{N}_L \quad (21)$$

Where S_V is the grain boundary area per unit volume, and $\bar{N}_L$ is the no. of intercepts per unit length. Because of the reason above, composites have shown better damping than the base alloy.

It is worth discussing the role of interfaces, i.e. AA6061/SiC, on damping. The interfaces also enhance damping, particularly at high temperatures [78]. The interface moves under cyclic loading conditions, as the matrix is softer than the SiC particles. The finer particles have a larger interface area, and thus the specimen with 9 μm particles should have exhibited better damping. However, the grain boundary area for the same sample was lower than the samples having larger particles. The present results suggest that the contribution from the grain boundary in enhancing the damping was higher than the contribution provided by the interface area.

4.4.7 Summary

The AA6061/SiC_p composites were produced by FSP, and the influence of SiC_p on the damping properties was investigated for the temperature range 25 °C to 300 °C. The average size of reinforcements were 9, 29.4 and 109 μm.

1. The average grain size has significantly reduced after friction stir processing (45 to 5.64 μm)

2. The damping capacity remarkably increased just after friction stir processing. Further, the damping increased with the particle size due to the larger plastic radius zone. The enhancement in damping was significant at high temperatures, i.e. 125 °C to 300 °C.

3. The plastic zone size increased with the particle size was and responsible for damping enhancement in the temperature range 25 °C to 125 °C.

4. The increase in grain boundary area was responsible for the enhancement in damping at high temperatures 125 °C to 300 °C.

4.5 Effect of friction stir process parameters on the damping capacity of Al6061/BN surface composites.

4.5.1 Objective

The objective of this work is to explore the effect of friction stir process parameters, i.e. tool rotational speed, tool traverse speed and number of passes, on damping capacity of Al6061/BN surface composites.

4.5.2 Experimental Methods

Al6061 alloy received in T6 condition machined in to the size of 200×100×6 mm^3 used for friction stir processing. The Boron Nitride (BN) reinforcements (3μm) were incorporated in to the alloy employing various FSP process parameters as shown in Table. 4.5.5. The amount of reinforcement was kept constant at 15 vol.%. The method of specimen preparation for various characterization is presented in Chapter 3.

Table. 4.5.1 Process variables under which samples are prepared for the study

Variable	**Fixed parameters**
Tool rotational speeds (RS): 600, 900 and 1200 rpm	TS: 40 mm/min
Tool traverse speed:40, 80, 120 and 160 mm/min	RS: 1200rpm
Number of passes: 1,2, and 3	RS:900 rpm; TS:80 mm/min

4.5.3 Microstructural characterization

4.5.3.1 Effect of rotational speed

Fig. 4.5.1 shows the SEM image of the as received alloy (Al6061), shows the coarser grains with an average grain size of 45μm. The effect of tool rotational speed on the microstructure of Al6061/BN surface composite produced at rotational speeds 600, 900, 1200 rpm and traverse speed 40 mm/min is shown in Fig. 4.5.2 (a-c). The SEM images clearly reveal the distribution of BN particles in the alloy matrix. The grain size and distribution of particles in the stir zone depends on the FSP parameters and the tool used. The distribution was not uniform at 600 rpm also agglomeration of BN particles observed at several locations. When tool rotational speed was increased, the agglomerations gradually disappeared [46]. The surface composite fabricated at 1200 rpm showed (Fig. 4.5.2 c) uniform distribution of BN particles. The stirring action of the tool was vigorous at rotational speed of 1200 rpm, which induced high plastic strain on the matrix and dispersed the particles effectively into the plasticized matrix.

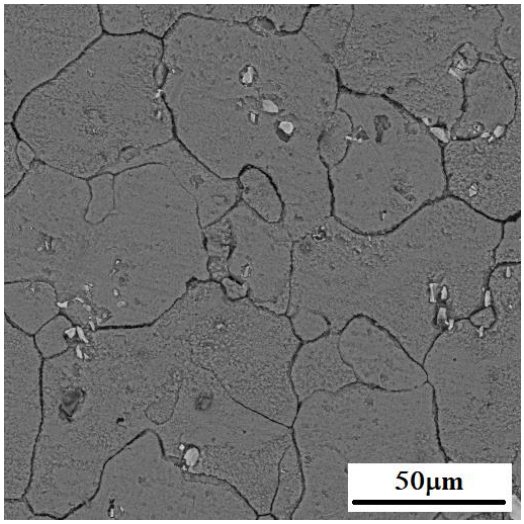

Fig. 4.5.1 SEM image of as received base metal.

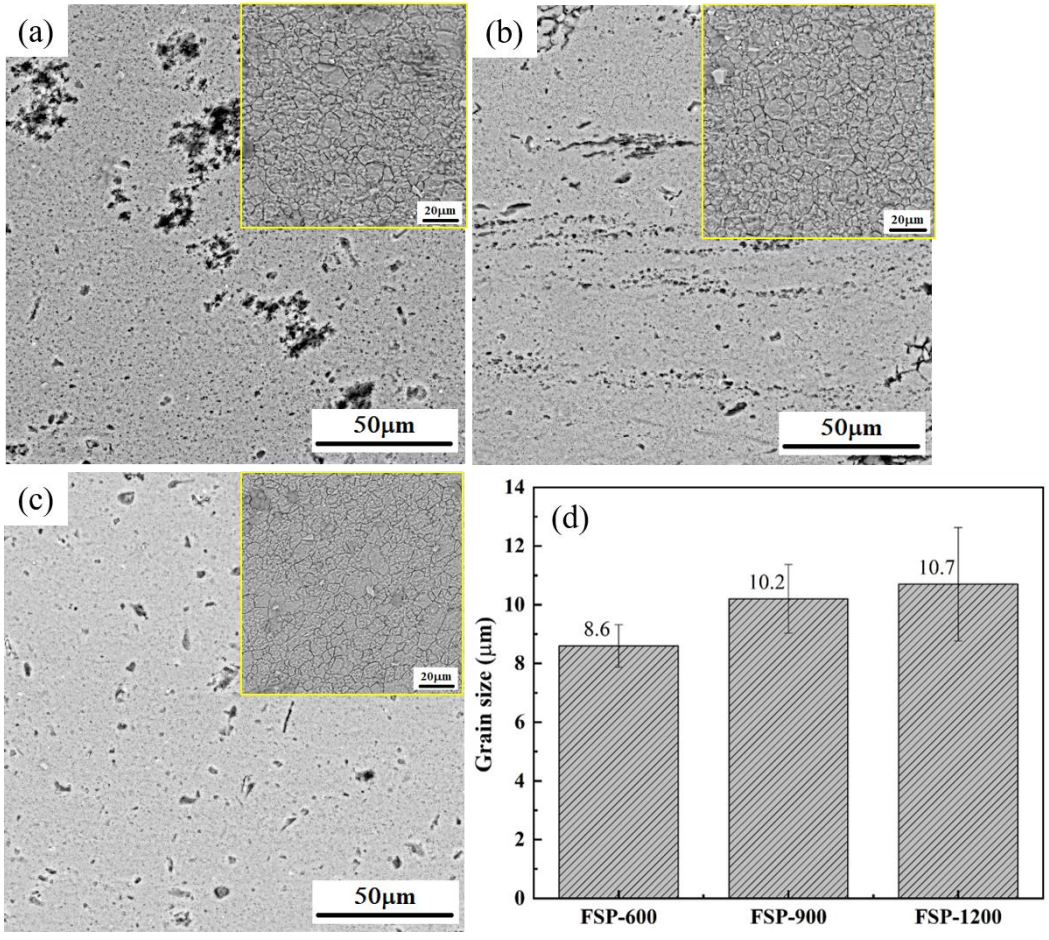

4.5.2 SEM image of FSPed Al6061/BN surface composites produced at constant traverse speed 40 mm/min and rotational speed of (a) 600 rpm (b) 900 rpm (c) 1200 rpm (d) effect of rotational speed on grain size. Subset figures show the microstructure at high magnification in which grains are clearly revealed.

The intense stirring and adequate material flow produced homogenous distribution. The increase in rotational speed was observed to increase the average grain size at the stir zone (Table 4.5.2). Increase of rotational speed increases the heat input into the region being processed thus enables coarsening of recrystallized grains.

Table. 4.5.2 Average grain size at the stir-zone

S. No.	Rotational speed (rpm)	Traverse speed (mm/min.)	No. of passes	Heat input	Grain size (μm)
Base metal	--	--	1	--	45
1	600	40	1	9	8.6 ± 3.4
2	900	40	1	20	10.16 ± 4.2
3	1200	40	1	36	10.67 ± 3.9
4	1200	80	1	18	8.15 ± 2.5
5	1200	120	1	12	6.27 ± 1.7
6	1200	160	1	9	5.10 ± 1.55
7	900	80	**1**	10.1	9.04 ± 3.05
8	900	80	**2**	--	8.56 ± 3.16
9	900	80	**3**	--	6.06 ± 1.65

4.5.3.2 Effect of traverse speed

The effect of traverse speed on the microstructure of the Al6061/BN composites (Fig. 4.5.3 a - c) fabricated through FSP at a constant speed of 1200 rpm and at various speeds of 40, 80 and 120 mm/min respectively. The SEM images of surface composites fabricated at 40 mm/min shows (Fig. 4.5.3 a) homogeneous distribution of BN particles and no particle clusters were observed. The distribution of BN particles was not uniform (Fig. 4.5.3 c) for the sample performed at a speed of 120mm/min. When the traverse speed was increased, the agglomerations gradually increased. The stirring action of the tool is vigorous at traverse speed of 40 mm/min, which induces high plastic strain on the Al matrix and disperses the particles effectively into the plasticized Al. The intense stirring and adequate material flow produces homogenous distribution [45]. The available stirring action of the tool is inadequate at traverse speed of 120 mm/min and leads to improper mixing of particles and plasticized Al. Hence, the particles are closely located and clusters are formed. From the Fig. 4.5.3 d with increasing the traverse speed in constant rpm causes reducing in grain size (Table. 4.5.2). The reason is related to the effect of the heat input on the grain growth. Increasing the traverse speed leads to a decrease in the duration of the time in which the material is affected by the process heat [45]. Therefore, the grain size decreases during dynamic re-crystallization. Fig. 4.5.5 shows the EDS images of base metal and FSPed composites. The indication of element nitrogen (N) confirms the presence of BN particles in the composite (Fig. 4.5.5 b).

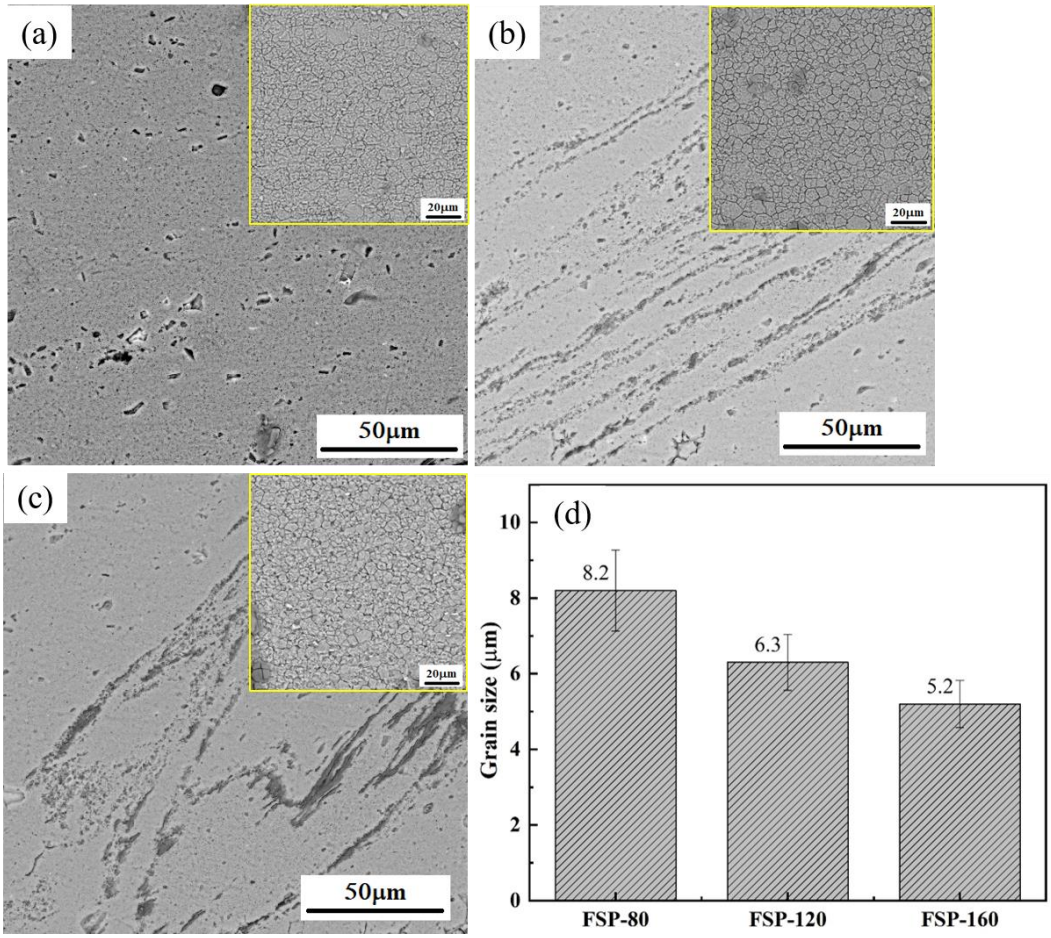

Fig. 4.5.3 SEM image of FSPed Al6061/BN surface composites produced at constant 1200 rpm (b) 40 mm/min. (c) 80 mm/min. (d) 120 mm/min. (d) effect of traverse speed on grain size. Subset figures show the microstructure at high magnification in which grains are clearly revealed.

4.5.3.3 Effect of no of passes

Fig. 4.5.4 (a-c) shows the microstructure of Al6061/BN composites in the stir zone produced at 1, 2, 3 passes. The first FSP pass refines microstructure and forms fine grains with a large area of grain boundaries. On the other hand, with increase in number of FSP passes, BN powder distribution becomes more homogenous and clusters of BN particles are not found in the stir zone. The grain size decreases with increasing no. of passes (Fig. 4.5.4 d). Bauri et al. [28] reported that increasing the number of passes uniformly distributes TiC reinforcements in the AA5082 matrix [94]. An analysis using EDS also confirmed the presence of BN particles in the matrix (Fig. 4.5.5 (a-b)).

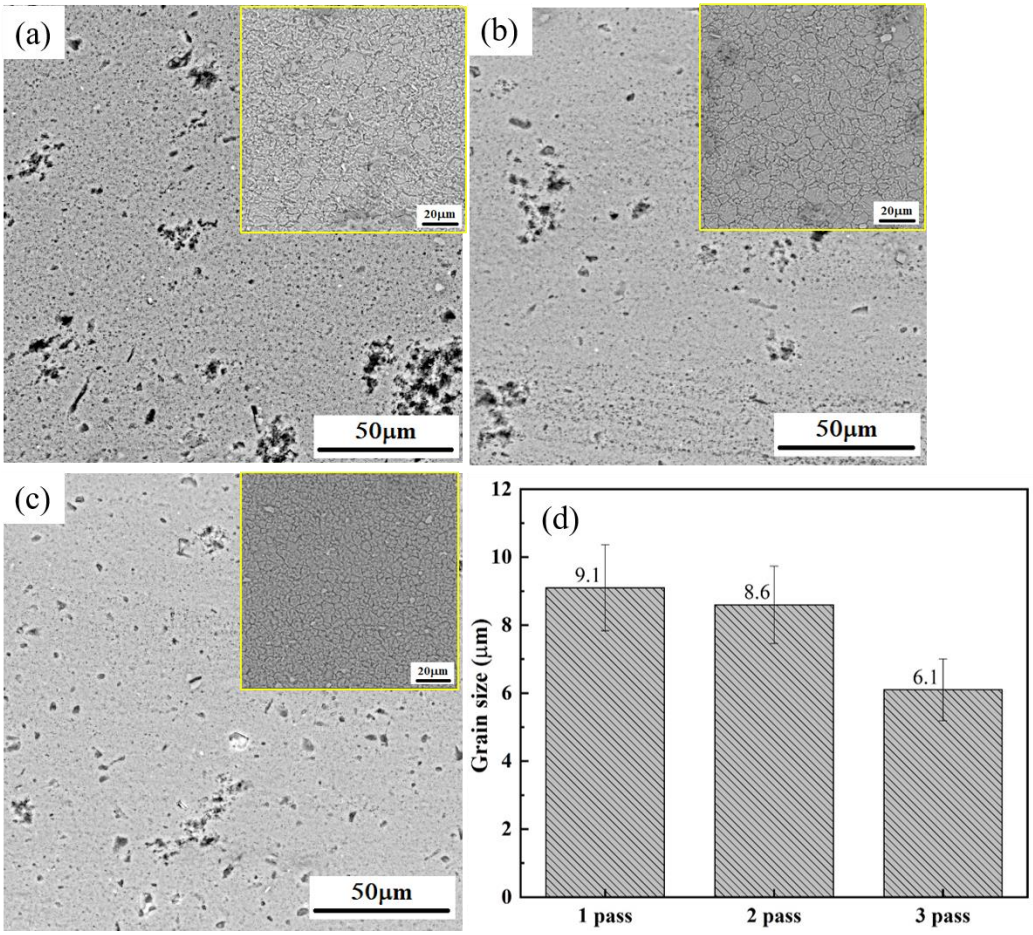

Fig. 4.5.4 SEM image of FSPed Al6061/BN surface composites produced at constant 900rpm and 80 mm/min.(a) 1 pass (b) 2 pass (c) 3 pass (d) effect of no. of pass on grain size. Subset figures show the microstructure at high magnification in which grains are clearly revealed.

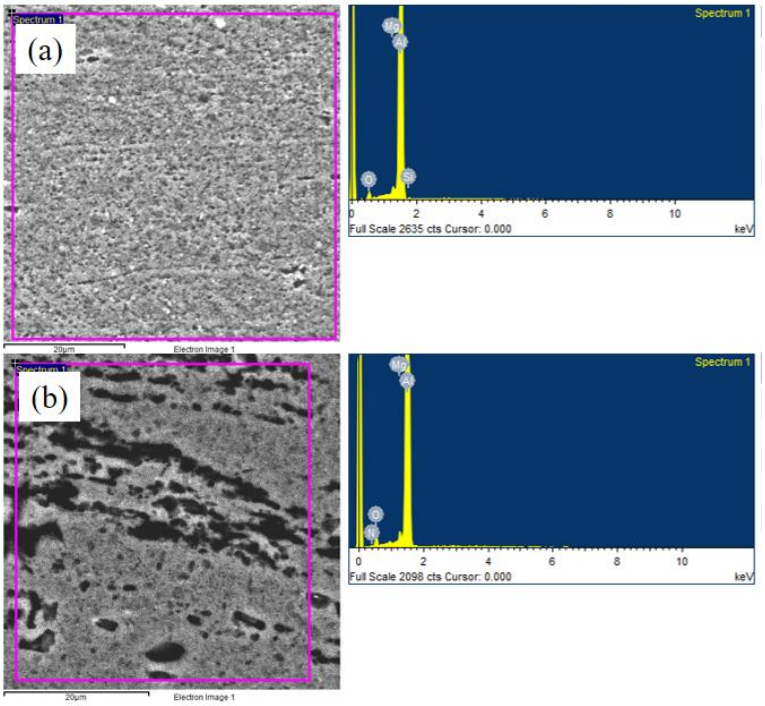

4.5.5 Elemental analysis of (a) base alloy (b) Al6061/BN surface composite by EDS

4.5.4 Damping capacity

4.5.4.1 Effect of rotational speed

Fig. 4.5.6 shows the temperature dependent damping capacity of base metal and FSPed samples. The effect of rotational speed on damping capacity of base metal and surface composites presented in Fig. 4.5.6 (a). The damping capacity of all samples increased with increasing temperature. There is no significant improvement in the damping capacity of the samples was observed till 150 °C but the damping capacity of FSPed samples improved than the base metal. The increase in damping capacity of the FSPed materials at lower temperature (below 150 °C) is due to the addition of BN particles. At higher temperature (above 150 °C) significant improvement in damping is observed. The increase in damping capacities of all samples with increasing temperature is due to the viscous flow at grain boundaries (GBs) converting mechanical energy into thermal energy as a result of damping at GBs [64]. Damping peaks were noticed in FSPed samples but not in the base metal. The damping peaks of Al materials is associated with viscous sliding along the GBs. The fine equiaxed grains in the FSP samples provide the excellent GB sliding capacities of these alloys at high temperature. Thus, the damping peaks caused by GB relaxation were observed in the temperature-dependent damping of the FSP samples [73]. FSPed surface composites shown better damping than the base metal because of the addition of BN particles. FSPed composite produced at 600 rpm and 40 mm/min displayed better damping (217%) than the base metal (Fig. 4.5.6 b) at 300 °C because the fraction of grain boundary is high in this sample due its fine grain structure (Table. 4.5.2). Increasing the rotational speed increases the heat input in stir zone, which leads to coarser grain size. Because of this reason FSPed at 1200 rpm shown less damping compared to other two composites. Similar trends i.e. rotational speed dependent high temperature damping capacity, were reported in literature [95].

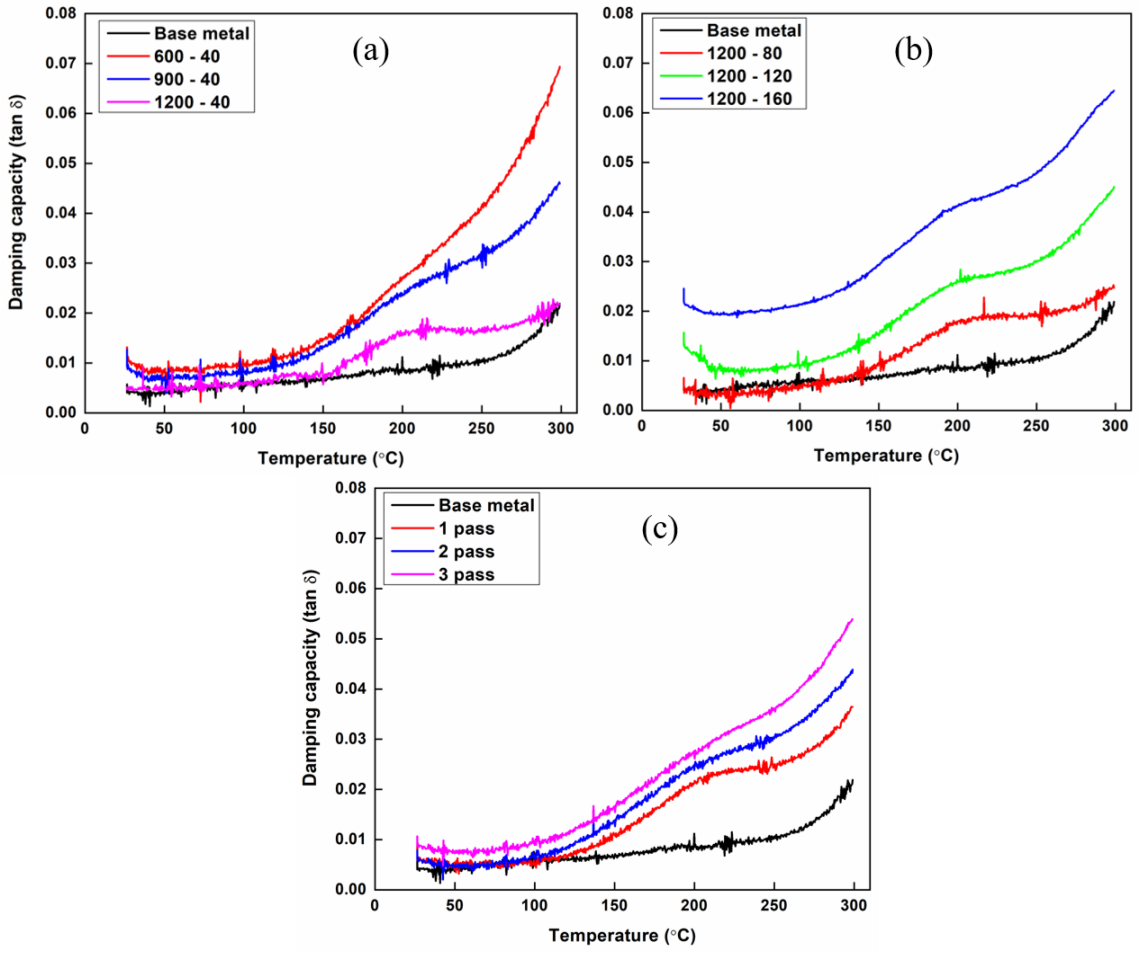

Fig. 4.5.6 Temperature damping capacity of Al6061/BN surface composites (a) effect of rotational speed (b) effect of traverse speed and (c) effect of no. of passes.

4.5.4.2 Effect of traverse speed

Fig. 4.5.6 (b) displays the effect of traverse speed on damping capacity of Al6061/BN surface composites. The damping capacity of all samples increased with increasing temperature. There was no significant improvement in the damping capacity of the samples observed till 150 °C, but the damping capacity of FSPed samples improved than the base metal. At higher temperature (above 150 °C) significant improvement in damping was observed. Damping peaks were noticed in FSPed samples but not in the base metal. The FSPed composites produced at 1200 rpm and 160 mm/min. shown highest damping capacity, which is very large (194%) as compared to the base metal. The tool residing time in stir zone reduces as traverse speed increases and the quantity of available heat input is decreased. Less heat input at traverse speed of 160 mm/min due to less residing time, which leads to finer grain size (Table. 4.5.2). Because of this reason FSPed at 1200 rpm and 160 composite shown better damping compared to other composites.

4.5.4.3 Effect of number of passes

Fig. 4.5.6 c displays the effect of no of FSP passes on damping capacity. The highest damping capacity was shown by FSPed composite developincreasedses. Once again, its fine grain size was attributed to its better damping capacity as compared to the 1- and 2- pass samples. The FSP samples presented a microstructure characterized by an equiaxed fine grain structure with a random grain misorientation distribution. Such microstructure provides the excellent GB sliding capacity at high temperature [64]. Thus, FSP samples exhibited higher damping capacity than the BM. The smaller grain size (Table. 4.5.2) increased the GB area of the FSP samples, dissipating more energy during vibration at high temperature, according to the GB damping mechanism [71].

4.5.5 Summary

Al6061T6-BN surface composites have been prepared by friction stir processing. Further, its vibration-damping properties have been studied through a dynamic mechanical analyser. The following conclusions can be drawn from the current study.

1. The chosen process parameters were observed to result in a processed regime without any defects. However, process parameters played a significant role in the distribution of reinforcement in the particle.
2. The particle distribution was observed to be uniform when using
    a. high tool rotational speed
    b. low tool traverse speed
    c. Increasing the number of passes

3. Severe microstructure refinement due to friction stir processing was observed to influence the damping properties at high temperatures significantly.

4. Addition of BN particles was observed to improve the damping capacity.

5. The highest damping capacity recorded for sample processed with a rotational speed of 1200 rpm/min and traverse speed of 160 mm/min. And it was 407% higher than the as-received Al6061.

4.6 Damping capacity of surface composites with metallic dispersions

In chapters 4.3-4.5, ceramic particles were used as reinforcements, further its influence on the damping properties of Al6061 was investigated. In this chapter, pure metallic powders, i.e. Fe and Ni, have been used as reinforcements. The reason for choosing powders was due to their excellent inherent damping capacity compared to Al6061 (Table 3.1.1). It was believed that incorporating these particles would enhance the damping capacity.

4.6.1 Objective

To study the effect of Fe/Ni reinforcements on the damping capacity of Al6061 prepared through friction stir processing.

4.6.2 Experimental Methods

AA6061 alloy received in T6 condition machined into the size of 200×100×6 mm^3. The Iron (Fe) and Nickel (Ni) reinforcements were incorporated into the alloy, employing a rotational tool speed of 600 rpm and traverse speed of 60 mm/min. The amount of reinforcement was fixed at 15 vol.%. The method of preparing surface composite and specimen preparation for various characterizations are presented in Chapter 3.

4.6.3 Microstructural characterisation

The scanning electron micrographs of base alloy (Al6061) and the surface composites are shown in Fig. 4.6.1. The base alloy consisted of large grains, as seen Fig.4.6.1a, whereas the grains were indistinguishable in the stir zone of the FSPed base alloy. This indicated severe grain refinement in the stir zone. The stir zone of surface composites consisted of fine grains and reinforced particles. The distribution of Fe and Ni particles can be seen in Fig. 1 (c, d), and at some locations, clustering of particles was observed. The presence of particles at the stir zone was also confirmed by EDS analysis (Fig. 4.6.2).

Table 4.6.1 Grain size measurements of base metal and FSPed composites.

Material	**Grain size (μm)**	**The crystallite size (nm)**	**Lattice strain**	**Dislocation density ($10^{14}/m^2$)**
Al6061	45±3.1	339.1241	0.00481	17.2
As FSPed	6.35±2.12	218.9573	0.00207	11.5
Al/Ni composite	6.02±1.78	190.9617	0.00174	11
Al/Fe composite	5.36±1.51	339.3732	0.00168	6

The average grain size of the base alloy was 45μm, whereas, in the stir zone, it was 6.35±2.12μm. The average grain size at the stir zones of composites was 5.36 ± 1.51μm for Al/Fe and 6.02 ± 1.78μm for Al/Ni. As discussed earlier, dynamic recrystallization phenomena are responsible for the microstructure refinement at the stir zones. Noting the difference in grain size reduction in the presence of particles, it can be concluded that particles pinned the grain boundaries, thereby hindering grain growth while processing.

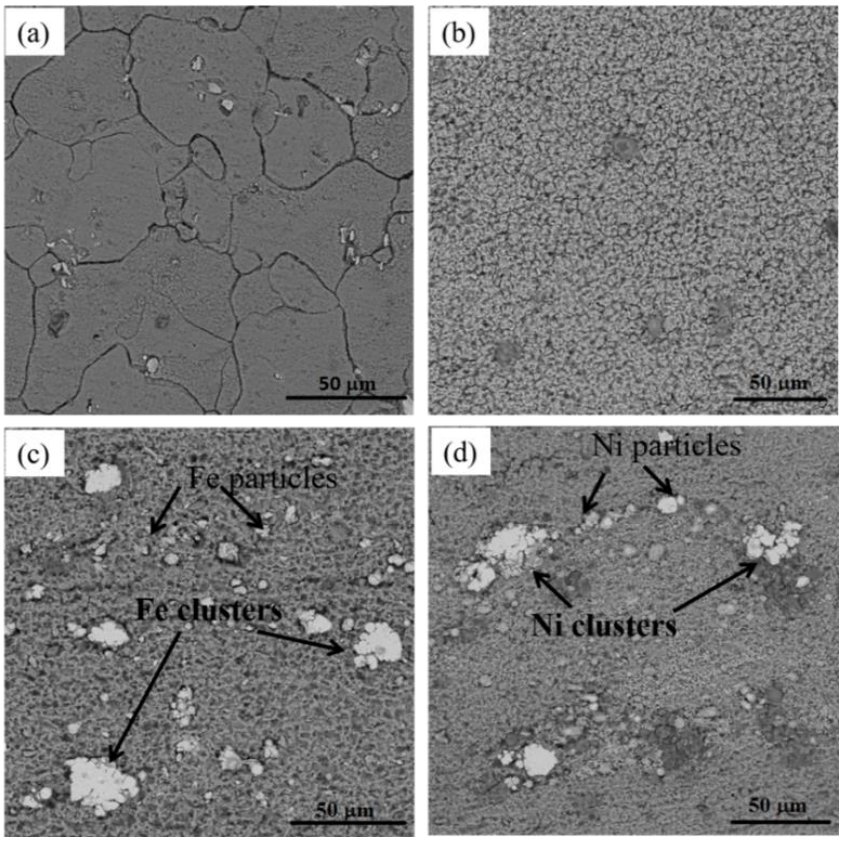

Fig. 4.6.1 SEM images of (a) base alloy (b) As FSPed sample (c) Al/Fe composite (d) Al/Ni composite.

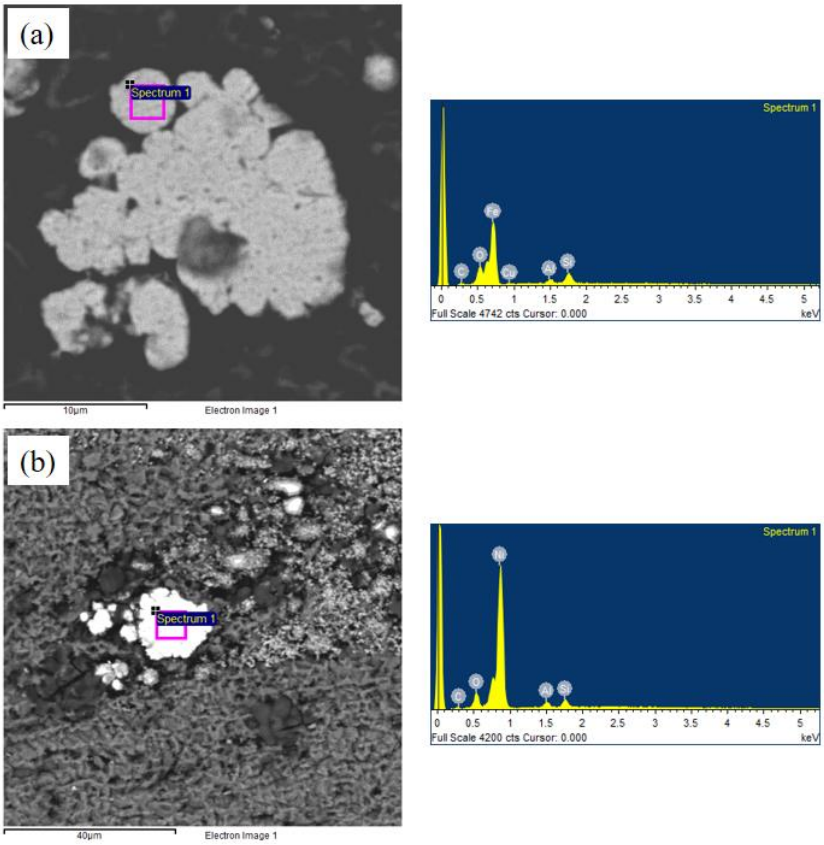

Fig. 4.6.2 Elemental analysis of (a) Al6061/Fe and (b) Al6061/Ni composite by EDX.

4.6.4 Hardness

Fig. 4.6.3 shows the hardness profile obtained across the processed regime. Hardness along a line was measured for the base alloy and presented in the plot as a reference. The average hardness of the base metal was 60 ± 4.3 Hv. Hardness was decreased just after FSP, i.e. 51 ± 3.4 Hv. The reduction in the stir zone was about 15%, which could be due to coarsening/dissolution of precipitates [96]. Average hardness at the stir zones of the Al6061/Fe and Al6061/Ni surface composites measured to be 114Hv and 80 ± 5.7 Hv, respectively. The hardness increment was about 90% and 33.3%, respectively, for Al/Fe and Al/Ni composites compared to the base alloy. This significant increase was majorly believed to be due to the reinforcement of particles.

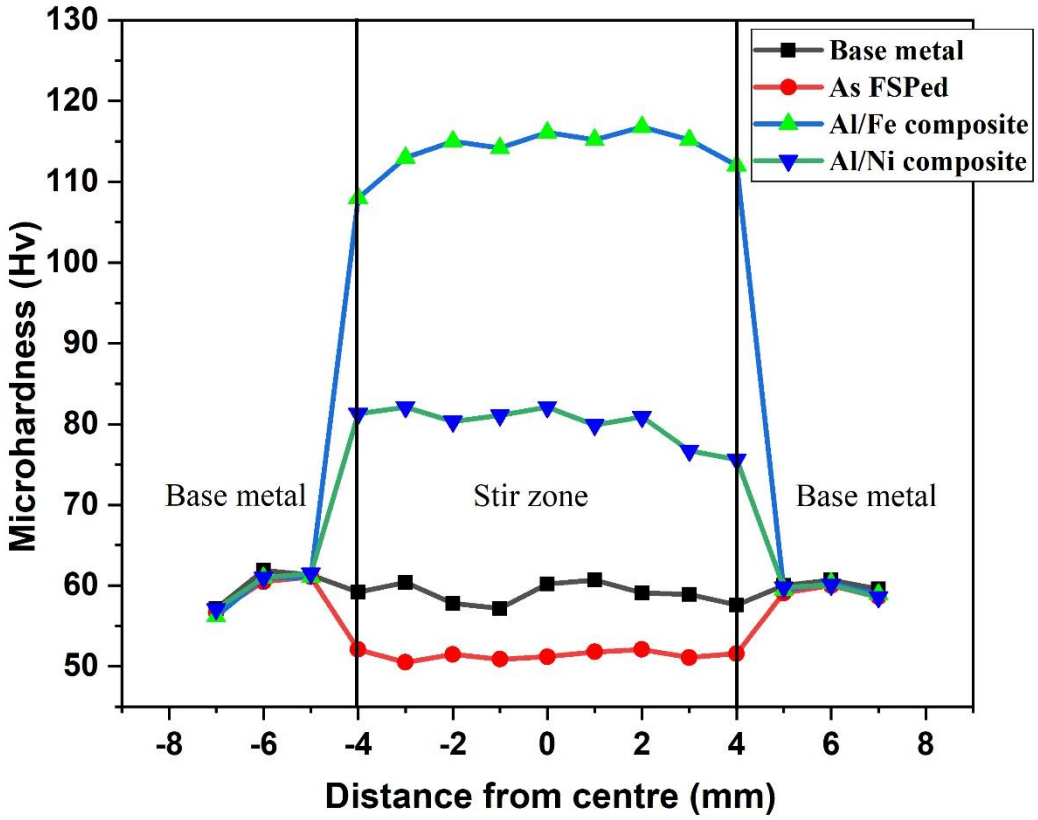

Fig. 4.6.3 Microhardness of base metal and FSPed composites.

4.6.5 Damping capacity of surface composites

Fig. 4.6.4 shows the temperature-dependent (30 to 300 °C) damping capacity of samples at 1 Hz. For all the samples, damping capacity increased with the temperature. The damping capacity was higher for the FSPed base alloy and the surface composites compared to the base alloy. The difference between the damping capacities of the composites and the base alloy was minimal at lower temperatures (30-100 ºC); the difference was significant at high temperatures (125-300 ºC). The highest damping capacity (tan $\delta = 55 \times 10^{-3}$) was observed at 300 ˚C, which is 2.89 times of the base alloy.

The following facts can be noted by comparing the damping curves of FSPed alloy and the surface composites:

(i) At low temperatures (25 to 100 °C), there was a minimal increment in damping due to the reinforcements

(ii) Nickel was observed to improve the damping better than the iron at low temperatures. This could be due to its higher inherent damping capacity than the iron.

(iii) At high temperatures, particularly in the range of 150-250°C, the reinforcements improve the damping. However, the contribution was observed to be marginal.

(iv) At high temperatures, the contribution to damping improvement was observed to be identical for nickel and iron.

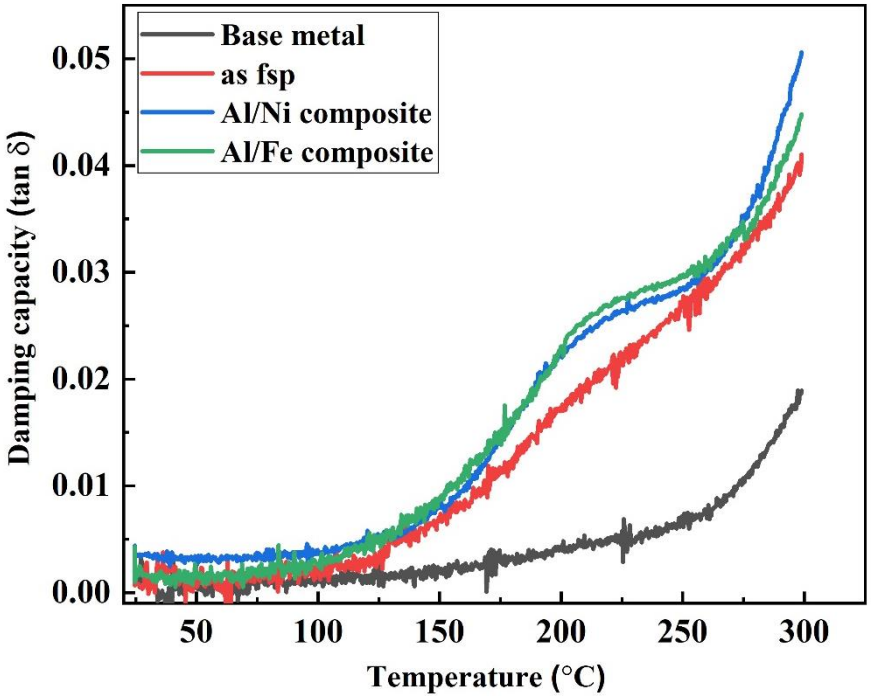

Fig. 4.6.4 Temperature damping capacity of (a) Al6061/Fe composite (b) Al6061/Ni composites.

4.6.6 Damping capacity of Al composites using Impulse excitation technique (IET)

Fig. 4.6.5 shows the decay of sound vibration as a function of time. The time required to decay the sound vibration represents the damping ability of the material. If the vibration amplitude decays quickly, it has better damping properties. It is evident from Fig. 4.6.5 that the time for decaying the vibration increased in the case of friction stir processed sample. Whereas it takes less time to decay the vibration in the case of composites. The damping factor (Q^{-1}) as calculated from these curves are shown in Fig. 4.6.6. It can be implied from the figure that the damping factor increased after adding the particles. The damping capacity of the FSPed sample decreased by 37%. However, the damping capacity for composites increased by 34% (Al/Fe) and 54% (Al/Ni) compared to the base alloy.

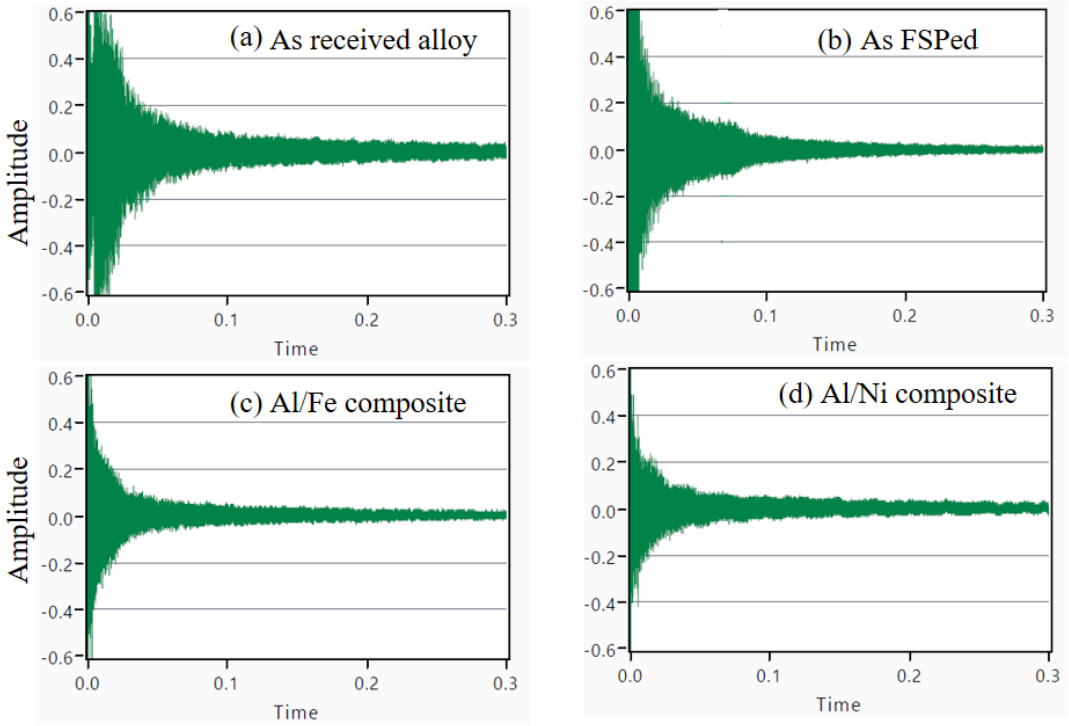

Fig. 4.6.5 Decay of sound vibration as a function of time

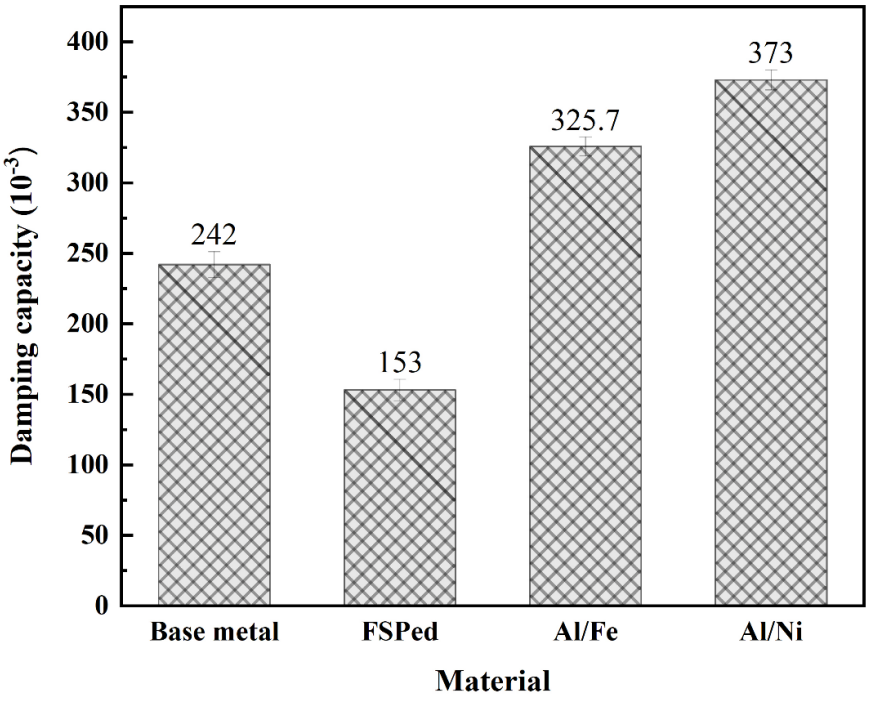

Fig. 4.6.6 Damping capacity of base metal, FSPed and Al composites using IET

From the above results, i.e. damping measurements by DMA and IET, the following conclusions can be drawn

a) The damping at room temperature was observed to be lower than the base alloy for FSPed alloy. This could be due to a reduction in the dislocation density just after FSP (Table 4.6.1). Dislocations are significant contributors to damping at low temperatures [3]. The decrease in dislocation density was due to frictional heat-assisted dynamic recrystallisation phenomena that occur at the processed regime. The recrystallisation results in the formation of grains with an equilibrium number of dislocations which was an established fact in earlier studies [64]. Similar observation has been made while measuring the damping of FSP-ed aluminium, as discussed in section 4.2.
b) The damping at high temperatures was observed to be significantly higher for the FSPed alloy and surface composites compared to the base alloy. This could be attributed to their fine grain size. Grain boundary sliding was reported to be a significant damping mechanism that operates at high temperatures [65]. The microstructure refinement increased the fraction of grain boundaries in the FSPed samples. Hence, sliding was enhanced at these boundaries so that these samples have shown excellent damping at high temperatures.
c) The contribution of iron/nickel was observed to be minimal for damping enhancement at high temperatures. From this, it can be concluded that the contribution of grain boundaries are predominant over the inherent damping of reinforcements.

4.6.7 Summary

The following conclusion can be drawn from this study

1. The chosen friction stir process parameters were appropriate to develop a defect-free processed regime.
2. The hardness of the AA6061/Fe and AA6061/Ni surface composites increased about 90% and 33.3% compared to base alloy, i.e. AA6061.
3. The dispersion of Fe and Ni in AA6061, observed to improve the damping at the resonant frequency by 34 and 54%, respectively.

The highest damping capacity (tan $\delta = 55 \times 10\text{-}3$) was observed at 300 ˚C for AA6061/Ni composite, which was 2.89 times of the base alloy.

4.7 Significant contributions of present research work

The purpose of this section is to highlight the significant contributions of present research work.

1. The present work undoubtedly established that friction stir processing is an effective tool to enhance the damping capacity of metallic materials.
2. The systematic studies brought out the influence of friction stir processing parameters on altering the high temperature (100 - 300 °C) damping capacity.
    - Increase of tool rotational speed decreased the damping property (Fig. 4.2.4b)
    - High traverse speeds were observed to be effective to improve the damping (Fig.4.2.5b)
    - An increase in number of passes increased the damping capacity; at the same time the improvement was observed to be insignificant (Fig.4.2.6b).
3. The results suggest that significant improvement in damping can be brought in to the materials just after friction stir processing i.e. the processed doesn't require additional heat treatment.
4. Does friction stir processing always result in improvement of damping? No (Fig.4.1.4). It depends on the processing history of the material. Generally cold/hot rolling samples consists of high dislocations. Friction stir processing of the samples resulted in significant grain refinement with equilibrium dislocations. The room temperature damping capacity and hardness of the as FSPed samples (without reinforcement) reduced even though there is a grain refinement. Room temperature damping capacity depends on the dislocations present in the samples. At high temperature the damping capacity of FSPed samples shown better than as received samples. Because, grain boundary sliding plays a major role at high temperatures (150-300 °C).
5. Intrinsic damping capacity of reinforcement plays an important role in improving the damping capacity of composites. For comparison purpose, Al6061/SiC, Al6061/Gr and Al6061/BN surface composites were prepared using the parameters 1120 rpm and 30mm/min (Fig. 4.7.1). All surface composites shown better damping capacity than as received sample and highest damping capacity was observed for Al6061/BN composite (585% at 200 °C as compared to the base alloy Al6061). The intrinsic damping capacity of BN is high (Table. 3.1.1) that's the reason why Al6061/BN composite exhibited better damping capacity.

6. Al6061/BN surface composites were produced at different rotational, traverse speed and no. of passes. Highest damping capacity is shown by FSPed sample at 1200 rpm &160 mm/min. (at 200 °C, 407% increased than Al6061) (Fig. 4.5.6).

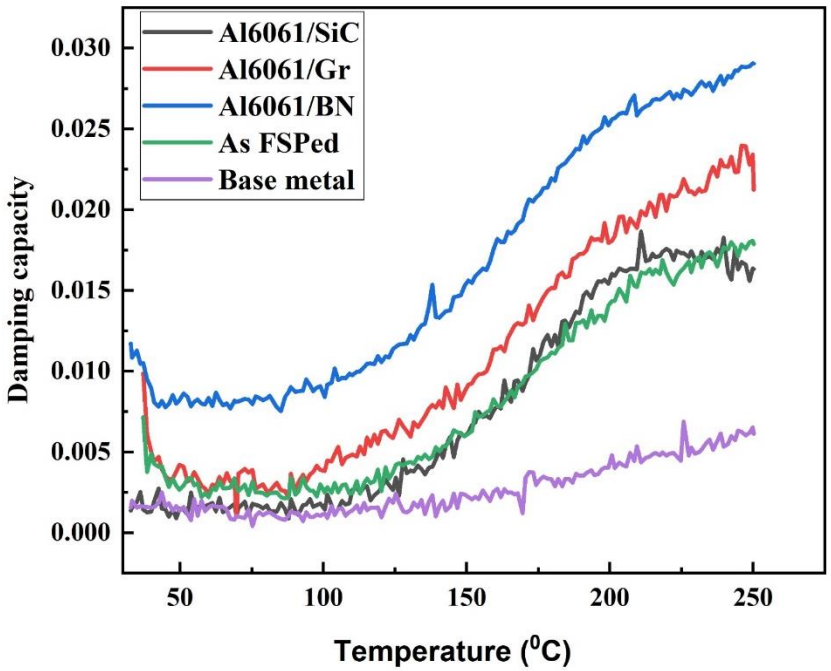

Fig. 4.7.1 Temperature damping capacity of base metal (Al6061) and Al6061 surface composites processed at 1120 rpm and 30 mm/min.

7. Table 4.7.1 compares the damping property improvement in the current study with some published works; the influence of FSP on enhancing the damping can be inferred from the Table 4.7.1.

Table 4.7.1 Comparison of Damping Capacity (Tanδ) of Al6061 Alloy and Its Composites with Other Al Alloys and their Composites.

Material	Reinforcement	Process	Test mode	Damping at 250 °C	Remarks % Increase	Reference
Al8090	Base metal	Stir casting	3 point bending	0.056	--	Ranjit Bauri and M. K. surappa [25]
	18% vol. SiC		--	0.081	44.6	
6061Al	Base metal			0.007	--	J. Zhang et. al. [78]
	Deposited Al6061	Spray atomization and deposition		0.013	85.7	
	5% SiC			0.039	457.1	
	10% SiC			0.040	471.4	
	5% Gr			0.027	285.7	
	10% Gr			0.040	471.4	
AlSi	Base metal	Hot pressing		0.03	--	
	8.6 % SiC			0.046	53.3	

	(113µm)		Single cantilever			S madeira et. al. [97]
Al6061	Base metal	Spray atomization and deposition		0.014	--	Can Wang [98]
	SiC			0.039	178.5	
Al6061	Base alloy	--	3- point bending	0.007	--	**Present work**
	As FSP 1120 rpm & 30 mm/min.	Friction stir processing (FSP)		0.018	157.1	
	15 Vol. % Gr (1120 rpm & 30 mm/min.)			0.025	257.1	
	As FSP 600 rpm & 60mm/min. (2 pass)			0.023	228.5	
	15 vol.% (SiC 9µm) 600 rpm & 60mm/min. (2 pass)			0.020	185.7	
	15 vol.% (SiC 29.4 µm) 600 rpm & 60mm/min. (2 pass)			0.031	342.8	
	15 vol.% (SiC 109µm) 600 rpm & 60mm/min. (2 pass)			0.032	357.1	
	15 vol.% BN (1200 rpm & 160 mm/min.)			0.047	571.4	
	As FSP (600 rpm & 60 mm/min.)			0.027	285.7	
	15 vol.% Ni 600 rpm & 60 mm/min.			0.028	300.0	
	15 vol.% Fe 600 rpm & 60 mm/min.			0.029	314.2	

Chapter 5

Conclusions and future scope

5.1 Conclusions

The principal objective of this doctoral research work is to explore the possibility of analysing the damping capacity of commercial pure metals (pure Al, Cu and Mg) through friction stir processing. Also, efforts were made to develop Al6061 surface composites incorporating ceramic and metallic reinforcements through friction stir processing. In all these efforts, the effect of friction stir processing on the development of microstructure further its effects on damping capacity and hardness properties are systematically investigated. This chapter summarises the significant observations of research work.

- The fine-grained microstructure developed due to friction stir processing with a rotational speed of 600 rpm and traverse speed of 40 mm/min enhanced the damping of aluminium, copper and magnesium at high temperatures.
- The increase of tool rotational speed decreased the damping capacity of pure aluminium. Whereas the increase of tool traverse speed and the number of passes increased the damping.
- The increase of graphite fraction resulted in improved damping (up to 293%) of AA6061 based surface composites at ambient and elevated temperatures. The optimum amount of graphite to enhance the damping was found to be 15 vol. %; a further increase of graphite was observed to decrease the damping.
- An increase of SiC particle size increased the damping capacity of AA6061 based surface composites; the reason was found to be a larger plastic zone built up with large particles.
- The role of process variables explored on the damping capacity of AA6061/BN composites. Damping, in general, improved after the processing compared to the as-received AA6061. The observed maximum improvement in damping was 407%.
- The dispersion of Fe and Ni in AA6061 improved the damping at the resonant frequency by 34 and 54%, respectively.

- The enhanced damping capacity of surface layers, particularly at high temperatures (around 300°C), is attributed to increasing grain boundary area due to grain refinement.

5.2 Scope for future research

Based on the knowledge and experience gained during the current study, the following research topics suggested those willing to explore friction stir processing to enhance the damping properties.

1. Study the influence of friction stir process parameters on the damping properties of magnesium and copper.
2. Study the effect of friction stir processing on the dissolution/ coarsening of precipitates, further influencing the damping properties of heat treatable aluminium alloys.
3. Exploring industrial wastes (rice husk ash, fly ash etc.) as reinforcements further its effect on the damping properties of aluminium based metal matrix composites.
4. Influence of friction stir processing on the grain boundary character distribution subsequently its effect on the damping properties of aluminium/ magnesium.
5. A study on the damping capacity of Al/cast iron composites through friction stir processing can be explored.
6. The effect of hybrid reinforcements on the damping capacity of Al composites can be explored.
7. The contribution of quantitative analysis of damping capacity of dislocations and grain boundaries can be explored.

References

[1] Y. Cui, J. Li, Y. Li, Y. Koizumi, and A. Chiba, “Damping capacity of pre-compressed magnesium alloys after annealing,” *Mater. Sci. Eng. A*, vol. 708, no. June, pp. 104–109, 2017, doi: 10.1016/j.msea.2017.09.096.

[2] B. M. Girish, K. R. Prakash, B. M. Satish, P. K. Jain, and P. Prabhakar, “An investigation into the effects of graphite particles on the damping behavior of ZA-27 alloy composite material,” *Mater. Des.*, vol. 32, no. 2, pp. 1050–1056, 2011, doi: 10.1016/j.matdes.2010.07.006.

[3] E. J. L. Jinmin Zhang, Robert J Perej, Catherin R Wong, “Effect of secondary phases on damping behaviour of metals, alloys and metal matrix composites,” vol. 16, pp. 97–159, 1996.

[4] H. ZHANG, Z., XU, C., WANG, J., & LIU, “Damping behaviour of ultrafine-grained pure aluminum l2 and the damping mechanism,” *Acta Metall. Sin. (English Lett.*, vol. 19, no. 3, pp. 223–227, 2006.

[5] J. Wang *et al.*, “Optimization of mechanical and damping properties of Mg-0.6Zr alloy by different extrusion processing,” *J. Magnes. Alloy.*, vol. 3, no. 1, pp. 79–85, 2015, doi: 10.1016/j.jma.2015.02.001.

[6] E. Emadoddin, M. Tajally, and M. Masoumi, “Damping behavior of Al/SiCP multilayer composite manufactured by roll bonding,” *Mater. Des.*, vol. 42, pp. 334–338, 2012, doi: 10.1016/j.matdes.2012.06.009.

[7] D. Yadav and R. Bauri, “Processing, microstructure and mechanical properties of nickel particles embedded aluminium matrix composite,” *Mater. Sci. Eng. A*, vol. 528, no. 3, pp. 1326–1333, 2011, doi: 10.1016/j.msea.2010.10.035.

[8] C. Y. Liu, H. J. Jiang, B. Zhang, and Z. Y. Ma, “High damping capacity of Al alloys produced by friction stir processing,” *Mater. Charact.*, vol. 136, no. November 2017, pp. 382–387, 2018, doi: 10.1016/j.matchar.2018.01.009.

[9] N. Gangil, A. N. Siddiquee, and S. Maheshwari, “Aluminium based in-situ composite fabrication through friction stir processing: A review,” *J. Alloys Compd.*, vol. 715, pp. 91–104, 2017, doi: 10.1016/j.jallcom.2017.04.309.

[10] A. P. Zykova, S. Y. Tarasov, A. V. Chumaevskiy, and E. A. Kolubaev, “A review of

friction stir processing of structural metallic materials: Process, properties, and methods," *Metals (Basel).*, vol. 10, no. 6, pp. 1–35, 2020, doi: 10.3390/met10060772.

[11] D. S. Prasad, C. Shoba, and K. R. Varma, "Damping behavior of commonly used reinforcement powders – An experimental approach," *Eng. Sci. Technol. an Int. J.*, vol. 18, no. 4, pp. 674–679, 2015, doi: 10.1016/j.jestch.2015.05.001.

[12] D. Siva Prasad, P. T. Radha, C. Shoba, and P. S. Rao, "Dynamic mechanical behavior of WC-Co coated A356.2 aluminum alloy," *J. Alloys Compd.*, vol. 767, pp. 988–993, 2018, doi: 10.1016/j.jallcom.2018.07.203.

[13] D. Siva, P. Chintada, D. Á. Dma, and Á. Rice, "Damping Behavior of Metal Matrix Composites," vol. 68, pp. 161–167, 2015, doi: 10.1007/s12666-014-0462-z.

[14] S. Singh and K. Pal, "Influence of surface morphology and UFG on damping and mechanical properties of composite reinforced with spinel MgAl2O4-SiC core-shell microcomposites," *Mater. Charact.*, vol. 123, pp. 244–255, 2017, doi: 10.1016/j.matchar.2016.11.042.

[15] R. J. Perez, J. Zhang, and E. J. Lavernia, "Damping Behavior of 6061AI / Gr Metal Matrix Composites," vol. 24, no. March, 1993.

[16] K. K. Deng, J. C. Li, K. B. Nie, X. J. Wang, and J. F. Fan, "High temperature damping behavior of as-deformed Mg matrix influenced by micron and submicron SiCp," *Mater. Sci. Eng. A*, vol. 624, pp. 62–70, 2015, doi: 10.1016/j.msea.2014.11.069.

[17] A. Granato and K. Lücke, "Theory of mechanical damping due to dislocations," *J. Appl. Phys.*, vol. 27, no. 6, pp. 583–593, 1956, doi: 10.1063/1.1722436.

[18] D. Siva Prasad and C. Shoba, "Experimental evaluation onto the damping behavior of Al/SiC/RHA hybrid composites," *J. Mater. Res. Technol.*, vol. 5, no. x x, pp. 2–9, 2015, doi: 10.1016/j.jmrt.2015.08.001.

[19] S. H. Kim and S. H. Park, "Improvement in damping capacity of extruded pure magnesium through precompression and subsequent annealing: Effects of dislocation and twin boundary motions," *J. Alloys Compd.*, vol. 835, p. 155257, 2020, doi: 10.1016/j.jallcom.2020.155257.

[20] S. K. Wu, S. H. Chang, and C. Chien, "Effect of cold-rolling on damping characteristics of multi-component Al-12% Si alloy measured by dynamic mechanical analyzer," *Mater. Trans.*, vol. 54, no. 5, pp. 738–744, 2013, doi:

10.2320/matertrans.M2012418.

[21] G. D. Fan, M. Y. Zheng, X. S. Hu, C. Xu, K. Wu, and I. S. Golovin, “Improved mechanical property and internal friction of pure Mg processed by ECAP,” *Mater. Sci. Eng. A*, vol. 556, pp. 588–594, 2012, doi: 10.1016/j.msea.2012.07.031.

[22] J. Wang, R. Lu, D. Qin, W. Yang, and Z. Wu, “Effect of arc-bending deformation on amplitude-dependent damping in pure magnesium,” *Mater. Sci. Eng. A*, vol. 615, pp. 296–301, 2014, doi: 10.1016/j.msea.2014.07.078.

[23] J. N. Wei, H. F. Cheng, Y. F. Zhang, F. S. Han, Z. C. Zhou, and J. P. Shui, “Effects of macroscopic graphite particulates on the damping behavior of commercially pure aluminum,” vol. 325, pp. 444–453, 2002.

[24] P. K. Rohatgi, D. Nath, S. S. Singh, and B. N. Keshavaram, “Factors affecting the damping capacity of cast aluminium-matrix composites,” *J. Mater. Sci.*, vol. 29, no. 22, pp. 5975–5984, 1994, doi: 10.1007/BF00366882.

[25] R. Bauri and M. K. Surappa, “Damping behavior of Al-Li-SiCp composites processed by stir casting technique,” *Metall. Mater. Trans. A*, vol. 36, no. 3, pp. 667–673, 2005, doi: 10.1007/s11661-005-0183-3.

[26] J. Zhang, R. J. Perez, and E. J. Lavernia, “Effect of sic and graphite particulates on the damping behavior of metal matrix composites,” *Acta Met. Mater*, vol. 42, no. 2, pp. 395–409, 1994.

[27] J. Gu, X. Zhang, M. Gu, M. Gu, and X. Wang, “Internal friction peak and damping mechanism in high damping 6061Al/SiCp/Gr hybrid metal matrix composite,” *J. Alloys Compd.*, vol. 372, no. 1–2, pp. 304–308, 2004, doi: 10.1016/j.jallcom.2003.10.021.

[28] O. Carvalho, G. Miranda, M. Buciumeanu, M. Gasik, F. S. Silva, and S. Madeira, “High temperature damping behavior and dynamic Young ’ s modulus of AlSi – CNT – SiC p hybrid composite,” vol. 141, pp. 155–162, 2016.

[29] S. Madeira, G. Miranda, V. H. Carneiro, D. Soares, F. S. Silva, and O. Carvalho, “The effect of SiCp size on high temperature damping capacity and dynamic Young’s modulus of hot-pressed AlSi-SiCp MMCs,” *Mater. Des.*, vol. 93, pp. 409–417, 2016, doi: 10.1016/j.matdes.2015.12.147.

[30] J. Gu, X. Zhang, M. Gu, Z. Liu, and G. Zhang, “The damping capacity of aluminum

matrix composites reinforced with coated carbon fibers," *Mater. Lett.*, vol. 58, no. 25, pp. 3170–3174, 2004, doi: 10.1016/j.matlet.2004.05.066.

[31] R. S. Mishra and Z. Y. Ma, "Friction stir welding and processing," *Reports A Rev. J.*, vol. 50, pp. 1–78, 2005.

[32] N. Gangil *et al.*, "Fabrication of magnesium-nitip composites via friction stir processing: Effect of tool profile," *Metals (Basel).*, vol. 10, no. 11, pp. 1–11, 2020, doi: 10.3390/met10111425.

[33] V. Sharma, U. Prakash, and B. V. M. Kumar, "Surface composites by friction stir processing: A review," *J. Mater. Process. Technol.*, vol. 224, pp. 117–134, 2015, doi: 10.1016/j.jmatprotec.2015.04.019.

[34] B. R. Sunil, G. P. K. Reddy, H. Patle, and R. Dumpala, "Magnesium based surface metal matrix composites by friction stir processing," *J. Magnes. Alloy.*, vol. 4, no. 1, pp. 52–61, 2016, doi: 10.1016/j.jma.2016.02.001.

[35] O. B. Bembalge and S. K. Panigrahi, "Influence of SiC ceramic reinforcement size in establishing wear mechanisms and wear maps of ultrafine grained AA6063 composites," *Ceram. Int.*, vol. 45, no. 16, pp. 20091–20104, 2019, doi: 10.1016/j.ceramint.2019.06.274.

[36] W. B. Lee *et al.*, "Microstructures and wear property of friction stir welded AZ91 Mg/SiC particle reinforced composite," *Compos. Sci. Technol.*, vol. 66, no. 11–12, pp. 1513–1520, 2006, doi: 10.1016/j.compscitech.2005.11.023.

[37] A. Devaraju, A. Kumar, and B. Kotiveerachari, "Influence of addition of Grp/Al2O3p with SiCp on wear properties of aluminum alloy 6061-T6 hybrid composites via friction stir processing," *Trans. Nonferrous Met. Soc. China (English Ed.*, vol. 23, no. 5, pp. 1275–1280, 2013, doi: 10.1016/S1003-6326(13)62593-5.

[38] A. Hosseinzadeh and G. G. Yapici, "High temperature characteristics of Al2024/SiC metal matrix composite fabricated by friction stir processing," *Mater. Sci. Eng. A*, vol. 731, no. April, pp. 487–494, 2018, doi: 10.1016/j.msea.2018.06.077.

[39] D. Yadav and R. Bauri, "Effect of friction stir processing on microstructure and mechanical properties of aluminium," *Mater. Sci. Eng. A*, vol. 539, pp. 85–92, 2012, doi: 10.1016/j.msea.2012.01.055.

[40] K. Li, X. Liu, and Y. Zhao, "Research status and prospect of friction stir processing

technology," *Coatings*, vol. 9, no. 2, 2019, doi: 10.3390/COATINGS9020129.

[41] R. S. Mishra, M. W. Mahoney, S. X. McFadden, N. A. Mara, and A. K. Mukherjee, "High strain rate superplasticity in a friction stir processed 7075 Al alloy," *Scr. Mater.*, vol. 42, no. 2, pp. 163–168, 1999, doi: 10.1016/S1359-6462(99)00329-2.

[42] C. Srinivasan and M. Karunanithi, "Fabrication of surface level Cu/SiCp nanocomposites by friction stir processing route," *J. Nanotechnol.*, vol. 2015, 2015, doi: 10.1155/2015/612617.

[43] T. Morishige, T. Hirata, M. Tsujikawa, and K. Higashi, "Comprehensive analysis of minimum grain size in pure aluminum using friction stir processing," *Mater. Lett.*, vol. 64, no. 17, pp. 1905–1908, 2010, doi: 10.1016/j.matlet.2010.06.003.

[44] F. S. Tooling, "Tool Materials and Designs, Chapter 2 in Friction Stir Welding and Processing," *ASM Int. Ed. Rajiv S. Mishra Murray W. Mahoney*, pp. 7–35, 2007, doi: 10.1361/fswp2007p001.

[45] D. K. Lim, T. Shibayanagi, and A. P. Gerlich, "Synthesis of multi-walled CNT reinforced aluminium alloy composite via friction stir processing," *Mater. Sci. Eng. A*, vol. 507, no. 1–2, pp. 194–199, 2009, doi: 10.1016/j.msea.2008.11.067.

[46] R. Sathiskumar, N. Murugan, I. Dinaharan, and S. J. Vijay, "Role of friction stir processing parameters on microstructure and microhardness of boron carbide particulate reinforced copper surface composites," *Sadhana - Acad. Proc. Eng. Sci.*, vol. 38, no. 6, pp. 1433–1450, 2013, doi: 10.1007/s12046-013-0184-7.

[47] W. Y. Gan, Z. Zhou, H. Zhang, and T. Peng, "Evolution of microstructure and hardness of aluminum after friction stir processing," *Trans. Nonferrous Met. Soc. China (English Ed.*, vol. 24, no. 4, pp. 975–981, 2014, doi: 10.1016/S1003-6326(14)63151-4.

[48] K. Surekha and A. Els-Botes, "Development of high strength, high conductivity copper by friction stir processing," *Mater. Des.*, vol. 32, no. 2, pp. 911–916, 2011, doi: 10.1016/j.matdes.2010.08.028.

[49] S. Salahi and V. Rezazadeh, "Fracture Mechanism in Friction Stir Processed Annealed Pure Copper Samples," *World Appl. Sci. J.*, vol. 23, no. 12, pp. 54–58, 2013, doi: 10.5829/idosi.wasj.2013.23.12.805.

[50] M. Barmouz, M. K. B. Givi, and J. Jafari, "Evaluation of tensile deformation properties

of friction stir processed pure copper: Effect of processing parameters and pass number," *J. Mater. Eng. Perform.*, vol. 23, no. 1, pp. 101–107, 2014, doi: 10.1007/s11665-013-0734-5.

[51] S. Singh and K. Pal, "Effect of texture evolution on mechanical and damping properties of SiC/ZnAl2O4/Al composite through friction stir processing," *J. Mater. Res. Technol.*, vol. 8, no. 1, pp. 222–232, 2019, doi: 10.1016/j.jmrt.2017.07.006.

[52] R. S. Mishra, Z. Y. Ma, and I. Charit, "Friction stir processing: A novel technique for fabrication of surface composite," *Mater. Sci. Eng. A*, vol. 341, no. 1–2, pp. 307–310, 2003, doi: 10.1016/S0921-5093(02)00199-5.

[53] W. Wang, Q. yu Shi, P. Liu, H. ke Li, and T. Li, "A novel way to produce bulk SiCp reinforced aluminum metal matrix composites by friction stir processing," *J. Mater. Process. Technol.*, vol. 209, no. 4, pp. 2099–2103, 2009, doi: 10.1016/j.jmatprotec.2008.05.001.

[54] L. Ke, C. Huang, L. Xing, and K. Huang, "Al-Ni intermetallic composites produced in situ by Friction Stir Processing," *J. Alloys Compd.*, vol. 503, no. 2, pp. 494–499, 2010, doi: 10.1016/j.jallcom.2010.05.040.

[55] E. R. I. Mahmoud, M. Takahashi, T. Shibayanagi, and K. Ikeuchi, "Wear characteristics of surface-hybrid-MMCs layer fabricated on aluminum plate by friction stir processing," *Wear*, vol. 268, no. 9–10, pp. 1111–1121, 2010, doi: 10.1016/j.wear.2010.01.005.

[56] A. Thangarasu, N. Murugan, and I. Dinaharan, "Production and wear characterization of AA6082-TiC surface composites by friction stir processing," *Procedia Eng.*, vol. 97, pp. 590–597, 2014, doi: 10.1016/j.proeng.2014.12.287.

[57] W. Woo, H. Choo, D. W. Brown, and Z. Feng, "Influence of the tool pin and shoulder on microstructure and natural aging kinetics in a friction-stir-processed 6061-T6 aluminum alloy," *Metall. Mater. Trans. A Phys. Metall. Mater. Sci.*, vol. 38, no. 1, pp. 69–76, 2007, doi: 10.1007/s11661-006-9034-0.

[58] N. Parumandla and K. Adepu, "Effect of Al2O3 and SiC nano reinforcements on microstructure, mechanical and wear properties of surface nanocomposites fabricated by friction stir processing," *Medziagotyra*, vol. 24, no. 3, pp. 338–344, 2018, doi: 10.5755/j01.ms.24.3.18220.

[59] M. Barmouz, M. K. Besharati Givi, and J. Seyfi, “On the role of processing parameters in producing Cu/SiC metal matrix composites via friction stir processing: Investigating microstructure, microhardness, wear and tensile behavior,” *Mater. Charact.*, vol. 62, no. 1, pp. 108–117, 2011, doi: 10.1016/j.matchar.2010.11.005.

[60] P. Asadi, G. Faraji, and M. K. Besharati, “Producing of AZ91/SiC composite by friction stir processing (FSP),” *Int. J. Adv. Manuf. Technol.*, vol. 51, no. 1–4, pp. 247–260, 2010, doi: 10.1007/s00170-010-2600-z.

[61] H. Sarmadi, A. H. Kokabi, and S. M. Seyed Reihani, “Friction and wear performance of copper-graphite surface composites fabricated by friction stir processing (FSP),” *Wear*, vol. 304, no. 1–2, pp. 1–12, 2013, doi: 10.1016/j.wear.2013.04.023.

[62] R. Sathiskumar, N. Murugan, I. Dinaharan, and S. J. Vijay, “Characterization of boron carbide particulate reinforced in situ copper surface composites synthesized using friction stir processing,” *Mater. Charact.*, vol. 84, pp. 16–27, 2013, doi: 10.1016/j.matchar.2013.07.001.

[63] V. Kishan, A. Devaraju, and K. Prasanna Lakshmi, “Influence of volume percentage of NanoTiB2 particles on tribological & mechanical behaviour of 6061-T6 Al alloy nano-surface composite layer prepared via friction stir process,” *Def. Technol.*, vol. 13, no. 1, pp. 16–21, 2017, doi: 10.1016/j.dt.2016.11.002.

[64] H. J. Jiang *et al.*, “Simultaneously improving mechanical properties and damping capacity of Al-Mg-Si alloy through friction stir processing,” *Mater. Charact.*, vol. 131, no. April, pp. 425–430, 2017, doi: 10.1016/j.matchar.2017.07.037.

[65] C. Y. Liu *et al.*, “Effects of pre-aging and minor Sc addition on the microstructure and mechanical properties of friction stir processed 7055 Al alloy,” *Vacuum*, vol. 149, no. July 2017, pp. 106–113, 2018, doi: 10.1016/j.vacuum.2017.12.030.

[66] J. Zhang, R. J. Perez, and E. J. Lavernia, “Documentation of damping capacity of metallic, ceramic and metal-matrix composite materials,” *J. Mater. Sci.*, vol. 28, no. 9, pp. 2395–2404, 1993, doi: 10.1007/BF01151671.

[67] H. I. Kurt, “Influence of hybrid ratio and friction stir processing parameters on ultimate tensile strength of 5083 aluminum matrix hybrid composites,” *Compos. Part B Eng.*, vol. 93, pp. 26–34, 2016, doi: 10.1016/j.compositesb.2016.02.056.

[68] Y. Yang, Y. Zhao, X. Kai, and R. Tao, “Superplasticity behavior and deformation

mechanism of the in-situ Al3Zr/6063Al composites processed by friction stir processing," *J. Alloys Compd.*, vol. 710, pp. 225–233, 2017, doi: 10.1016/j.jallcom.2017.03.246.

[69] A. Dhal, S. K. Panigrahi, and M. S. Shunmugam, "Insight into the microstructural evolution during cryo-severe plastic deformation and post-deformation annealing of aluminum and its alloys," *J. Alloys Compd.*, vol. 726, pp. 1205–1219, 2017, doi: 10.1016/j.jallcom.2017.08.062.

[70] A. K. Swarnakar, L. Donzel, J. Vleugels, and O. Van der Biest, "High temperature properties of ZnO ceramics studied by the impulse excitation technique," *J. Eur. Ceram. Soc.*, vol. 29, no. 14, pp. 2991–2998, 2009, doi: 10.1016/j.jeurceramsoc.2009.04.039.

[71] Y. H. Jeong *et al.*, "Effects of friction stir processing on the thermal conductivity of a strain-hardened Al-Mg alloy," *Int. J. Precis. Eng. Manuf.*, vol. 16, no. 9, pp. 1969–1974, 2015, doi: 10.1007/s12541-015-0256-1.

[72] G. M. Xie, Z. Y. Ma, and L. Geng, "Development of a fine-grained microstructure and the properties of a nugget zone in friction stir welded pure copper," *Scr. Mater.*, vol. 57, no. 2, pp. 73–76, 2007, doi: 10.1016/j.scriptamat.2007.03.048.

[73] Y. Chen *et al.*, "Effects of friction stir processing and minor Sc addition on the microstructure, mechanical properties, and damping capacity of 7055 Al alloy," *Mater. Charact.*, vol. 135, no. November 2017, pp. 25–31, 2018, doi: 10.1016/j.matchar.2017.11.030.

[74] P. P. Pal-Val *et al.*, "Unusual Young's modulus behavior in ultrafine-grained and microcrystalline copper wires caused by texture changes during processing and annealing," *Materials Science and Engineering A*, vol. 618. pp. 9–15, 2014, doi: 10.1016/j.msea.2014.08.069.

[75] H. J. Jiang *et al.*, "Fabrication of Al–35Zn alloys with excellent damping capacity and mechanical properties," *J. Alloys Compd.*, vol. 722, pp. 138–144, 2017, doi: 10.1016/j.jallcom.2017.06.091.

[76] Z. M. Zhang, C. J. Xu, J. C. Wang, and H. Z. Liu, "Damping behavior of ultrafine-grained pure aluminum L2 and the damping mechanism," *Acta Metall. Sin. (English Lett.*, vol. 19, no. 3, pp. 223–227, 2006, doi: 10.1016/S1006-7191(06)60048-3.

[77] Y. Zhang, N. Ma, X. Li, and H. Wang, “Study on damping capacity of aluminum composite reinforced with in situ TiAl3 rod,” *Mater. Des.*, vol. 29, no. 5, pp. 1057–1059, 2008, doi: 10.1016/j.matdes.2007.04.001.

[78] E. J. Lavernia, R. J. Perez, and J. Zhang, “Damping behavior of discontinuously reinforced ai alloy metal-matrix composites,” *Metall. Mater. Trans. A*, vol. 26, no. 11, pp. 2803–2818, 1995, doi: 10.1007/BF02669639.

[79] M. Azizieh, D. Iranparast, M. A. G. Dezfuli, Z. Balak, and H. S. Kim, “Fabrication of Al/Al2Cu in situ nanocomposite via friction stir processing,” *Trans. Nonferrous Met. Soc. China (English Ed.*, vol. 27, no. 4, pp. 779–788, 2017, doi: 10.1016/S1003-6326(17)60089-X.

[80] R. J. Arsenault and N. Shi, “Dislocation generation due to differences between the coefficients of thermal expansion,” *Mater. Sci. Eng.*, vol. 81, no. C, pp. 175–187, 1986, doi: 10.1016/0025-5416(86)90261-2.

[81] A. Devaraju, A. Kumar, and B. Kotiveerachari, “Influence of addition of Grp/Al2O3p with SiCp on wear properties of aluminum alloy 6061-T6 hybrid composites via friction stir processing,” *Trans. Nonferrous Met. Soc. China (English Ed.*, vol. 23, no. 5, pp. 1275–1280, 2013, doi: 10.1016/S1003-6326(13)62593-5.

[82] Y. M. Hwang, P. L. Fan, and C. H. Lin, “Experimental study on Friction Stir Welding of copper metals,” *J. Mater. Process. Technol.*, vol. 210, no. 12, pp. 1667–1672, 2010, doi: 10.1016/j.jmatprotec.2010.05.019.

[83] K. Venkateswara Reddy, R. Bheekya Naik, G. R. Rao, G. Madhusudhan Reddy, and R. Arockia Kumar, “Microstructure and damping capacity of AA6061/graphite surface composites produced through friction stir processing,” *Compos. Commun.*, vol. 20, no. April, p. 100352, 2020, doi: 10.1016/j.coco.2020.04.018.

[84] Z. Liu, H. Zhang, Z. Hou, H. Feng, P. Dong, and P. K. Liaw, “Microstructural origins of mechanical and electrochemical heterogeneities of friction stir welded heat-treatable aluminum alloy,” *Mater. Today Commun.*, vol. 24, no. April, p. 101229, 2020, doi: 10.1016/j.mtcomm.2020.101229.

[85] J. Osten, B. Milkereit, C. Schick, and O. Kessler, “Dissolution and precipitation behaviour during continuous heating of Al-Mg-Si alloys in a wide range of heating rates,” *Materials (Basel).*, vol. 8, no. 5, pp. 2830–2848, 2015, doi:

10.3390/ma8052830.

[86] Y. S. Sato, M. Urata, and H. Kokawa, “Parameters controlling microstructure and hardness during friction-stir welding of precipitation-hardenable aluminum alloy 6063,” *Metall. Mater. Trans. A*, vol. 33, no. 3, pp. 625–635, 2002, doi: 10.1007/s11661-002-0124-3.

[87] G. C. Li, Y. Ma, X. L. He, W. Li, and P. Y. Li, “Damping capacity of high strength-damping aluminum alloys prepared by rapid solidification and powder metallurgy process,” *Trans. Nonferrous Met. Soc. China (English Ed.*, vol. 22, no. 5, pp. 1112–1117, 2012, doi: 10.1016/S1003-6326(11)61291-0.

[88] D. S. Prasad and A. R. Krishna, “Effect of T6 heat treatment on damping characteristics of Al / RHA composites,” vol. 35, no. 6, pp. 989–995, 2012.

[89] D. Dunand and A. Mortensen, “Thermal mismatch dislocations produced by large particles in a strain-hardening matrix,” *Mater. Sci. Eng. A*, vol. 135, no. C, pp. 179–184, 1991, doi: 10.1016/0921-5093(91)90557-4.

[90] S. Madeira, O. Carvalho, V. H. Carneiro, D. Soares, F. S. Silva, and G. Miranda, “Damping capacity and dynamic modulus of hot pressed AlSi composites reinforced with different SiC particle sized,” *Compos. Part B Eng.*, vol. 90, pp. 399–405, 2016, doi: 10.1016/j.compositesb.2016.01.008.

[91] P. J. Withers, “the Application of the Eshelby Method of Internal Stress Determination To Short,” *Acta Met.*, vol. 37, no. 11, pp. 3061–3084, 1989.

[92] C. Y. Barlow and N. Hansen, “Deformation structures and flow stress in aluminium containing short whiskers,” *Acta Metall. Mater.*, vol. 39, no. 8, pp. 1971–1979, 1991, doi: 10.1016/0956-7151(91)90166-X.

[93] Y. Suzuki *et al.*, “Effect of surface area of grain boundaries on stress relaxation behavior in pure copper over wide range of grain sizes,” *Mater. Sci. Eng. A*, p. 139585, 2020, doi: 10.1016/j.msea.2020.139585.

[94] R. Bauri, D. Yadav, and G. Suhas, “Effect of friction stir processing (FSP) on microstructure and properties of Al-TiC in situ composite,” *Mater. Sci. Eng. A*, vol. 528, no. 13–14, pp. 4732–4739, 2011, doi: 10.1016/j.msea.2011.02.085.

[95] H. J. Jiang, C. Y. Liu, Z. X. Yang, Y. P. Li, H. F. Huang, and F. C. Qin, “Effect of Friction Stir Processing on the Microstructure, Damping Capacity, and Mechanical

Properties of Al-Si Alloy," *J. Mater. Eng. Perform.*, vol. 28, no. 2, pp. 1173–1179, 2019, doi: 10.1007/s11665-018-3844-2.

[96] D. Aruri, K. Adepu, K. Adepu, and K. Bazavada, "Wear and mechanical properties of 6061-T6 aluminum alloy surface hybrid composites [(SiC + Gr) and (SiC + Al2O3)] fabricated by friction stir processing," *J. Mater. Res. Technol.*, vol. 2, no. 4, pp. 362–369, 2013, doi: 10.1016/j.jmrt.2013.10.004.

[97] S. Madeira, G. Miranda, V. H. Carneiro, D. Soares, F. S. Silva, and O. Carvalho, "The effect of SiCp size on high temperature damping capacity and dynamic Young's modulus of hot-pressed AlSi-SiCp MMCs," *Mater. Des.*, vol. 93, pp. 409–417, 2016, doi: 10.1016/j.matdes.2015.12.147.

[98] C. Wang and Z. Zhu, "Internal friction at medium temperature in an al matrix composite reinforced by sic particles," *Acta Metall.*, vol. 38, no. 12, pp. 1739–1745, 1998.

List of publications

1. **K Venkateswara Reddy**, R. Bheekya Naik, G Madhusudhan Reddy, Chakravarthy Pammi, Sabavath Janakiram, R. Arockia Kumar, Damping capacity of aluminium surface layers developed through friction stir processing, **Materials Letters** (2021) 298(4):130031 DOI: 10.1016/j.matlet.2021.130031.
2. **K Venkateswara Reddy**, R. Bheekya Naik, G. Rama Rao, G Madhusudhan Reddy, R. Arockia Kumar, Microstructure and damping capacity of AA6061/graphite composites produced through friction stir processing, **Composite Communications**, 20 (2020) 100352.(https://doi.org/10.1016/j.coco.2020.04.018.
3. **K. Venkateswara Reddy**, R. Bheekya Naik, G. Madhusudhan Reddy, P. Chakravarthy, R. Arockia Kumar, "Damping capacity of Al6061/SiC$_P$ surface composites developed through friction stir processing". **Journal of Materials Engineering and Performance**, 2021.(https://doi.org/10.1007/s11665-021-06201-5)
4. **K Venkateswara Reddy**, R. Bheekya Naik, Sandeep Yadav, G Madhusudhan Reddy, R. Arockia Kumar, Measurement of Elastic Modulus and Damping Properties of Friction Stir Processed Pure Metals Using Impulse Excitation Technique, **Advances in Applied Mechanical Engineering** (2019) 521-528. (https://doi.org/10.1007/978-981-15-1201-8_58).
5. **K Venkateswara Reddy**, RB Naik, GM Reddy, RA Kumar, Damping capacity of friction stir processed commercial pure aluminium metal, **Materials Today: Proceedings** (https://doi.org/10.1016/j.matpr.2019.09.059)

International/National Conferences attended

1. **K. Venkateswara Reddy**, Ramavath Bheekya Naik, R. Arockia Kumar, Preparation of Shape memory alloy layer through Friction Stir Process, **Poster presentation,** NCAMPC – 2016, NIT Warangal**,** 4 – 6 January, 2016.
2. **K. Venkateswara Reddy**, Golla Rama Rao, G. Madhusudhan Reddy, R. Arockia Kumar, Microstructure and damping capacity of Al/Gr surface composites fabricated through friction stir processing, **Poster presentation** in NMD-ATM 2017 held in BITS, KK Birla Campus, Goa, 11-14 Nov 2017.
3. **K. Venkateswara Reddy**, R. Bheekya Naik, G. Madhusudhan Reddy, R. Arockia Kumar**,** Damping capacity of friction stir processed metallic materials, **Poster presentation** in NMD-ATM 2018 held in Kolkata, India, 11-14 Nov 2018.
4. **K. Venkateswara Reddy**, R. Bheekya Naik,, Sandeep Yadav, G. Madhusudhan Reddy R. Arockia Kumar, Measurement of elastic modulus and damping properties of friction stir processed pure metals using impulse excitation technique, ICAMER – 2019, NIT Warangal, 2 – 4 May 2019.
5. **K. Venkateswara Reddy**, R. Bheekya Naik, G. Madhusudhan Reddy, R. Arockia Kumar, Damping capacity of friction stir processed commercial pure aluminium metal, MMM – 2019, NIT Trichy, 5 – 7 July 2019.
6. **K. Venkateswara Reddy**, Sandeep Yadav, G. Madhusudhan Reddy, R. Arockia Kumar, Damping capacity of friction stir processed Magnesium, ICAM^{5} – 2019, NIT Warangal, 25 – 27 September 2019.
7. **K. Venkateswara Reddy**, G. Madhusudhan Reddy, R. Arockia Kumar, Damping capacity of Al surface composites produced by friction stir processing, **Poster presentation** in NMD-ATM 2019 held in Trivandrum, Kerala, 13-16 Nov 2019.

Annexure 1

Dislocation density measurement for Al6061/SiC 9µm composite.

2θ	θ	Sin θ	Cos θ	FWHM (Bo)	B_o (rad)	B_o^2	Bi^2	$Br^2 = Bo^2 - Bi^2$
38.6	19.30	0.33	0.94	0.1261	0.002194	4.81E-06	1.07545E-06	3.7388E-06

Br	Br Cosθ	$D = \frac{\kappa\lambda}{\beta Cos\theta}$	D*D	Dislocation density = 1/D2	Dislocation density of FSPed Al6063/Al_3Zr composite [68]
0.001933597	0.001825	75.95144575	5768.622	17.3	14.2